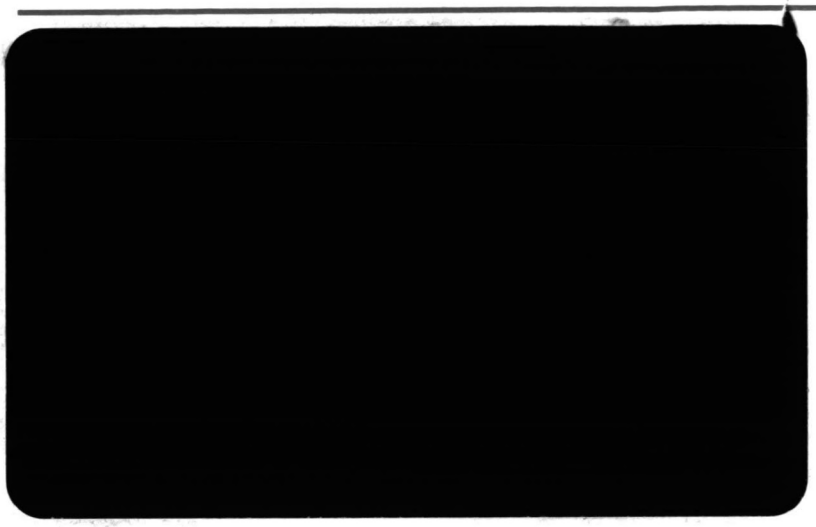

TU Delft
Technische Universiteit Delft

Faculteit der Civiele Techniek
Vakgroep Waterbouwkunde

P.J. de Wit

5.11

Liquefaction and erosion of mud due to waves and current

Uitgeleend aan:

Naam: Datum: Tel.nr.

Liquefaction and erosion of mud due to waves and current

Experiments on China Clay

P.J. de Wit

report no. 10-92

January 1994

Hydromechanics Section
Hydraulic and Geotechnical Engineering Division
Department of Civil Engineering
Delft University of Technology
Delft, The Netherlands

Abstract

A research project was started at the Delft University of Technology in order to study the interaction between waves as well as a current and a muddy bed. For this purpose several experiments were made on artificial clays. In the present report only flume experiments on China Clay are discussed. In the experiments made special attention was paid to the liquefaction mechanism, the turbulence structure over a liquefied bed and the influence of liquefaction on the wave damping.

The experimental results showed, among other things, that a layer of fluid mud was generated as soon as the wave height exceeded a certain threshold value. This value increases with the consolidation period.

Pressure induced shear stresses in the bed calculated under the assumption of China Clay being a poro-elastic material, show that these stresses play an important role in the liquefaction process of mud.

The waves were significantly damped as soon as a layer of fluid mud was generated. The damping was only little influenced by a current. Furthermore, it was observed that the fluid mud was transported very easily by a current and hardly any mud was entrained into the water layer during this process.

The velocity measurements showed that the turbulence intensities decreased in a stationary current when a layer of fluid mud was present, which result corresponds with visual observations made when dye was injected into the flow.

The observations and pressure measurements usually made at the transparent sidewall of a set-up are not representative of the actual physical processes away from the sidewalls. Only measurements carried out far from a wall give a quantitative description of the processes inside the bed.

Pore-pressure measurements showed a transient decrease, possibly caused by the break down of the aggregate structure, succeeded by a gradual build-up of an excess pore pressure so as to compensate for the vanishing effective stress.

The wave damping and velocity amplitudes in the fluid mud which were determined during the experiments, correspond well with the calculated results using a modified version of Gade's model (1958).

Acknowledgements

This research project was partly funded by the Commission of the European Communities, Directorate General for Science, Research and Development under MAST2 (G8 Morphodynamics research programme) and supported financially by Rijkswaterstaat. It was conducted in the framework of the Netherlands Centre of Coastal Research.

The extensive laboratory experiments could not be carried out without the continuous support of the staff of the Hydromechanics Laboratory of the Delft University of Technology. In particular I wish to thank Dirk Post, for his always enthusiastic assistance in the preparation and making of the experiments, just as Karel de Bruin, Fred van der Brugge, Mr. J. Groeneveld, Hans Tas, Frank Kalkman and Arie den Toom who's support always could be counted on. Special thanks go to Manon Moot for her continuous help during my employment as a PhD student.

Delft Hydraulics is acknowledged for making available their Haake viscometer. The suggestions of ir. Han Winterwerp and ir. John Cornelisse of Delft Hydraulics are highly appreciated.

However, most of all I would like to thank dr.ir. Cees Kranenburg who provided continuous guidance, valuable comments and highly appreciated constructive criticism throughout this research project.

Contents

Chapter 1

Introduction

The interest in the complex behaviour of cohesive sediments has increased considerably during the last decades, for these sediments are becoming more and more a menace to human activities and the environment. Mud, for instance, once was a fertile medium for all kinds of flora forming an habitat for various life forms or a fertile layer which was left behind on the arable land after a flooding. Today, in industrialised countries mud usually contains large amounts of various contaminants, such as pesticides and heavy metals and consequently forming a hazard to various life forms, including man. Furthermore, the continuous accumulation of mud in harbours or channels may become a hindrance to navigation. The costs involved in the removal and disposal of these unwanted mud accumulations are very high.

Consequently, authorities all over the world are searching for measures that could be taken to decrease the undesired accumulation of mud. As a result, various research projects are initiated to study the complex behaviour of mud under several hydraulic conditions; the erosion and deposition of mud by currents has been studied intensively and various empirical relationships were derived from the experimental results. These relationships were adopted in various mathematical models to simulate the transport of mud (Partheniades, 1984). The erosion of mud due to waves has also been studied by several researchers, for instance Maa & Mehta (1987). In some experiments a layer of fluid mud was formed which could be transported very easily by a current (Lindenberg et al., 1989).

However, the interaction between waves and current on the one hand and a cohesive bed on the other hand is hardly studied. In particular the mechanisms underlying the generation of a layer of fluid mud, the resulting near-bed turbulence structure and wave damping require further study. The flow-induced displacements and velocities in (fluid) mud, for instance, have usually been studied making (visual) measurements at a sidewall of an experimental set-up (Maa, 1986; Cornelisse, 1993; Feng, 1993). These measurements may be incorrect because of a thick boundary layer at the sidewall. Furthermore, the available data on flow-induced (pore) pressures in the bed, which play an important role in the generation of fluid mud, are inaccurate because of the inaccuracy and drift of the pressure gauges used (Maa, 1986; Feng, 1992). Therefore, a research project was started on the erosion and liquefaction of mud due to waves and current in the Hydromechanics Laboratory some four years ago. Prior to this date, hardly any experimental experience with mud was present in this laboratory. An existing flume was adapted for the experimental study on the influence of waves on the liquefaction process and the influence of both waves and current on the transport and erosion processes of mud. During this study, among other things, pore pressures and velocities in the bed, and wave heights were accurately measured when waves and/or current were present in the flume. Furthermore, turbulence intensities over a non-liquefied and liquefied bed were determined for stationary flow.

In the present report three experiments on an artificial clay called China Clay are discussed. The characterisation of the sediment used in the experiments is discussed in chapter 2. The experimental set-up, procedures and results of the first experiment are presented in chapter 3. The results of the second and third experiment are discussed in chapters 4 and 5, respectively. This report is concluded by summarizing the main results of the experiments on China Clay (chapter 6).

Chapter 2

Characterisation of the artificial clays

The sediment used in this series of experiments was an artificial clay called China Clay. It is a dry, white powder packed in sacs with a content of 25 kg and it is designed as a general purpose anti-caking agent for the fertilizer industry. Altogether three experiments were carried out on this sediment. However, the sediment used in the third experiment was from a different lot than the China Clay used in the first two experiments.

A clay sample was taken at random prior to every experiment. This sample was analyzed by Delft Geotechnics and by the X-ray Laboratory of the Department of Mining and Petrol Engineering (D.U.T.) in order to determine several physical and chemical parameters. A brief description of the experimental procedures used to determine these parameters and the results of these analyses will be given in the next sections. The results will be compared with the specifications as given by the supplier Johnson Matthey B.V., Colour and Print Division, Maastricht, The Netherlands. This company was called Blythe Colours B.V. before March 1992. The clay used can be ordered under product code RM 225, Kaolin gty powder.

2.1 The bulk density

An outline of a so-called pycnometer is shown in figure 2.1.1. Such an instrument has been used by Delft Geotechnics to determine the bulk density of the China Clay. The following procedure has been used to determine the density of the clay sample.

First the weight of the empty pycnometer M_{pyc} and the weight of the pycnometer completely filled with hexane $M_{pyc+hex}$ are determined. The temperature of the hexane (C_6H_{14}) during the complete procedure is 20°C and the accompanying density ρ_{hex} is 0.6599 g·cm^{-3}. Then clay (mass M_{clay}) is put into the pycnometer and hexane is added until the pycnometer is completely filled. Finally the filled pycnometer is weighed (M_{filled}). Now the density of the clay can be calculated using

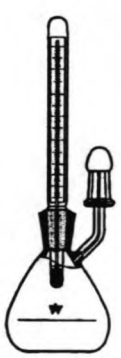

Figure 2.1.1 *Pycnometer.*

$$\rho_{clay} = \frac{M_{clay}\,\rho_{hex}}{M_{pyk+hex} + M_{clay} + M_{filled}}. \qquad (2.1.1)$$

The measurements showed that the average density of the China Clay used in the first two experiments was 2.593 ± 0.001 kg·m^{-3}. The average density of the China Clay used in the third experiment was 2.622 ± 0.001 kg·m^{-3}.

2.2 The particle size distribution

The particle size distribution of the China Clay was also determined by Delft Geotechnics using the Micromeritics Sedigraph 5000 D, serial 8641027 600 VA. The principle of operation of the Sedigraph is based on Stokes' settling law for spherical particles; a sample cell is filled with a homogeneous suspension (concentration C_0) of particles in a liquid (density ρ_0, viscosity η), then at time t=0 the particles are allowed to settle. After a time interval t a particle of diameter D has settled a distance h given by Stokes' law,

$$D = \sqrt{\frac{18\eta h}{(\rho - \rho_0)gt}} \tag{2.2.1}$$

where ρ is the density of the particle. Consequently, after a given time t_i all particles larger than the corresponding diameter D_i will have settled over a distance greater than h_i. By determining the concentration in the sample cell as a function of time and height a distribution of particle size in terms of equivalent spherical diameter can be calculated. The concentration in the cell is determined by measuring the transmittance of a finely collimated beam of X-rays. A detailed description of this instrument is given by Hendrix and Orr (1970). The sample was suspended in a peptising solution of 0.2 % sodium pyrophosphate in de-ionised water with a density of 0.996 g·cm^{-3}, a viscosity of 0.801 cp (1 cp ≡ 10^{-3} Pa·s) and a temperature of 30°C. The results are shown in figure 2.2.1.

Table 2.2.1 *Particle size specifications according to supplier.*

	cumulative mass percent
300 mesh residue	< 0.01
> 10 μm	15.00
< 2μm	43.00

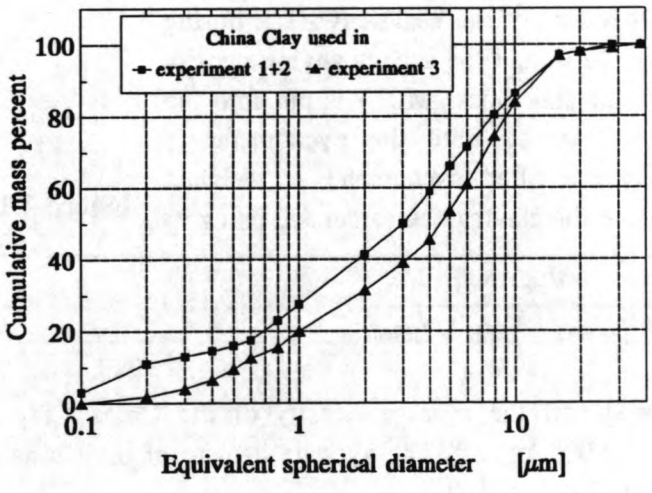

Figure 2.2.1 *Particle size distribution of China Clay used.*

The particle size distribution of the China Clay used in the first two experiments corresponds quite well with the specifications provided by the manufacturer (table 2.2.1). The China Clay used in the third experiment consisted of somewhat larger particles.

2.3 The specific surface area

The analytical determination of the specific surface area is based on the adsorption of a chemical substance onto the particles outer surface, or into the interlayer regions of the plate-like clay particles. At Delft Geotechnics Ethylene Glycol Monoethyl Ether (EGME) has been used as the adsorbing agent. To determine the specific surface area the clay sample is dried in a vacuum desiccator, in which P_2O_5 is used as desiccant. The sample was kept inside the desiccator until the mass of the sample did not decrease any more. For this sample it took about 162 hours before the mass was constant (W_0). Then approximately 6 ml EGME was added to the sample. After 45 minutes the excess EGME was carefully removed and then the sample was put into a vacuum desiccator in which $CaCl_2$ was used as desiccant. Only the EGME which is not adsorbed to a particle will evaporate. The sample is put under vacuum until the mass of the sample and the adsorbed EGME has become constant. Then the sample is weighted again (W_t) and the specific surface area (Sa) is calculated according to Carter et al. (1965),

$$Sa = \frac{W_t - W_0}{0.000286 * W_0} \qquad [m^2 \cdot g^{-1}] \qquad (2.3.1)$$

The tests showed that the specific surface area of the China Clay used in the first two experiments was 29.9 ± 0.1 $m^2 \cdot g^{-1}$ and the specific surface area of the clay used in the third experiment 23.9 ± 0.1 $m^2 \cdot g^{-1}$, which does not agree at all with the specifications provided by the supplier (8 - 10 $m^2 \cdot g^{-1}$).

2.4 Chemical properties

Several chemical properties of the clay samples were determined by Delft Geotechnics, such as the Cation Exchange Capacity (C.E.C.) and the concentration of various cations.

In order to determine the C.E.C. the sample was treated with a surplus of sodium acetate. Then the treated sample was shaken with a solution of ammonia acetate. A flame technic was used to determine the atomic adsorption spectrum, with which the C.E.C. can be determined. It was found that the C.E.C. of the China Clay used in the first two experiments was 5.0 meq per 100 g dry substance and the C.E.C of the clay used in the third experiment was 3.3 meq per 100 g dry substance.

The concentration of cations was determined in the following way. The sample was shaken in a solution of sodium acetate and ethanol. This solution was used to determine the atomic adsorption spectrum using the flame technic. The results found are listed in table 2.4.1. This determination was only made on the China Clay used in the first two experiments.

Table 2.4.1 *Chemical properties of the China Clay used in the first two experiments as determined by Delft Geotechnics.*

cation	concentration [meq/100g]
magnesium (Mg)	3.4
calcium (Ca)	1.5
sodium (Na)	0.7
potassium (K)	0.3

2.5 Mineralogical and chemical composition

A Philips PW 1370 X-ray diffractometer was used to determine the mineralogical composition of the sample. The chemical composition of the sample was determined using a Philips PW 1400 X-ray spectrometer. These instruments are placed in the X-ray laboratory of the Department of Mining and Petrol Engineering. The sample was scanned for elements with a atomic number larger than 12 (magnesium). It was found that the main elements within the China Clay used in the three experiments were silicon and aluminium. Potassium was also present, however in smaller quantities. Furthermore, traces of Zr, Sr, Rb and Fe were detected.

A quantitative analysis of the sample was performed by preparing a glass pearl (0.5 g sample + 5.0 g $Li_2B_4O_7$). This pearl was analyzed using the Philips PW 1400 and the results found for the China Clay used in the first two experiments are listed in table 2.5.1. The estimated standard deviation of the measurements is ± 2%. The specifications provided by the manufacturer are also printed in table 2.5.1. The accuracy of these specifications is unknown. A more extensive test was carried on the China Clay used in the third experiment. The results of this test are listed in table 2.5.2. The results agree quite well.

Table 2.5.1 *Chemical composition of the China Clay used in the first two experiments.*

substance	mass percentage according to supplier	mass percentage determined by X-ray Laboratory
SiO_2	46.88	48.9
Al_2O_3	37.65	33.2
K_2O	1.60	3.72
Fe_2O_3	0.88	0.74
MgO	0.13	0.25
CaO	0.03	0.08
TiO_2	0.09	0.07
Loss On Ignition (LOI)	12.45	12.6

Table 2.5.2 *Mineralogical composition of the China Clay used in the third experiment.*

Substance	percentage by weight	standard deviation	Substance	percentage by weight	standard deviation
SiO_2	53.0	0.2	CaO	0.077	0.006
Al_2O_3	31.7	0.2	TiO_2	0.043	0.005
K_2O	3.5	0.09	Rb_2O	0.036	0.003
Fe_2O_3	0.88	0.04	SO_3	0.029	0.01
Na_2O	0.34	0.2	MnO	0.021	0.003
MgO	0.20	0.06	ZrO_2	0.011	0.004
P_2O_5	0.13	0.02	In_2O_3	0.011	0.04
LOI	9.94				

The qualitative analysis made with the X-ray diffractometer showed that the samples mainly consisted of kaolinite. Furthermore, traces of muscovite or illite, α-quarts and microcline were detected. The specifications according to the supplier are printed in table 2.5.3.

Table 2.5.3 *Mineralogical composition according to supplier. (analysis by X-ray diffraction)*

mineral	percentage by weight
kaolinite	85
mica	15
feldspar	trace
quartz	trace

Chapter 3

The pilot experiment on China Clay

Around the first half of 1991 actual preparations were made for the first experiment in a series of experiments on China Clay (pilot experiment). In this chapter a complete description will be given of the experimental set-up (section 3.1), the preparation of the bed (3.2), the experimental procedure and program (3.3). In section 3.4 the experimental results will be discussed and finally the main conclusions which can be drawn from the results will be summarized in section 3.5.

3.1 Experimental set-up

In the Hydromechanics Laboratory of the Delft University of Technology an existing flume, the so-called "sediment transport flume", was adapted for the research on cohesive sediments. The flume has been made up of several segments and the total length is approximately 40 m, see figure 3.1.1. A side and sectional view of a mid-flume segment are shown in figure 3.1.2. The sidewalls are made of glass, which enables making visual observations during an experiment. The end segments are completely made of steel and the outlines of these segments are shown in figure 3.1.3 and figure 3.1.4.

This flume was modified in order to study experimentally the behaviour of cohesive sediments under waves and current. A recirculation pipe was installed below the flume, figure 3.1.5, to be able to generate a steady current. At the downstream end the fluid is withdrawn from the flume. In the end segment of the flume wooden plates were fixed in such a way that the accumulation of mud was prevented. Subsequently the fluid passes an electromagnetic flowmeter (FOXBORO 8004-WCR) and a centrifugal pump (STORK SUH 25-25, serial no. K806015) before it reenters the flume. See for further information about the electromagnetic flowmeter De Wit (1992b). The capacity of the centrifugal pump at 975 rpm is 6 m^3 per minute and the head is 3.4 m. The entire interior of the pump, including the fan, were made of cast iron.

The fluid reenters the flume via a smooth wooden duct which is installed just below the mechanical wave generator. The duct is 0.20 m high and approximately 4 m long. The wood used was 18 mm thick, so-called "Betonplex, berken door en door". The upstream, circular (∅ 22 cm) cross-section of the duct smoothly evolves to a rectangular (0.20 × 0.80 m^2) cross-section at the downstream side. The mechanical wave generator, which was designed and built in the Hydromechanics Laboratory, is only capable of generating regular waves. The wave paddle is sinusoidally translated using a Scotch Yoke construction. During the translation the wave paddle is also able to undergo a rotation. The period of oscillation, the amplitudes of translation and the rotation are variable. See the original design drawings (DCW, 1973) for further mechanical specifications. In order to smoothen the wave form and to dampen possible wave reflections a bundle of 32 small-mesh wire-netting sheets (mesh size 5 × 5 mm^2) is installed approximately 1 m downstream of the wave paddle. At the other side of the paddle a stack of plastic corrugated plates (centre to centre: 7.5 cm, depth of corrugations: 1.0 cm) was fitted to prevent the generation of standing waves in this part of

the flume.The corrugated plates (length: 80 cm, width: 50 cm) were made of a synthetic material. The height of the stack was approximately 50 cm.

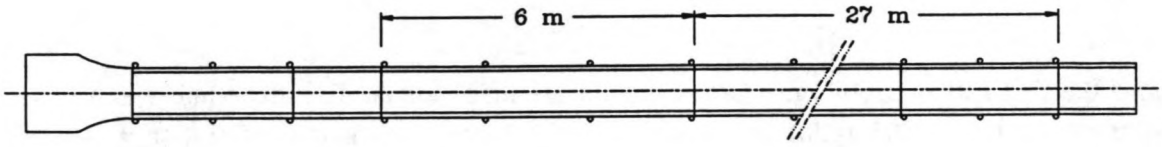

Figure 3.1.1 *Top view of the experimental set-up.*

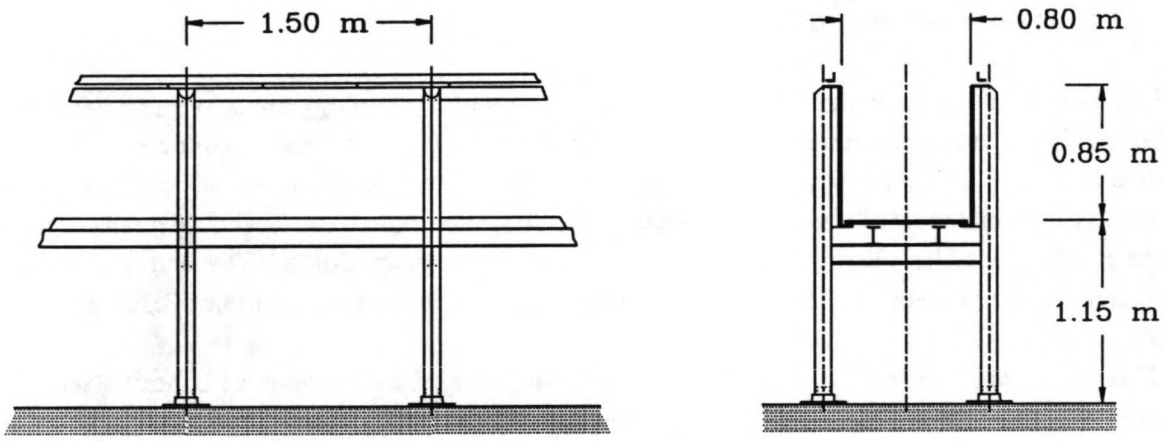

Figure 3.1.2 *Side and sectional view of a flume segment.*

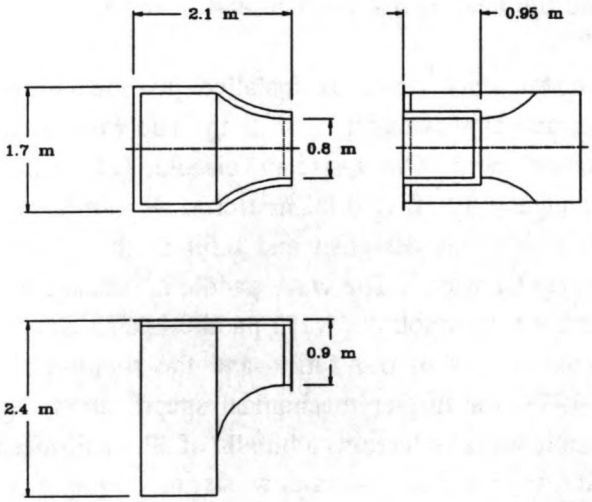

Figure 3.1.3 *Views of the upstream end of the flume.*

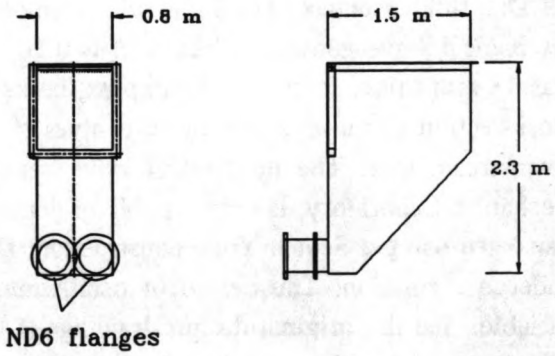

Figure 3.1.4 *Views of the downstream end of the flume.*

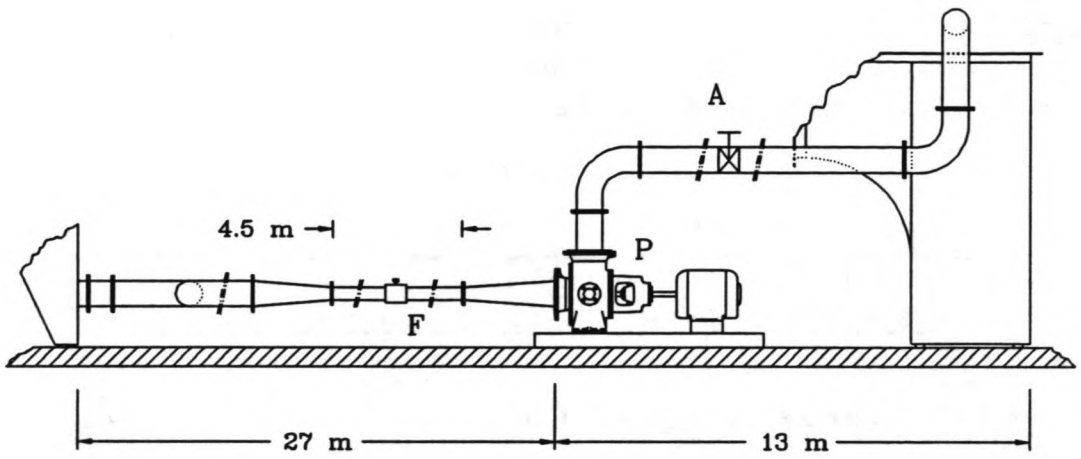

Figure 3.1.5 *Recirculation pipe below the flume.*
(F : flow meter, P : pump, A : valve)

At the other end of the flume a wave damper was installed to reduce wave reflection. The wave damper was constructed of three plates of Betonplex which were installed in such a way that the waves were dampened and a possible current would not be hindered by the construction. An outline of the wave damper is shown in figure 3.1.6.

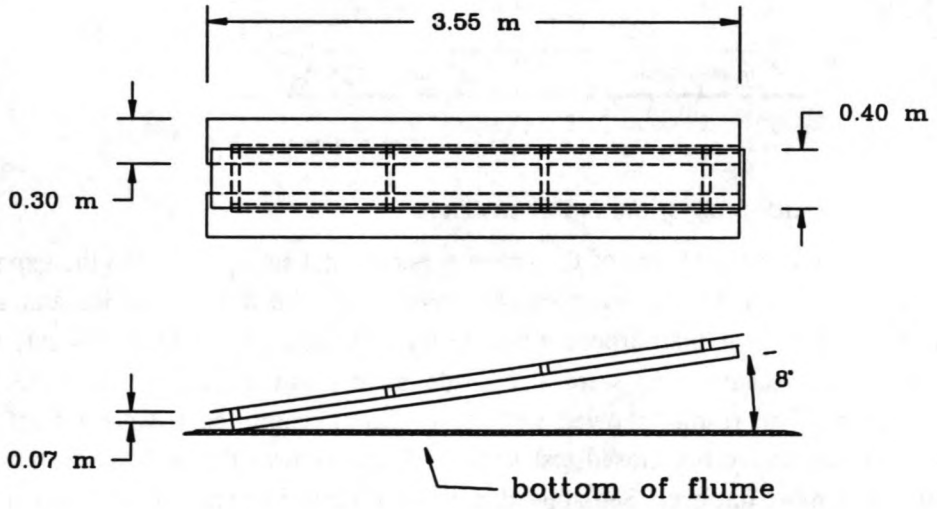

Figure 3.1.6 *Top and side view of the wave damper used.*

A false bottom was built to hold the sediment in a 14 m long test section, forming a trench with side slopes of 1:15 and a depth of 0.20 m. This configuration was chosen because a flow will always be parallel to the bottom whether the test section is filled entirely or not. In both the upstream and downstream direction the false bottom was kept horizontal over an interval of 5 m, measured from the ends of the test section. An outline of the configuration of the test section and other parts of the cement false-bottom are shown in figure 3.1.7. The upper part of the false bottom was made of cement, except for an approximately 2 cm wide band along the glass sidewalls. Directly to the glass wall a small piece of foam was installed, which was glued to a Betonplex lath. The foam was

necessary because otherwise the glass side walls would burst owing to expansion of the wood caused by adsorption of water. The lath was fixed in such away that it could be used as a gauge when the cement upper layer was fixed; a scraper, guided by the lathes, was used to form the ultimate upper cement layer. Ordinary sand is used as filling material.

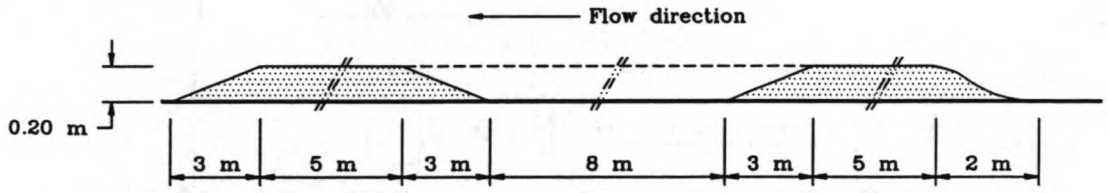

Figure 3.1.7 *Side view of the false bottom.*

The fluid which left the duct and reentered the flume was led via a streamlined wedge-shaped part of the false bottom into the flume. Waves generated by the wave generator and progressing over the wooden duct were disturbed and reflected due to the instantaneous increase of the water depth at the end of the duct, see figure 3.1.8. In order to reduce this disturbance as much as possible, the top of the wooden duct was enlarged in the downstream direction, dashed line in figure 3.1.8. The total enlargement was empirically determined in such a way that the disturbances of both the current and the progressive waves were as small as possible.

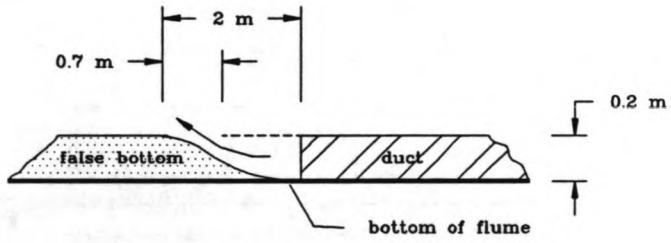

Figure 3.1.8 *Side view of the inflow structure.*

In figure 3.1.9 an outline is shown of the entire experimental set-up. Prior to the experiments on China Clay, tests were carried out to measure the wave decay, the wave reflection and the velocity distribution in the flume. For this purpose a temporary false bottom, made of cement, was placed over the test section. Measurements were also made in this configuration when both waves and current were present. The results showed that there was no significant wave reflection and no significant wave decay above the closed test section. Furthermore, the velocity distribution for a steady current was almost uniform. See appendix A for further information on these tests and the results.

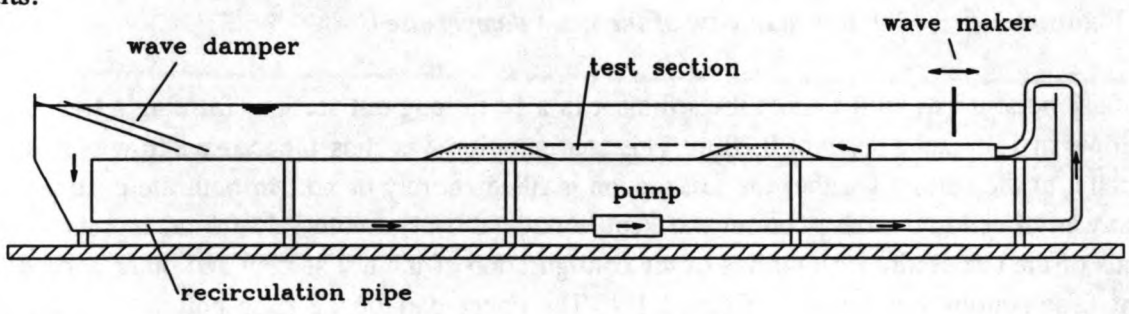

Figure 3.1.9 *Sketch of the complete experimental set-up.*

3.2 Preparation of the bed

The China Clay is provided as a dry, white powder. The powder was mixed with tap water in which sodium chloride is dissolved (salinity 5 ‰). The salt was added to increase the flocculation of the kaolinite and to eliminate the possible influence of small quantities of other chemicals on the characteristics of the China Clay, as for instance the settling velocity. According to Van Leussen (1988) the settling velocity of kaolinite is maximal for chloride concentrations ranging from 2 to 18 ‰. As soon as the China Clay is mixed with water several processes will be initiated, e.g. some material of the China Clay will be dissolved and diffuse double layers will be formed around a clay particle (Van Olphen, 1977). However, at a certain moment an equilibrium condition of the suspension will be established. The physical properties of such a suspension are strongly depended on the state in which the suspension is. As long as no equilibrium condition is reached the physical properties of the suspension will not be constant. In order to get reproducible measurements it is therefore very important to mix the China Clay long enough. Several researchers have used various kinds of China Clay and they all used different mixing times. Maa (1986), for instance, used an arbitrarily mixing period of one month.

As the consolidation characteristics of a suspension depend, among other things, on the chemical conditions of the suspension, it was tried to determine the minimal mixing period of China Clay from consolidation tests. For that purpose a series of consolidation tests were initiated in the physico-chemical laboratory, which is situated within the Hydromechanics Laboratory.

A China Clay suspension with a concentration of 275 $kg \cdot m^{-3}$ and a salinity of 5 ‰ was mixed daily for c. 2 hours using a propeller-like mixing device. The suspension was in a container with a content of 15 dm^3. In order to reduce the evaporation of the water, the container was closed when the suspension was not mixed. A sample was taken approximately every fourth day from this container and put into a glass graduated measuring cylinder with a volume of 1 dm^3 and a diameter of about 5.9 cm. The initial height h_0 of the suspension was about 36.60 ± 0.05 cm. Another sample was taken in order to determine the exact concentration of the suspension. Then the suspension was allowed to consolidate. The tests were carried out in a temperature controlled room in which the temperature was set at 21.5 °C. After a few moments an interface became visible and the position of the interface h as a function of time was monitored. As soon as the position of the interface did not change any more the height of the final mud layer was measured and a concentration profile was

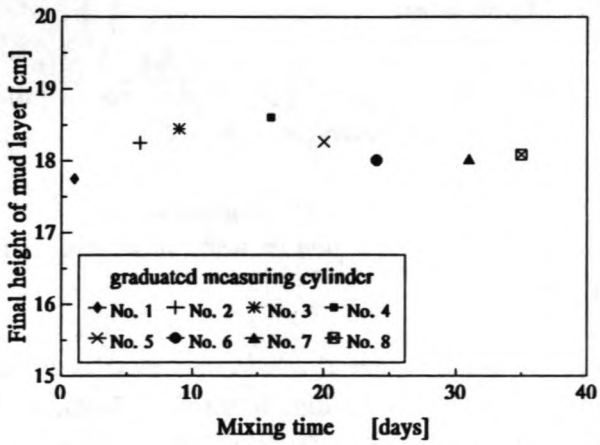

Figure 3.2.1 *Final height of completely consolidated mud layer as a function of the mixing time of the initial suspension.*

measured using a conductivity probe. See De Wit (1992b) for more information on this probe. The results of these tests are shown in figure 3.2.1. This graph shows the final height of the consolidated mud layer as a function of the mixing time. The thickness of the consolidated mud layer increases when the mixing time is increased until an apparent maximum is reached. Then it decreases again until the height of the consolidated mud layer is fairly constant after a mixing period of about 24 days.

The monitored position of the water-mud interface as a function of time of some of the measuring cylinders are shown in figure 3.2.2. It can be seen that the position of interface of the measuring cylinder no. 1 is initially changing vary fast compared to the other measuring cylinders. However, they are all fully consolidated after approximately 200 hours.

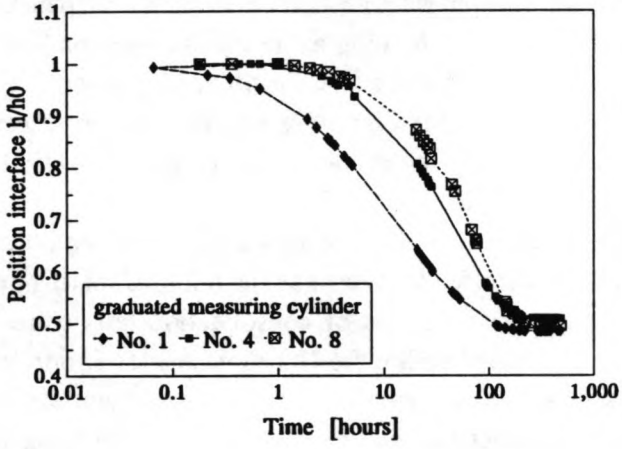

Figure 3.2.2 *The position of the water-mud interface during consolidation.*

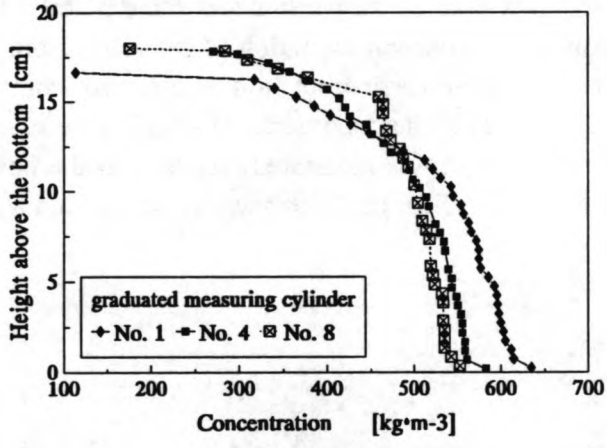

Figure 3.2.3 *Concentration profiles after consolidation.*
(The uppermost data points were measured below the water-mud interface.)

Using the conductivity probe, the concentration was measured as a function of the height above the bottom of the cylinder (figure 3.2.3). According to the specifications of this device the accuracy is estimated at 10 % of the local concentration (De Wit, 1992b). These concentration profiles were used to verify the accuracy of the probe. The total dry weight of the clay in a measuring cylinder was determined using the measured concentration and the amount of initial suspension. The total dry

weight of clay was also calculated from the results found using the conductivity probe. The apparent accuracy for China Clay was better, namely 6 % of the local concentration.

The conclusion drawn from these results was that the China Clay had to be mixed for at least 3 weeks before an equilibrium suspension was formed.

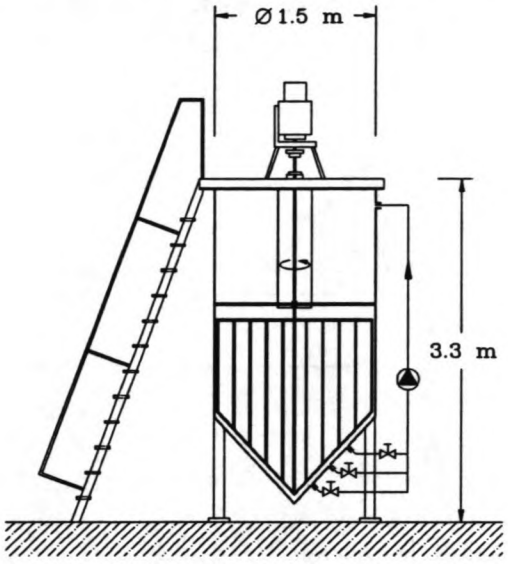

Figure 3.2.4 *Outline of the mixing tank.*

The results of these consolidation tests were used to estimate how much clay was needed to completely fill the test section with a deposited bed from a China Clay suspension with a concentration of c. 275 $kg \cdot m^{-3}$. It was found that about 4.5 m^3 of such a suspension was necessary to fill the test section. In order to mix such a large quantity of mud a bulk mixing device was built. An outline of the device is shown in figure 3.2.4. It is a large tank in which a revolving grid was installed. An electric motor (380 V, 3 kW, 50 Hz) was used to rotate the grid at a speed of approximately 32 rpm. Three outlets (∅ 4.5 cm) were installed in the lower part of the tank. Through these outlets fluid was withdrawn from the tank using a Delta sludger (type: FFC 3-218-2 AX) with a capacity of 15 m^3 per hour at a head of 3.5 m. The fluid reentered at the top of the tank. A riser pipe was installed to monitor the actual amount of fluid in the tank. The top of the tank was closed, except for a small hatch, in order to prevent the escape of China Clay dust when the tank was filled. The content of the tank was approximately 4.0 m^3. Consequently, an insufficient amount of suspension could be mixed in one time to fill the test section, so that it had to be mixed in two parts. The exact procedure of filling the test section is discussed later.

The mixing procedure of the China Clay was as follows. First tap water was put into the mixing tank, then sodium chloride was dissolved until the salinity of the solution was 5 ‰. Finally the dry China Clay powder was added and the circulation pump was started. During the whole procedure the grid inside was continuously revolving. The suspension was kept inside the tank for 14 days. During this period the grid was continuously revolving except for the week-ends. The sludger was only running during office-hours.

At the end of the mixing period the test section was separated from the rest of the flume by installing two boards in the cross-section of the flume at both ends of the test section. The entire content of the mixing tank was pumped to the separated test section using the Delta sludger. The remaining part of the flume was filled with tap water in order to decrease the leakage of mud out of the test section. The tank was filled again with China Clay and saline tap water and this suspension

was mixed for 21 days. In the meanwhile the suspension in the test section was prevented from consolidating by using a mixer (Premier, type: Pioneer 26600). The velocity of rotation of the stirring rod was made adjustable using a Danfoss variable speed drive (VLT, type 3002). The mixer, see figure 3.2.5, was installed on a remote-controlled measuring carriage which runs automatically back and forth above the test section along a rail mounted on top of the flume. The position of the mixing rod relative to the bottom and the side walls was varied during the mixing period.

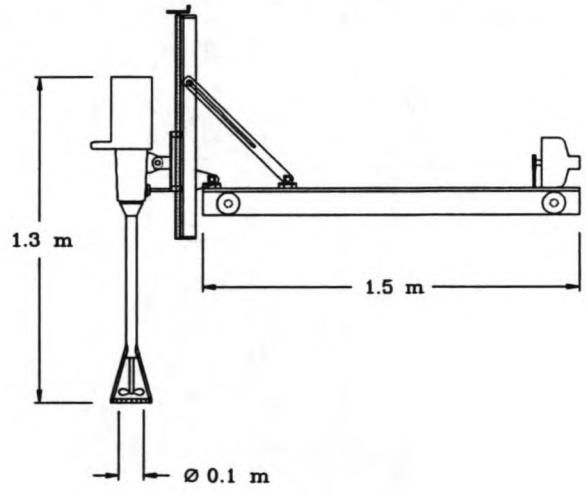

Figure 3.2.5 *Mixing device mounted on the measuring carriage.*

After 21 days the content of the mixing tank was added to the suspension in the test section. The mixing was continued for a few hours to be sure that a thoroughly mixed suspension was formed. As soon as the mixing had stopped one pore-pressure transducer was positioned at 15 cm above the bottom of the flume in the middle of the test section. See De Wit (1992b) for further details about this pore-pressure transducer. Then the suspension was allowed to consolidate.

Only a few minutes after the mixing had stopped an interface was formed between the mud and the clear water. At the surface of the water-mud interface small craters were formed through which the water was pressed out of the mud. After approximately one week, cracks became visible on the mud surface, especially near the walls.

After a consolidation period of about 14 days the bed thickness in the middle of the test section was about 21 cm. Due to the through-shaped test section the surface of the bed was not horizontal, but it had a concave shape as is shown in figure 3.2.6. In order to get a horizontal bed the surplus of mud was carefully removed using a scraper. The tap-water in the rest of the flume was replaced by tap water in which sodium chloride was dissolved (salinity 5‰). The solution was also mixed in the mixing tank. The two plates which separated the test section from the rest of the flume were carefully removed as soon as the water levels in both parts of the flume had become equal. The water depth above the 20 cm height false bottom was 30 cm when the filling had been completed.

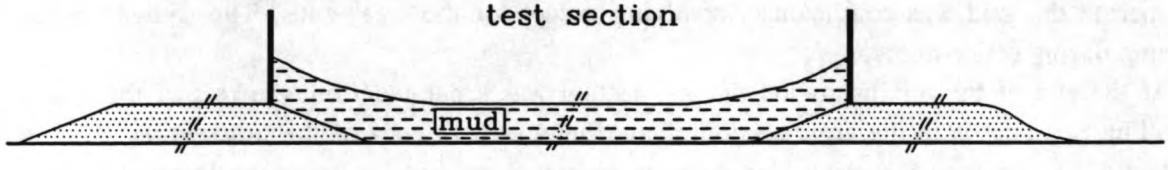

Figure 3.2.6 *Schematic presentation of the bed after consolidation.*

During the consolidation period it was observed that all kinds of organisms, such as unicellular organisms, bacteria, algae and fungi, found a perfect matrix in the wooden parts of the interior of the flume. Large populations of organisms were found especially on those places were the brown surface coating of the Betonplex was damaged or completely absent. Additional tests also showed that a small amount of the brown coating dissolved, which resulted in a light brown colour of the water.

3.3 Experimental procedure and program

Prior to and during the consolidation process of the mud several instruments were installed. First of all a pore-pressure transducer (Druck PDCR81, range 150 mbar) was fixed 15 cm above the bottom of the flume in the middle of the test section. A detailed description of this instrument is given by De Wit (1992b). The transducer was clamped in a custom-made PVC holder. A drawing of this holder is shown in figure 3.3.1. The holder was screwed on top of a stainless steel rod (diameter 5 mm). The latter was mounted on a bracket, which was fixed in the mud suspension as soon as the mixing was stopped.

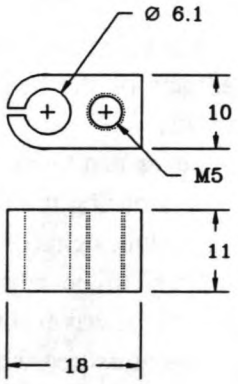

Figure 3.3.1 *Top and side views of the PVC holder which was used to position the pore-pressure transducer (dimensions in mm).*

Furthermore, 6 wave height meters (WHM), 3 electromagnetic current meters (ECM) and 3 optical suspended-sediment concentration meters (OCM) were installed in the centre-line of the flume. The electromagnetic current meters used are able to measure the velocity components in the longitudinal as well as in the transverse direction. However, in this experiment only the velocity components in longitudinal direction were measured, because the preliminary measurements made over a false bottom showed that the velocity component was almost zero in the transverse direction (appendix A). The optical concentration meters were used in combination with a peristaltic pump (Velp Scientifica SP311/60) which continuously withdrew and returned fluid (flow rate c. 7 $cm^3 \cdot s^{-1}$) from and into the flume via stainless steel tubes. These tubes are installed perpendicularly to the direction of the flow (transverse suction). The instruments were all fixed at gauging-rods, which made it possible to alter the vertical measuring position during the experiment. The locations of these instruments during the experiment is shown in figure 3.3.2. See De Wit (1992b) for further information about these instruments.

The measurements were logged on the hard disk of a personal computer using the DACON data-

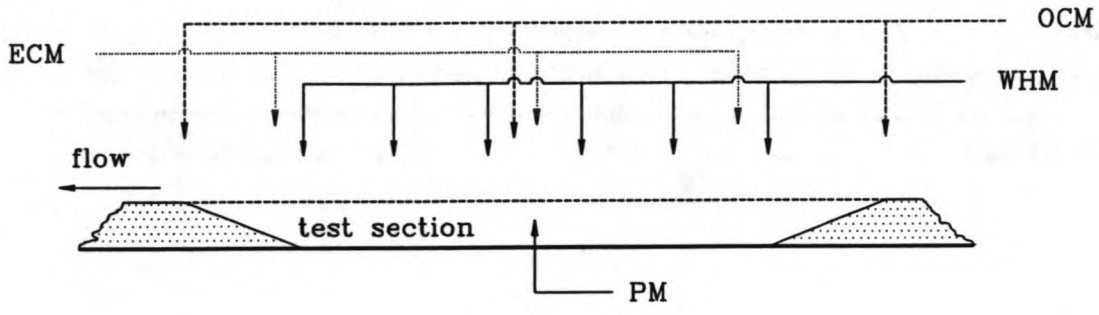

Figure 3.3.2 *Positions of the instruments.*
WHM: wave height meter, OCM: optical concentration meter,
ECM: electromagnetic current meter, PM: pressure meter.

acquisition software (ver. 1.2) designed for the Data Acquisition Processor DAP 2400 and the Simultaneous Sampling Board of Microstar Laboratories. The resolution of the processor is 12 bits (signed) for input voltages ranging from c. -10 V to c. 10 V and maximal 16 input signals can be logged simultaneously. The signals are logged in realtime as two's complement binary data. See Dacon (1990a, 1990b) for further information.

Video recordings were made during the tests using two recording units. One stationary camera was used to record a small part of the upper part of the bed. The other camera was used to make recordings at several locations during the tests.

Prior to the experiment several measurements had to be made. The wave height meters had to be calibrated on every range which could be used during the experiment. See for a correct calibration procedure De Wit (1992b). Furthermore, the output signal of the electromagnetic current meter, when it was immersed in the quiescent water, had to be adjusted to zero. In order to correct the measurements to be made for the zero-flow drift it was recommended to log this signal also (See De Wit, 1992b). The maximal concentration to be measured with the optical concentration meter had to be set, after the output voltage was set to zero when clear water was pumped through the sensor. Finally, concentration profiles of the consolidated bed were measured at several locations using a conductivity probe. See appendix B for additional information on the instruments used.

After the preliminary measurements were made, the actual pilot experiment was started at June 11th, 1991. The pilot experiment comprised 7 tests.

In the first test it was tried to determine the critical erosion velocity of the mud bed by increasing the flow rate until the onset of erosion was determined. During these tests no waves were present in the flume.

The subsequent tests were started with the generation of waves with a constant wave height for approximately half an hour. The wave period was set at 1.5 s. Then the pump was started and a steady current was generated. The flow rate was set at approximately 12 $dm^3 \cdot s^{-1}$ which corresponds with an average velocity of 5 $cm \cdot s^{-1}$ in the flume. After about 5 minutes the flow rate was increased until the average velocity in the flume was c. 10 $cm \cdot s^{-1}$. This procedure was repeated until the maximal average velocity in flume was reached (22.5 $cm \cdot s^{-1}$). Then the average velocity in the flume was carefully reduced to zero. Subsequently the wave height was increased and the whole procedure was started again. The average wave heights were ranging from 15 to 93 mm. In figure 3.3.3 a schematical overview is shown of the average velocity in the flume as a function of time during such a test. The experimental program of the pilot experiment is summarized in table 3.3.1.

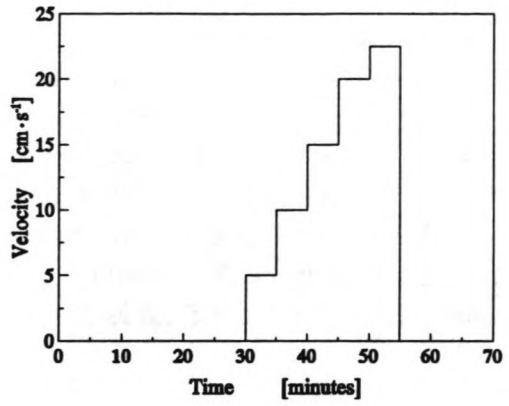

Figure 3.3.3 *Characteristic average flow velocity as a function of time.*

Table 3.3.1 *Experimental program of the pilot experiment (11 June 1991).*

test no.	details
1	* Determination of the critical erosion velocity of the mud bed.
2	* No net current. Generation of waves for half an hour; *average wave height 15 mm.* * Both waves and current. Flow rate increased step by step every five minutes (see fig 3.3.3).
3	* No net current. Generation of waves for half an hour; *average wave height 32 mm.* * Both waves and current. Flow rate increased step by step every five minutes (see fig 3.3.3).
4	* No net current. Generation of waves for half an hour; *average wave height 52 mm.* * Both waves and current. Flow rate increased step by step every five minutes (see fig 3.3.3).
5	* No net current. Generation of waves for half an hour; *average wave height 60 mm.* * Both waves and current. Flow rate increased step by step every five minutes (see fig 3.3.3).
6	* No net current. Generation of waves for half an hour; *average wave height 81 mm.* * Both waves and current. Flow rate increased step by step every five minutes (see fig 3.3.3).
7	* No net current. Generation of waves for half an hour; *average wave height 93 mm.* * Both waves and current. Flow rate increased step by step every five minutes (see fig 3.3.3).

3.4 Results

The results of the separate tests will be discussed in the next sections. The concentration profiles measured prior to the experiment will be presented in section 3.4.1. The results of the attempt to measure a critical erosion velocity of the mud are discussed in section 3.4.2, and finally the results of the wave/current tests are presented in section 3.4.3. For all of the results presented in this report t=0 is defined as the moment at which every test was started. If a test was started with the generation of waves, t=0 is defined as the moment at which the first waves reached the test section. If a test was started with the generation of a steady current, t=0 is defined as the moment at which the preselected flow rate was set.

3.4.1 Concentration measurements prior to the tests

Prior to the tests profiles in the bed were measured using a conductivity probe. These measurements were made at several locations in the test section.

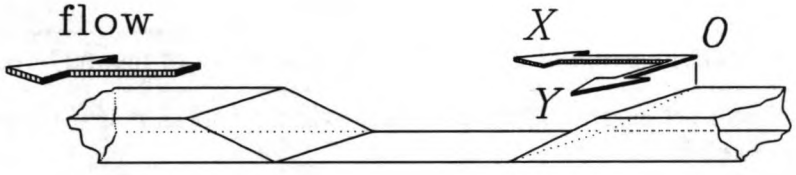

Figure 3.4.1 *Cartesian coordinate system used to pinpoint the measuring positions.*

Consider a cartesian coordinate system, the origin of which is at the upstream end of the through-shaped test section at the right-hand sidewall of the flume when looking in downstream direction, see figure 3.4.1. This coordinate system is used to pinpoint the exact position of every concentration measurement. The results of these measurements are shown in figures 3.4.2, and 3.4.3. It can be seen that the bed was not quite uniform; the variation in concentration in a cross-section is significant and the surface of the bed is not horizontal at all. The procedure which was pursued to fill the test section is probably the reason of these inhomogenities in the bed. Furthermore, the structure of the bed was disturbed because of the local removal of the surplus of China Clay on the slopes of the test section after the consolidation period.

The pH of the clear water in the flume was 8.4.

3.4.2 Determination of the critical erosion velocity (test 1)

In test 1 the average flow velocity was increase almost linearly in time. The average velocity measured at about 5.0 cm above the mud interface as a function of time is shown in figure 3.4.4. The height at which velocities and suspended sediments concentrations were measured was kept constant (5.0 cm above the initial mud interface) in all of the tests of the pilot experiment. At first a large amount of ferric oxide was pumped into the flume, shortly after the pump was turned on. The ferric oxide originated from the interior of the pump, which was made of cast iron. At a velocity of approximately 18 $cm \cdot s^{-1}$ the onset of erosion of the upper part of the bed was observed. However,

the erosion was very locally and only a very thin layer (< 0.5 mm) was eroded. This erosion did not develop further when the flow velocity was increased.

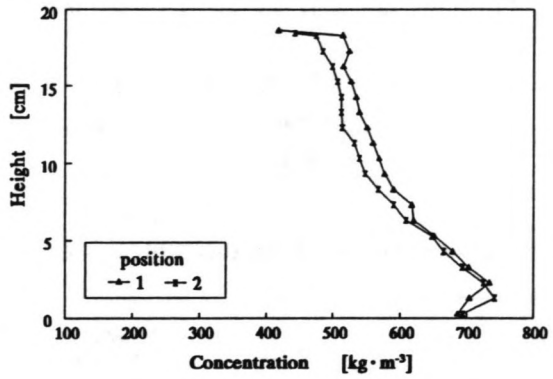

Figure 3.4.2 *Concentration profiles in the bed at x=4.25 m. (Position 1: y=0.2 m, position 2: y=0.6 m)*

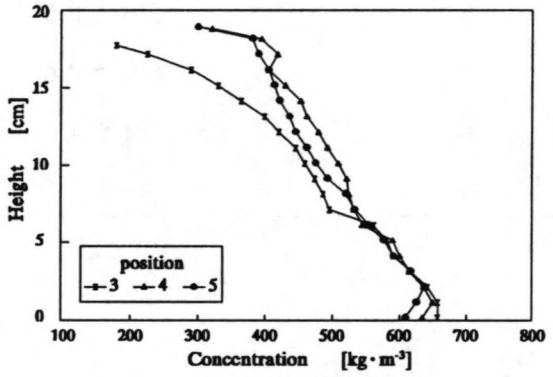

Figure 3.4.3 *Concentration profiles in the bed at x=9.40 m. (Position 3: y=0.20 m, position 4: y=0.40 m, position 5: y=0.60 m)*

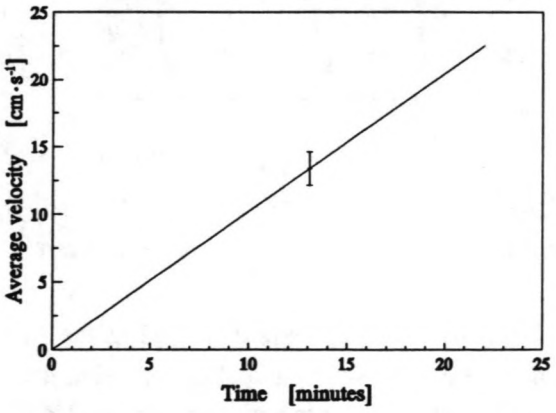

Figure 3.4.4 *Average velocity as a function of time measured at approximately 5 cm above the water-mud interface during test no. 1.*

3.4.3 Wave/current tests (2-7)

Waves were generated for the first time in test no. 2. When starting this test it was noticed that the only pore-pressure transducer used was defective. After half an hour the pump was started and then the average flow velocity was increased every five minutes. The wave height was increased in every test. The average wave height of the incoming waves during the various tests is shown in table 3.4.1. A representative wave profile is shown in figure 3.4.5.

Table 3.4.1 *Average wave height of the incoming waves during the tests.*

Test no.	Average wave height [mm]
2	15.0 ± 0.3
3	32.0 ± 0.3
4	52.0 ± 0.5
5	60.0 ± 0.6
6	81 ± 1
7	93 ± 2

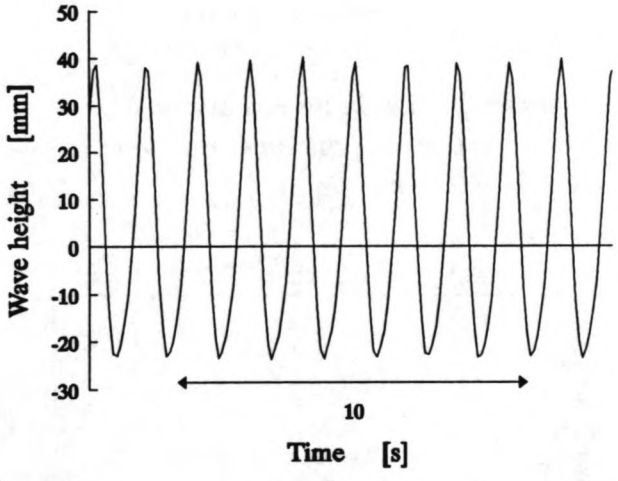

Figure 3.4.5 *Wave profile measured at x=6.04 m during test 5.*

In the tests 2, 3, 4 and 5 no visual changes were observed in the structure of the bed; not under wave action solely and not under combined wave/current action. Measurements showed that there was no significant decrease in wave height over the test section, figure 3.4.6. However, in test no. 6 the upper part of the bed started to liquefy locally. Visual observations, made at the sidewall of the flume, indicated a fluid-mud layer of about 0.5 cm thick. Internal waves were generated; the amplitude was about 0.2 cm. The damping of the waves became significant due to the increase in

dissipation of wave energy in the fluid-mud layer, which can be seen in figure 3.4.7. The damping of waves was also noticeable when both waves and current were present in the flume; the wave height of the incoming wave had decreased due to the current, and continued to decrease when travelling over the test section, see figure 3.4.7. As soon as a current was generated it looked as if the liquefaction process came to a halt and the fluid mud was transported very easily in the downstream direction. During this process hardly any fluid mud was entrained into the water layer.

Injections with a solution of potassium permanganate seemed to indicate that the turbulence intensities in the overlying water decreased when fluid mud was present.

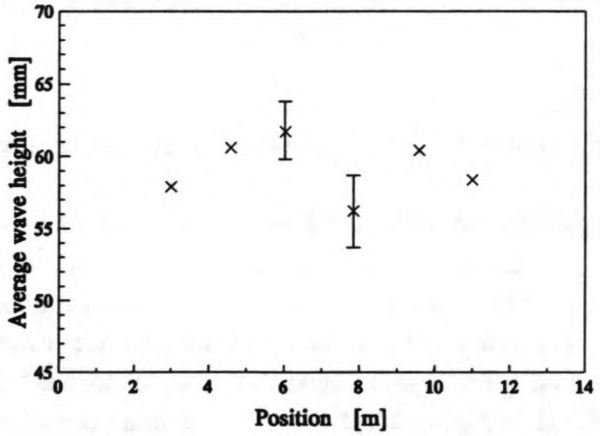

Figure 3.4.6 *One-minute averaged wave heights during test 5.*

Visual observations through the side walls of the flume gave the impression that a thick boundary layer was formed along the side wall when fluid mud was present; velocity amplitudes near the wall were much smaller than those observed near the centre-line of the flume.

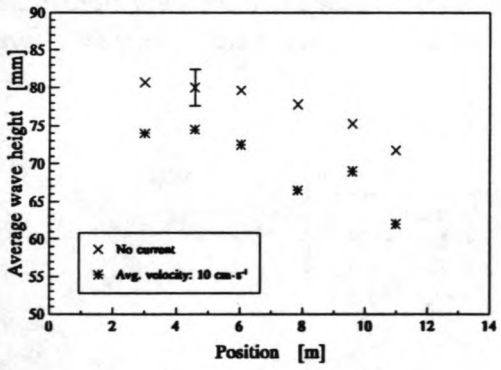

Figure 3.4.7 *One-minute averaged wave heights (test 6).*

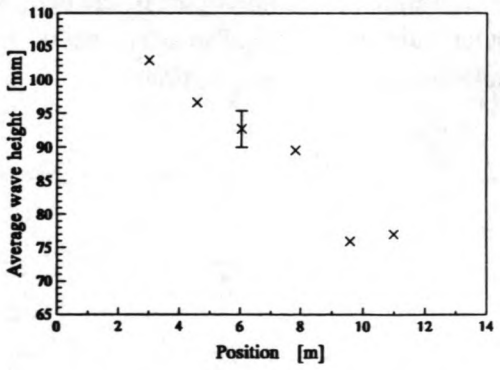

Figure 3.4.8 *One-minute averaged wave heights (test 7).*

These phenomena were also observed in test 7. Significant wave damping was measured, figure 3.4.8, and the generated fluid-mud was easily transported in the downstream direction by the current. However, in the end phase of test 7 the fluid mud became trapped in the through-shaped test section. The bed surface then slightly sloped upwards in the direction of the flow. Furthermore, a recirculation

zone was observed at the downstream end of the test section, which was probably initiated by the shearing caused by the stationary current. A sketch of this recirculation zone is shown in figure 3.4.9.

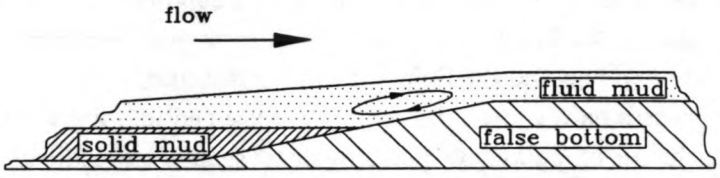

Figure 3.4.9 *Outline of the recirculation zone as observed in test 7. (side view)*

3.4.4 Suspended sediment concentration measurements during the tests

The optical concentration meter has to be adjusted before every experiment as already mentioned in section 3.3. An estimate of the maximal suspended sediment concentration which may occur in an experiment has to be made in order to make a proper adjustment of the instrument. Assuming that the entire bed would erode very easily, the maximal concentration was calculated and set. However, during the tests hardly any mud was suspended and the maximal suspended sediment concentration was considerably overestimated, which resulted in very inaccurate concentration measurements that will not be presented here.

3.4.5 Bed concentrations after the tests

The bed was allowed to consolidate for 13 days after these tests. Then some additional concentration profiles were measured. The results are shown in figure 3.4.10. Notice the relatively high concentration in the upper part of the bed, which is probably caused by the rapid consolidation of the former fluid-mud layer. The alignment of the plate-like particles due to the wave action may also have resulted in higher concentrations.

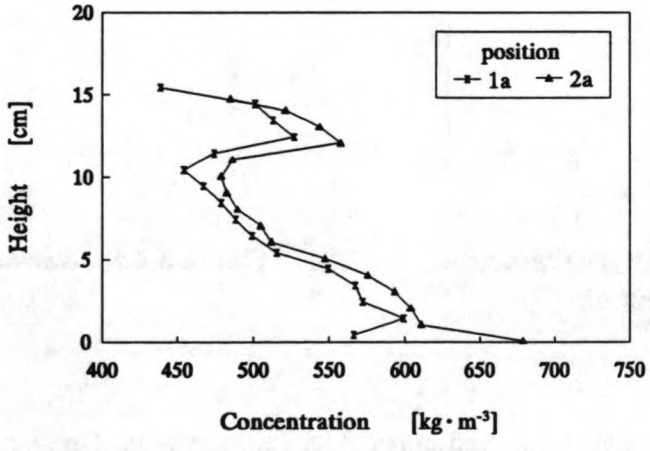

Figure 3.4.10 *Concentration profiles 13 days after the tests. (y: 0.40 m, position 1a: x=5.32 m, position 2a: x=10.02 m)*

3.5 Conclusions

The following conclusions may be drawn from the results of the pilot experiment.

- The so-called Betonplex was used to build parts of the interior of the experimental set-up. The coating of this material turned out to be partly dissolvable in water and an ideal matrix for all kind of organisms. It is known from the literature that the influence of organisms and small quantities of dissolved chemicals may have a large effect on the physical properties of the mud. Because the growth of organisms and the amount of dissolved material from the Betonplex cannot be controlled, the use of this material should be avoided as much as possible.

- After the pump was started a large amount of ferric oxide entered the flume. Due to the susceptibility of the mud to all kinds of chemicals, this pump should be replaced by a pump which has a non-rusting interior.

- The measured concentration profiles showed that the bed was not completely uniform. The preparation of the bed from one initial suspension, instead of two, should give better results.

- Fluid mud was generated if the wave height exceeded a threshold value.

- Significant wave damping was observed only when fluid mud was present in the flume.

- The fluid mud was easily transported by a current and hardly any mud was entrained into the water layer during this process.

- Visual observations gave the impression that a boundary layer was present along the glass side wall when fluid mud was present. Consequently, observations made through the side walls should be carefully interpreted.

- Injections with potassium permanganate seemed to indicate that turbulence intensities decrease when fluid mud was present. In order to get quantitative results about the turbulence intensities measurements should be made at different heights above the bed using the electromagnetic current meter.

- The shape of the test section was not well chosen. After the consolidation the bed surface is not horizontal and the excess mud has to be removed prior to the experiments. As a result the bed structure will be disturbed. Furthermore, the fluid mud will be trapped in the through shaped test section in a later phase of the experiments when some of the mud has been eroded. A recirculation zone in the fluid mud will be formed at the downstream end of the test section when a steady current is present in the flume. A better configuration of the test section may overcome all these problems.

- When the fluid mud was allowed to consolidate after the tests, it was observed that the concentration in the upper part of the consolidated bed was relatively high. This may be caused by the rapid consolidation of the layer of fluid mud. Furthermore, changes in the aggregate structure after liquefaction may also result in a higher concentration.

Chapter 4

The second experiment on China Clay

In the first experiment on China Clay several unexpected features of mud were observed. Furthermore, all kinds of practical experiences were gained. This newly obtained knowledge was used, among other things, to improve the configuration of the experimental set-up and to optimize the experimental procedure.

A detailed description of the improved experimental set-up is given in section 4.1. Section 4.2 is concerned with the experimental procedure and program for the second experiment on China Clay and in section 4.3 the experimental results are discussed and some conclusions are drawn. Finally, the conclusions are summarized in section 4.4.

4.1 The modified experimental set-up

The wooden parts of the interior of the flume were replaced in order to prevent the growth of all kinds of organisms. The wave damper and the complete duct below the wave generator were replaced by stainless steel duplicates. The wooden parts that were used to prevent the mud from settling in the downstream end of the flume, below the wave damper, were replaced by identical asbestos cement plates. The laths, which were used to build the false cement bottom, were removed and the gap was carefully filled up with cement and approximately 5 mm thick pieces of polystyrene which were fitted next to the glass sidewall. The wooden wave paddle mounted on the mechanical wave generator was replaced by a stainless steel one too. Furthermore, every corroded part of the flume was removed and provided with a non-corroding coating, including the interior of the pump. The cast iron fan was replaced by a bronze one and the interior of the pump was provided with a coating, called Epasfill, from Stork Standaard Pompen Nederland.

The geometry of the test section was drastically changed. The trough-shaped test section did not answer to the expectations; the surplus of mud on the slopes after the consolidation was troublesome and the mud could not leave the test section in a later phase of the experiment. Two design criteria should be met for the new test section. Firstly, the mud should not be hindered during the consolidation process, in order to obtain a homogeneous, horizontal bed without removing some local surplus of mud. Secondly, the flow has to be parallel to the bottom of the flume during the entire experiment, which means that no abrupt changes in the water depth should be formed during the experiment.

A configuration which meets these criteria is outlined in figure 4.1.1. This figure shows the upstream part of the new geometry. The slopes of the old test section were removed. Instead two metre long plates provided with hinges were installed. The position of the hinges is at x=0, according to the coordinate system defined in section 4.4.1. The plates are 1 cm thick and are made of asbestos cement. At the downstream end of the plate a plastic flexible skirt was fixed. An outline of this skirt is also shown in figure 4.1.1. The position of the downstream end of the plate is adjustable by means of two positioning rods. These rods are 2 mm thick stainless-steel bands, which are installed close

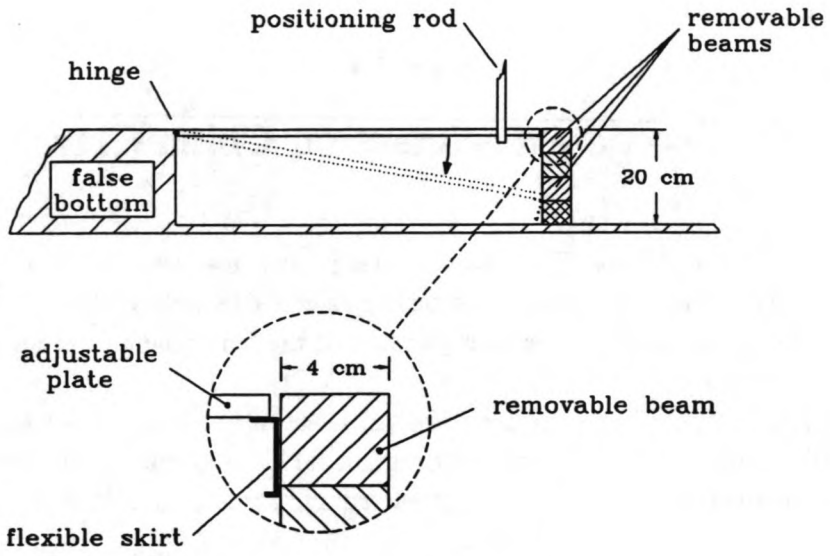

Figure 4.1.1 *Side view of the upstream part of the test section used in the second experiment on China Clay.*

to the sidewalls in order to reduce the disturbance of the flow as much as possible. The mud is kept inside the test section by means of 4 beams, of which 3 can be easily removed during an experiment through two bands (not shown in figure 4.1.1) which were fixed at either end of each beam. The beams are also made of stainless steel, except for the lowest, unremovable beam which is made of cement covered by plastic. The beams are 5 cm high and 4 cm wide. The downstream end of the test section is closed with an almost identical structure; only the hinges of the adjustable plate are fixed to the bottom of the flume. The removable beams in combination with the flexible skirt make it possible to continuously change the height of the endwalls of the test section, and should prevent the mud from being trapped in the test section in a later phase of an experiment. An overview of the entire geometry of the test section is shown in figure 4.1.2.

Having this geometry of the test section, a more convenient coordinate system has to be defined. Using the old coordinate system, the origin is translated in downstream direction to the bottom of the upstream end of the test section indicated as *O* in figure 4.1.2.

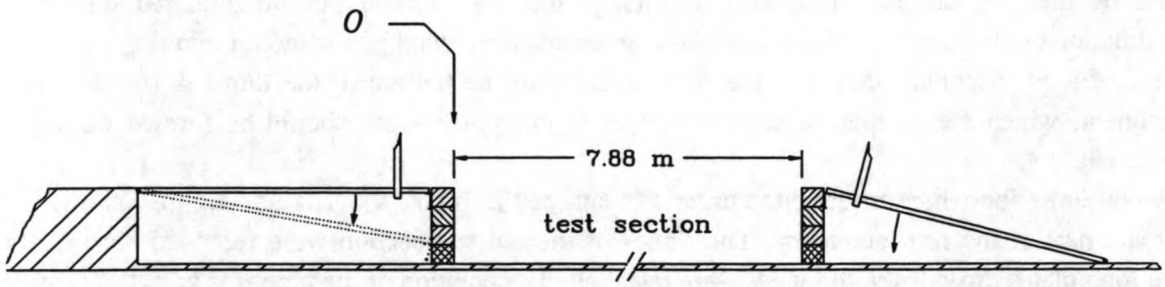

Figure 4.1.2 *Outline of the new geometry of the test section.*

4.2 Experimental procedure and program

The mixing tank was filled with 3.2 m^3 of tap water, then the grid was started to revolve and 16 kg of sodium chloride was carefully added. When the sodium chloride had dissolved, 880 kg of China Clay was added and this suspension was mixed for 3 weeks. The measured concentration of the suspension was 250 $kg \cdot m^{-3}$.

The test section was separated from the rest of the flume by two boards which were installed at both ends of the test section. The suspension was pumped from the mixing tank into the test section until the height of the suspension was 44.5 cm above the bottom of the flume. During the filling of the test section the rest of the flume was filled at the same time with tap water, keeping the fluid levels in and outside the test section almost equally. After the filling of the flume the suspension was mixed for approximately 30 minutes using the mixer installed on the measuring carriage. Then a frame containing four pressure transducers was lowered in the suspension and fixed to the flume. A sketch of this frame is given in the next section.

The mud started to consolidate as soon as the mixing was stopped and after only a few minutes an interface formed between the clear water and the mud. The position of this water-mud interface was monitored. On the mud surface small craters were formed and in a later phase of the consolidation process cracks became visible. The position of the interface in the middle of the test section is shown in figure 4.2.1 as a function of time.

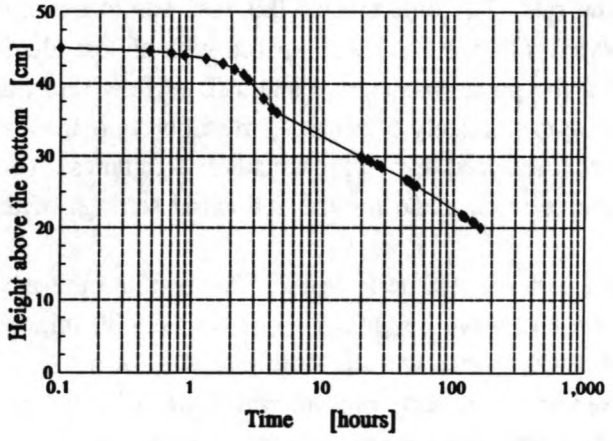

Figure 4.2.1 *Position of the water-mud interface during the consolidation period.*

As in the pilot experiment, 6 wave height meters, 3 electromagnetic current meters and 3 optical concentration meters were used in the second experiment on China Clay. See appendix C for more details on the exact location of the instruments. Only the velocity components in longitudinal direction (positive in the downstream direction) were measured. The procedure followed to calibrate and adjust these instruments was identical to the procedure described in section 3.3.

In this experiment three additional pressure meters were installed. The pressure transducers were mounted on a frame which was fixed in the test section after the test section was filled. The pressure transducers were fixed on several heights above the bottom of the flume. In figure 4.2.2 an outline of the frame and the exact locations of the pressure transducers are shown. Pressure transducer number 4 was used as a reference and the range of this pressure transducer was 350 mbar. The range

of the other pressure transducers was 75 mbar. The measurements were logged on a personal computer using the data-acquisition set. More details on the logging of the measurements are presented in appendix C.

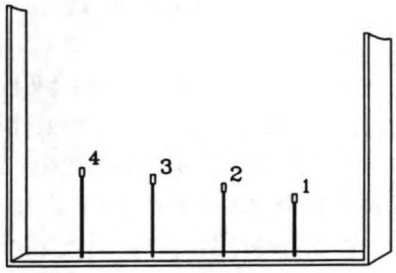

Figure 4.2.2 *Pressure transducers fixed on a frame. (Height above the bottom; no. 1: 14.8 cm, no. 2: 17.3 cm, no. 3: 19.3 cm and no. 4: 21.0 cm)*

After concentration profiles had been measured in the bed, the experiment was started on December 5th, 1991. This experiment comprised four tests.

In the first test velocity profiles were measured above the consolidated layer of mud for three settings of the average flow rate. The objective of this test was to determine velocity profiles and turbulence intensities. These results were to be compared with almost identical measurements above the false bottom. In this test the pump was started and a fixed flow rate was adjusted using valve A (figure 3.1.5). Then, after approximately 5 minutes, the flow velocities at 2, 3 ,4, 5, 10, 15 and 20 cm above the bed were measured for approximately 2 minutes. The sample frequency was ± 45 Hz. These measurements were made for the following settings of the flow rate; 12, 24 and 36 $dm^3 \cdot s^{-1}$.

Waves were generated for the first time in test 2. This test and the next tests were started with generating waves with a constant wave height for approximately 30 minutes. The wave period was set at 1.5 s. Then the pump was started and the flow rate was set a 12 $dm^3 \cdot s^{-1}$, which resulted in a steady current superimposed on the already present wave-induced flow in the flume. Subsequently, velocities and suspended sediment concentrations were measured at five levels (2.5, 5, 10, 15 and 20 cm) above the initial bed. This procedure was reiterated for two other settings of the average flow rate, namely 24 and 36 $dm^3 \cdot s^{-1}$. As soon as these measurements had been completed, valve A was carefully shut and the wave height was set to a higher value (test 3) and the entire programme was repeated. Test 4 concluded the experiment in which the largest wave height was employed. The complete experimental program of the second experiment is summarized in table 4.2.1.

Table 4.2.1 *Experimental program of the second experiment. (5 December 1991)*

test no.	details
1	* No waves. Measuring velocity profiles and turbulence intensities over a rigid bed for three settings of the flow rate; 12, 24 and 36 $dm^3 \cdot s^{-1}$. Velocity measurements at 2, 3, 4, 5, 10, 15 and 20 cm above the bed.
2	* No net current. Generation of waves for half an hour; *average wave height c. 23 mm.* * Both waves and current. Flow rate increased step by step every five minutes (flow rates: 12, 24 and 36 $dm^3 \cdot s^{-1}$). Measuring velocities at 2.5, 5, 10, 15 and 25 cm above the bed for every setting of the flow rate.
3	* No net current. Generation of waves for half an hour; *average wave height c. 45 mm.* * Both waves and current. Flow rate increased step by step every five minutes (flow rates: 12, 24 and 36 $dm^3 \cdot s^{-1}$). Measuring velocities at 2.5, 5, 10, 15 and 25 cm above the bed for every setting of the flow rate.
4	* No net current. Generation of waves for half an hour; *average wave height c. 75 mm.* * Both waves and current. Flow rate increased step by step every five minutes (flow rates: 12, 24 and 36 $dm^3 \cdot s^{-1}$). Measuring velocities at 2.5, 5, 10, 15 and 25 cm above the bed for every setting of the flow rate.

4.3 Results

In the next sections the results of the second experiment on China Clay are presented. Concentration profiles in the bed measured prior to the tests are presented in section 4.3.1. The velocity profiles and turbulence intensities measured will be discussed in section 4.3.2. The results of the wave/current tests are presented in section 4.3.3. This section is concluded by showing the concentration profiles in the bed measured after the tests (section 4.3.4).

4.3.1 Concentration measurements prior to the tests

The concentration profiles in the bed prior to the tests are shown in figures 4.3.1 and 4.3.2. These measurements were made using the conductivity probe. The coordinate system used to pinpoint the locations of these measurements was defined in section 4.1.

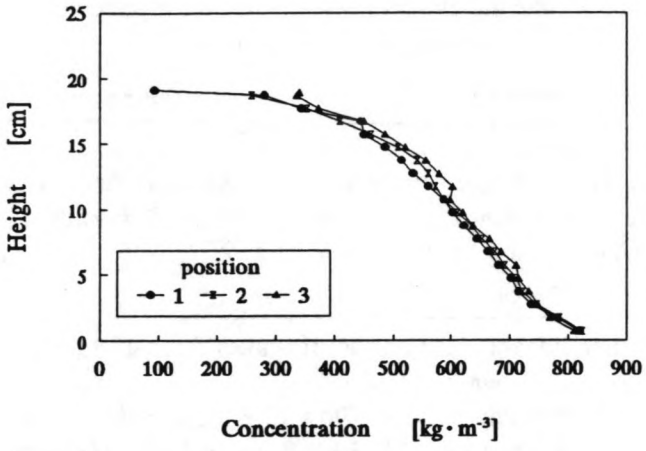

Figure 4.3.1 *Concentration profiles in the bed at x=2.11 m.*
(Position 1: y=0.2 m, position 2: y=0.4 m, position 3: y=0.6 m)

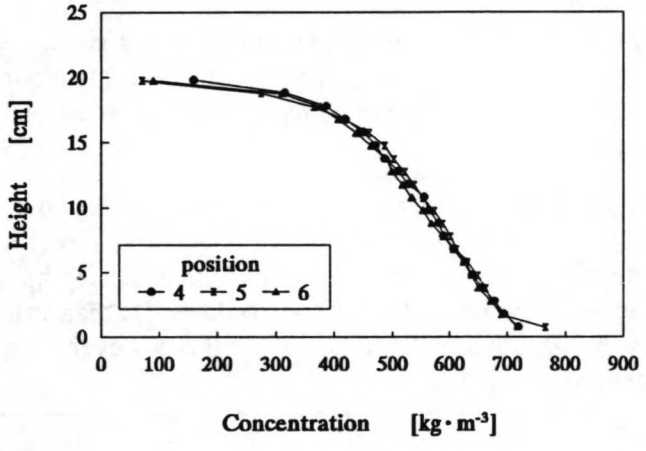

Figure 4.3.2 *Concentration profiles in the bed at x=5.48 m.*
(Position 4: y=0.2 m, position 5: y=0.4 m, position 6: y=0.6 m)

The measurements made at position x=2.11 and x=5.48 m show that the bed is much more uniform in transverse direction than it was in the pilot experiment. Furthermore, comparing figures 4.3.1 and 4.3.2 shows that the uniformity of the bed in longitudinal direction is also much better. However, in the downstream part of the test section there seems to be a larger concentration in the lower part of the bed than in the upstream measuring location. This gradient in the concentration in the downstream direction is however not significant because of the accuracy of the conductivity probe (maximal error: ± 6% of the local concentration). It may be concluded that, the alteration of the geometry of the test section produced a positive effect on the uniformity of the bed, mainly because the section could be filled with only one content of the mixing tank and no mud had to be removed after consolidation.

4.3.2 Velocity profiles and turbulence intensities over a rigid bed

The measurements were used to calculate the average local velocities U in the longitudinal direction at several levels, z, above the bed. Furthermore, root-mean-square values of the velocity (u') were calculated. The results are shown in figure 4.3.3 for three settings of the flow rate.

The profiles measured were found to agree with a logarithmic velocity profile for turbulent flow, which was to be expected because the Reynolds number based on the hydraulic radius varied from 8500 for a flow rate of 12 $dm^3 \cdot s^{-1}$ to 25500 for a flow rate of 36 $dm^3 \cdot s^{-1}$.

The calculated root-mean-square (rms) values are shown on the right hand side of figure 4.3.3. The rms values tend to increase with increasing mean velocity and they seem to decrease with increasing height above the bottom.

Nezu and Nakagawa (1993) proposed universal expressions for the turbulence intensities, normalized with the friction velocity, for open channel flow which are independent of the Reynolds and Froude numbers. These expressions are

$$\left.\begin{aligned} \frac{u'}{U_*} &= 2.30 \exp\left[\frac{-z}{h}\right] \\ \frac{v'}{U_*} &= 1.27 \exp\left[\frac{-z}{h}\right] \\ \frac{w'}{U_*} &= 1.63 \exp\left[\frac{-z}{h}\right] \end{aligned}\right\} \qquad (4.3.1)$$

where z is positive in upward direction from the bottom, h is the water depth and U_* is the friction velocity.

Nezu and Nakagawa (1993) also proposed relations for the relative turbulence intensities (u'/U) in open-channel flows. A distinction was made between a smooth and a rough bed. For a smooth bed the following relation was found

$$\frac{u'}{U} = \frac{2.3 \exp(-\xi)}{\kappa^{-1} \cdot \ln(\xi) + w(\xi) + A'} \qquad \text{for a smooth bed} \qquad (4.3.2)$$

where

$$A' \equiv \kappa^{-1} \cdot \ln(Re_*) + A,$$

$$\xi = \frac{z}{h},$$

$$w(\xi) = \frac{2\Pi}{\kappa} \sin^2\left[\frac{\pi z}{2h}\right].$$

Here κ is the Karman constant (≈ 0.4), ψ is Coles' wake strength parameter, Re_* is the Reynolds

number based on the friction velocity U_* and the flow depth h, and A is a constant. The function $w(\xi)$ is the so-called wake function and is used to account for the deviations from the standard log-law. This function was obtained empirically by Coles (1956).

A similar relation is found for the relative turbulence intensities over a rough bed (Nezu and Nakagawa, 1993)

$$\frac{u'}{U} = \frac{2.3\exp(-\xi)}{\kappa^{-1}\cdot\ln(\xi) + w(\xi) + A''} \qquad \text{for a rough bed} \qquad (4.3.3)$$

where $$A'' \equiv -\kappa^{-1}\cdot\ln(k_s/h) + A_r.$$

Here k_s is Nikuradse's equivalent sand roughness and A_r is a constant.

In figure 4.3.4 (Nezu and Nakagawa, 1993) various experimental results are compared with the curves calculated from equation 4.3.1. It can be observed that the relative turbulence intensities tend to decrease with increasing Reynolds number especially for $\xi < 0.1$. The effect of the roughness on the relative turbulence intensities (equations 4.3.2 and 4.3.3) is shown in figure 4.3.5 (Nezu and Nakagawa, 1993); the relative turbulence intensity tends to increase with the roughness of the bed.

The relative turbulence intensities calculated from the measurements made with the electromagnetic current meters were compared with the relations obtained by Nezu and Nakagawa (1993) in order to validate the use of an electromagnetic current meter for turbulence measurements. First the measurements made above the false floor were re-analyzed; the relative turbulence intensities were plotted with the relative height above the bottom (see figures A.3.7 and A.3.8). Comparing these figures with figure 4.3.4 clearly shows that the measured turbulence intensities coincide well with the results found by Nezu and Nakagawa. Furthermore, the relative turbulence intensities tend to decrease if the Reynolds number increases, which is also found by Nezu and Nagawaka.

It may be concluded that, the turbulence intensities measured using the electromagnetic current meters agree very well with results known from the literature.

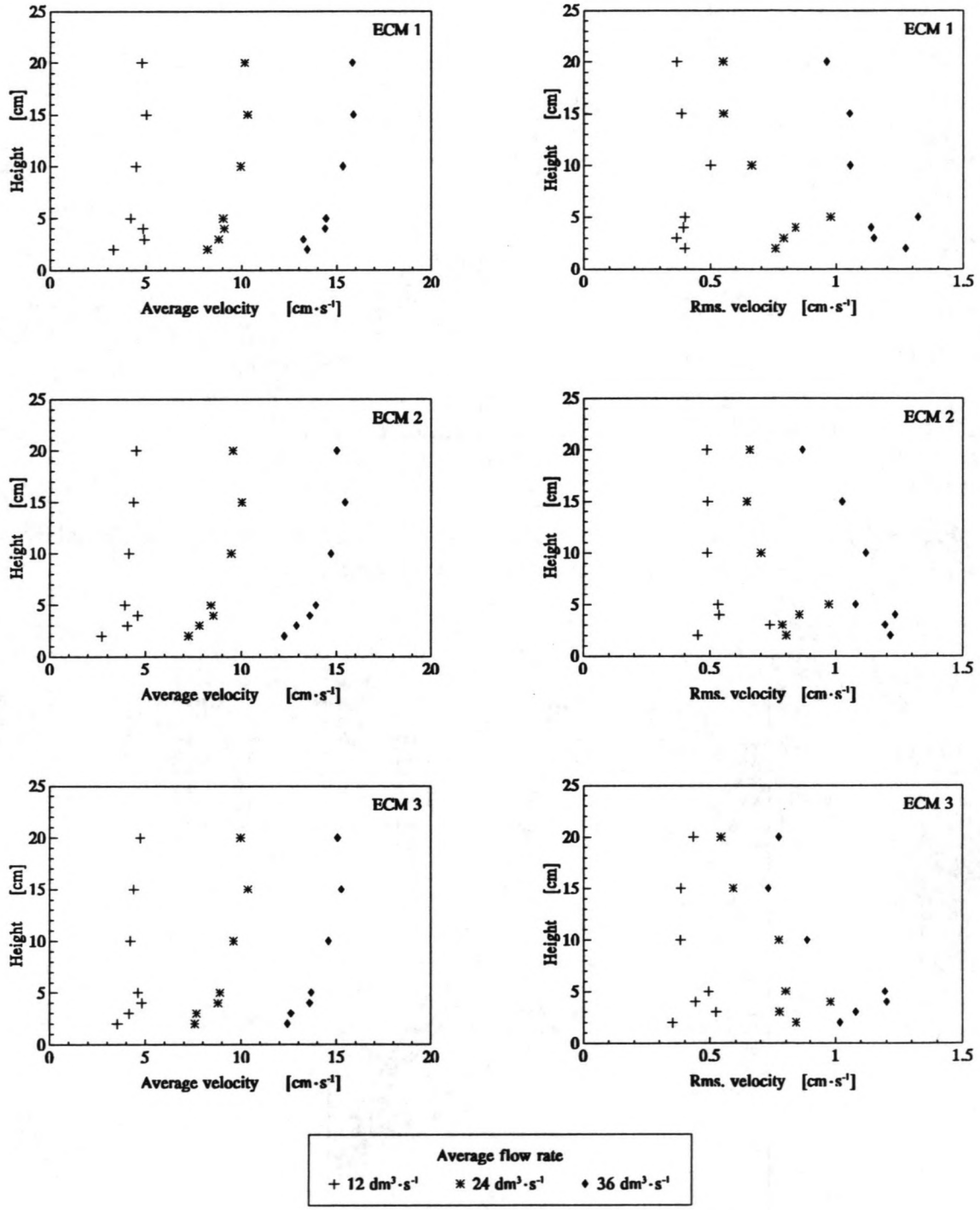

Figure 4.3.3 *Average and root-mean-square velocities in the longitudinal direction measured using the three electromagnetic current meters (ECM).*

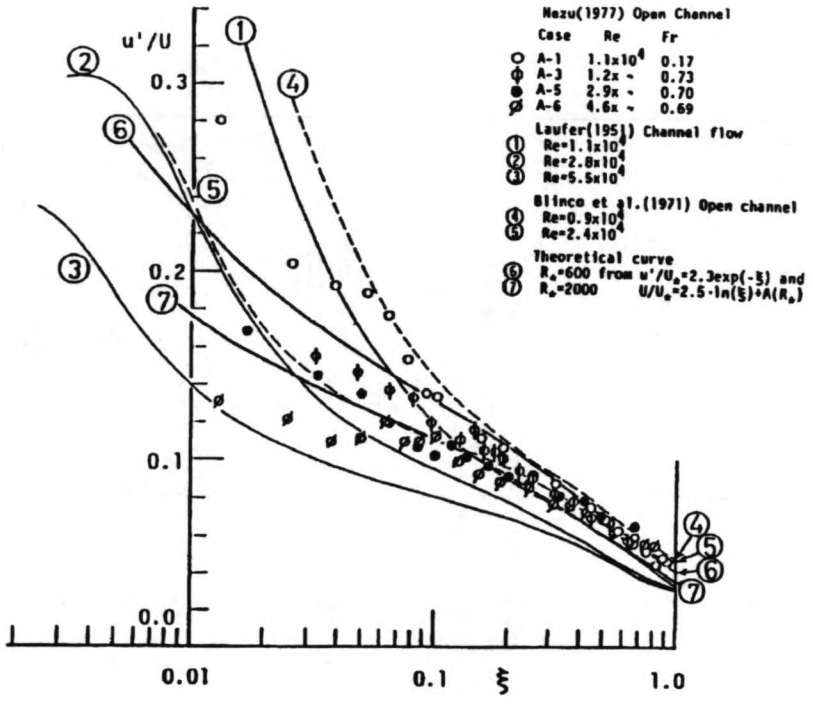

Figure 4.3.4 *The variation of the relative turbulence intensity for several Reynolds numbers (from Nezu and Nakagawa, 1993).*

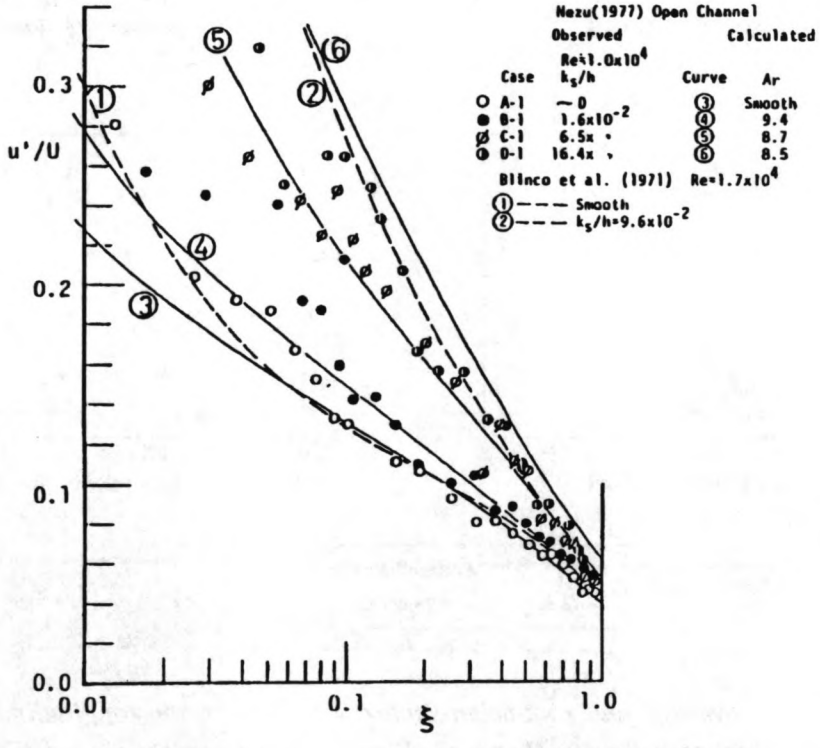

Figure 4.3.5 *The effect of the roughness on the relative turbulence intensity (from Nezu and Nakagawa, 1993).*

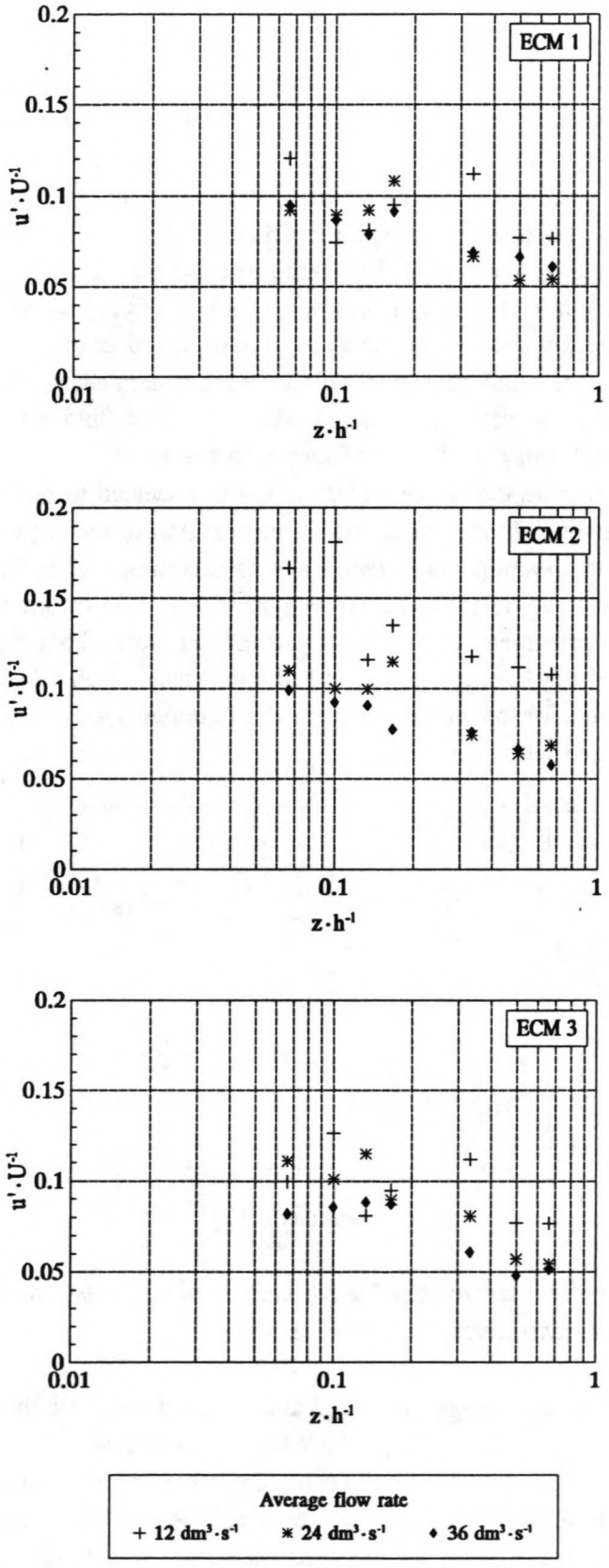

Figure 4.3.6 *Relative turbulence intensities measured over a non-liquefied bed.*

4.3.3 Wave/current tests (2-4)

Test 2

The bed was cyclicly loaded for the first time in test 2. The wave height and period were set at c. 23 mm and 1.5 s, respectively. The generation of waves continued for half an hour. Due to a minor technical defect the logging of the data was delayed for a moment and unfortunately the arrival of the first waves over the test section was not recorded. During this half hour the measuring position of the concentration and current meters was kept at z=25 cm.

As soon as the first waves had travelled over the test section movements were observed in the uppermost part of the bed. It looked as if a very thin top layer of the bed was eroded, which eroded material was moving over the bed. No movements were observed in the remaining part of the bed. Then, after about one minute small spots of fluid mud were generated, apparently at random, at the bed surface. The size of these patches increased with time. The fluid mud was oscillating in the patches and its movement seemed to be out of fase with the movement of the water just above it. After approximately 15 minutes the entire surface of the bed seemed to be liquefied.

The results of the wave height measurements of the first part of test 2 (waves only) are shown in figure 4.3.7. In this graph one-minute-averaged wave heights measured at five locations are shown. The measurements of the wave height meter no. 6 (position: x=7.33 m) are not shown because of a malfunctioning of this instrument during this part of the test. This figure shows that after approximately 23 minutes the liquefaction of the bed has reached such a level that significant wave damping due to the dissipation of wave energy in the liquefied mud layer can be observed. The damping seems to increased with time.

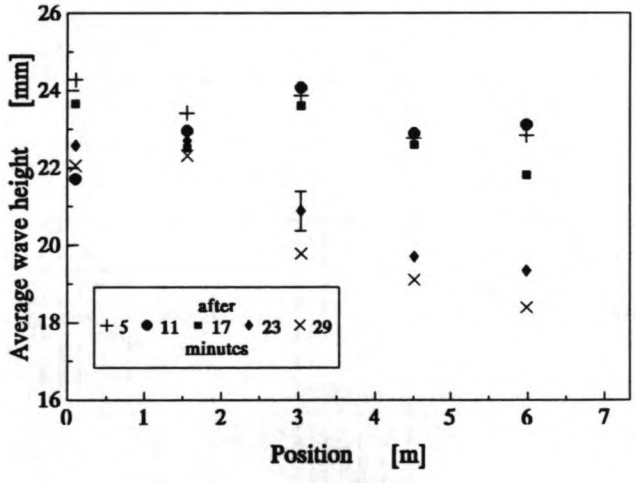

Figure 4.3.7 *One-minute-averaged wave heights over the bed measured at various moments during test 2 (waves only).*

The wave-averaged pressure changes measured at the start of test 2 are shown in figure 4.3.8. The pressure measurements were averaged using a Fast Fourier Technique; the oscillations were filtered out by removing the main frequencies from the spectrum generated by a forward Fourier transform. This filtered spectrum was inversely transformed and subsequently this signal was filtered using a 10 point filter. The initial pressures were not recorded because of a technical problem. Consequently, in figure 4.3.8 only pressure changes are shown and the zero value is chosen arbitrarily. The moment at which the first data point was logged was defined as t=0.

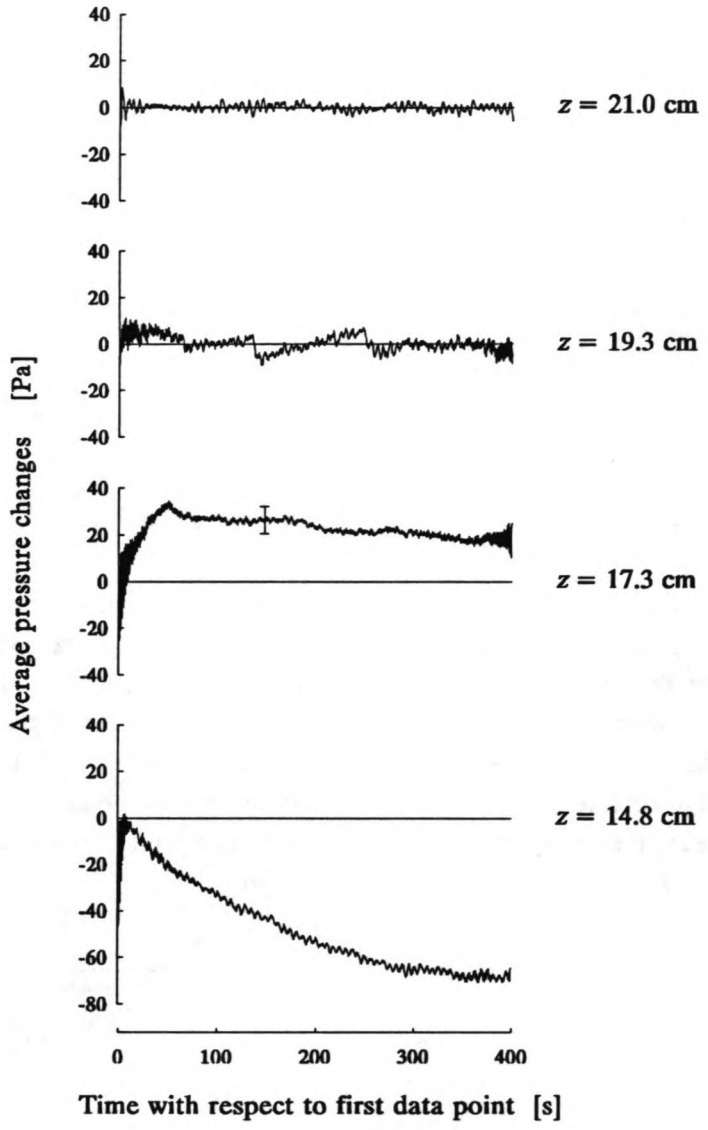

Figure 4.3.8 *Wave-averaged pressure changes (test 2). The bed surface was at $z \approx 19.5$ cm.*

In figure 4.3.8 four signals are shown; the upmost graph shows the pressure changes measured just above the bed. The other three graph show the pore-pressure changes measured in the bed. The vertical positions at which these signals had been measured are also shown in the figure. The maximum error in these signals is approximately ± 7 Pa. The reference measurement at z=21.0 cm shows that there is no significant change in pressure, which means that the average water depth is constant. The pore-pressure in the top of the bed also shows no significant pressure change. However, the pore-pressure at 17.3 cm above the bottom of the flume shows a transient increase followed by a gradual decrease. The same trend can be observed in the pore-pressure change at z=14.8 cm. Initially there is a sudden increase in pore-pressure followed by a more gradual decrease.
Pressure changes during the initial 400 s are shown in figure 4.3.8. In figure 4.3.9 the averaged pressures measured during the entire wave-only part of test 2 are shown.

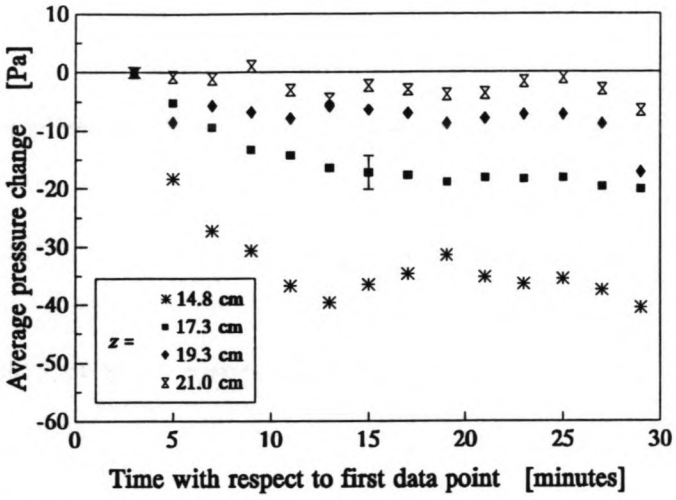

Figure 4.3.9 *Wave-averaged pressure changes during test 2.*

An example of the actual pressure changes as measured after approximately 14 minutes is shown in figure 4.3.10. The variation of the reference pressure is almost sinusoidal and the amplitude of the pressure is larger than that measured at z=19.4 cm, but smaller than the amplitudes measured at z=17.8 and z=14.8 cm. Furthermore, comparing the phases of the four signals it is observed that there is a phase lag between the pore-pressure measured at z=19.4 cm and the reference pressure. Furthermore, a negative retardation is found between the reference pressure changes and the pore-pressure changes measured at z=17.8 and z=14.8 cm. The pore-pressure variation measured close to the bottom of the flume has the largest negative retardation.

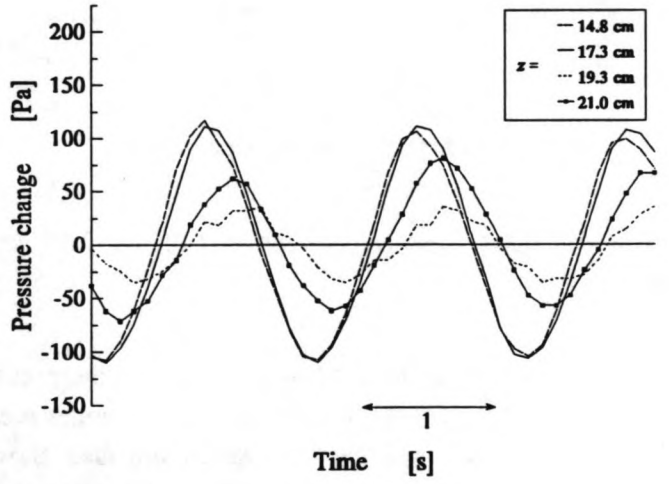

Figure 4.3.10 *A representative example of the average pressure variations measured during test 2 (waves only).*

The mean pore-pressures seem to decrease significantly, also at the upmost location in the bed, for approximately the first 15 minutes of the experiment. Then an equilibrium pore-pressure is apparently formed. The pressures shown in figures 4.3.8 and 4.3.9 are the wave-averaged pressures. The amplitudes of the pressures as a function of time are shown in figure 4.3.11.

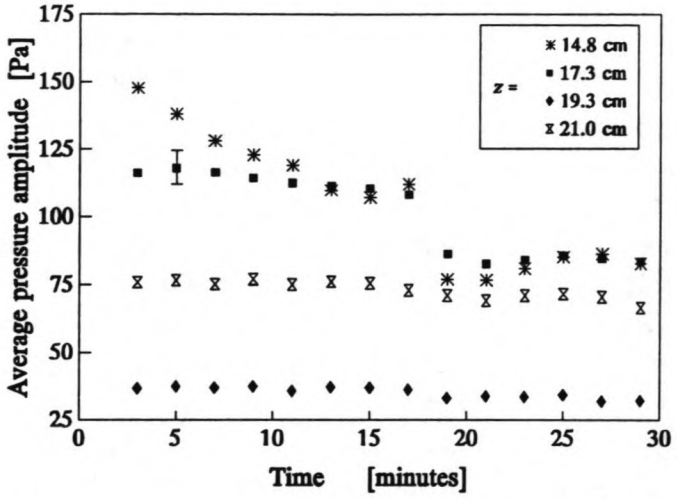

Figure 4.3.11 *Average pressure amplitudes as a function of time in test 2 (waves only).*

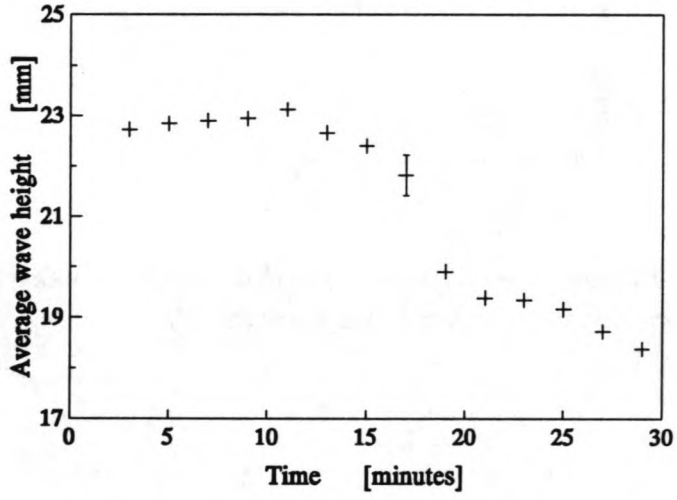

Figure 4.3.12 *Averaged wave heights measured at x=4.51 m during test 2.*

The amplitudes measured at the two upmost locations are fairly constant. The amplitudes at z=17.3 cm show a sudden decrease after approximately 17 minutes. At z=14.8 cm the pressure amplitude decreases with time. However, after approximately 17 minutes also an instantaneous decrease is observed, after which the amplitude remains constant. If a comparison is made between the average pore-pressure amplitudes and the wave height measured at x=4.51 m as a function of time, which are shown in figure 4.3.12, a correlation can be observed between these graphs. The moment at which an abrupt increase in wave damping is observed matches with a decrease in average pore-pressure amplitude.

The quick liquefaction of the China Clay was probably caused by the pressure-induced shear stresses in the bed. The order of magnitude of these shear stresses were approximated assuming that the initial China Clay bed has poro-elastic properties and applying Spierenburg's model (appendix F) to a layer of China Clay on a smooth base under similar flow characteristics as in this test (water depth: 0.30 m, wave period: 1.5 s, wave amplitude: 0.01 m). It is found that the deviatoric stress at the surface of the bed is of the order of 20 Pa and near the base approximately 52 Pa. In this calculation it was assumed that Poisson's ratio ν=0.45 and the shear modulus G=100 Pa (Chou

(1989), Kaolinite, concentration c. 600 kg·m^{-3}, for strain amplitude < 0.01). Comparing these deviatoric stresses with the yield strength of such a suspension as determined in rheological tests (De Wit, 1992a) it is found that the deviatoric stresses are one order higher than the yield stress, which probably results in a breakdown of the aggregate structure and the generation of fluid mud.

After having generated waves for half an hour, the pump was started which resulted in a steady current in the flume. The settings of the wave generator were not altered. Velocity profiles were measured for four different settings of the average flow rate. The wave heights decreased due to this steady current. The average wave heights measured above the test section for the different settings of the average flow rate are shown in figure 4.3.13. The average velocities and the average velocity amplitudes measured using electromagnetic current meter E013 (x=7.0 m, y=0.40 m) at several levels above the bottom of the flume are shown in figure 4.3.14.

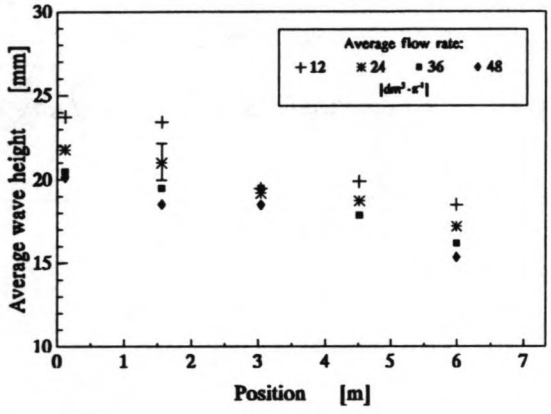

Figure 4.3.13 *Average wave heights measured at x=4.51 m when both waves and current were present in the flume (test 2).*

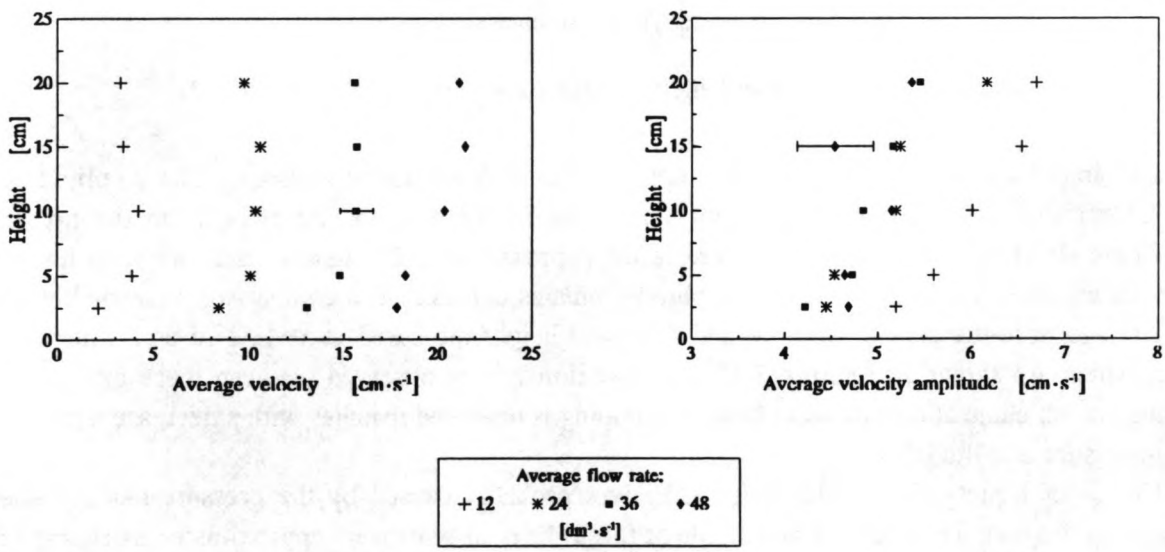

Figure 4.3.14 *Wave-averaged velocities and average velocity amplitudes when both waves and current were present in the flume (test 2).*

The damping is not influenced very much when a current was present, as can be seen in figure 4.3.13. Part of the fluid mud was easily transported in the downstream direction by the current. An increase in suspended sediment concentration as measured at the end of the wave-only part of test 2 was not observed.

Test 3

After test 2 the wave height was increased. The average wave height during the first part of test 3 are shown in figure 4.3.15. The damping of the waves was almost constant over the measuring period.

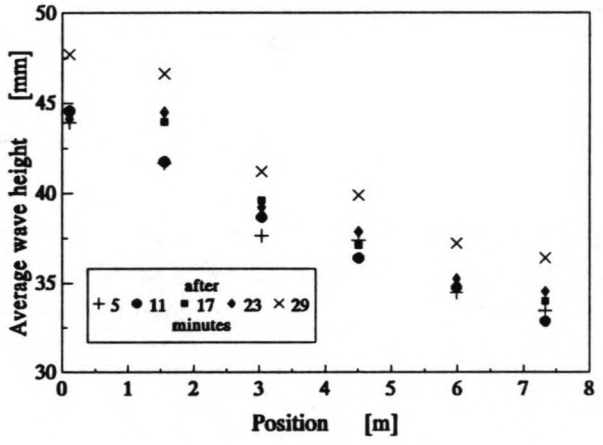

Figure 4.3.15 *Average wave heights during test 3 (waves only).*

The average pressure changes and average pressure amplitudes are shown in figures 4.3.16 and 4.3.17, respectively. The pore-pressures at z=14.8 and z=17.3 cm decreased with time. Only the pore-pressure measured at z=19.3 cm tended to increase a little. However, the average pressure amplitudes were constant over the whole period (figure 4.3.17).

The average suspended sediment concentration just before a current was generated was less than 0.01 $kg \cdot m^{-3}$.

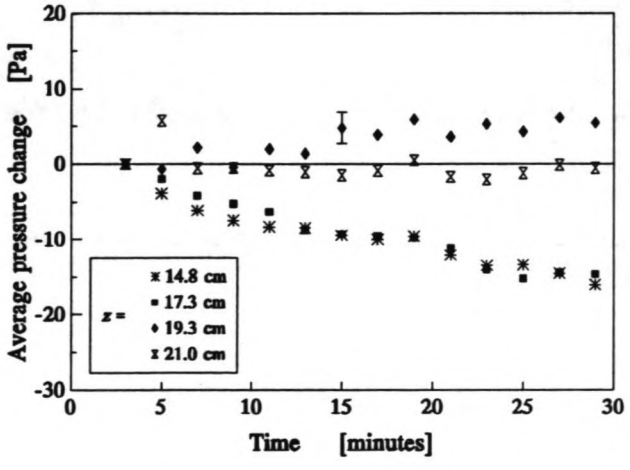

Figure 4.3.16 *Average pressure changes with respect to the first data point as functions of time (test 3, waves only).*

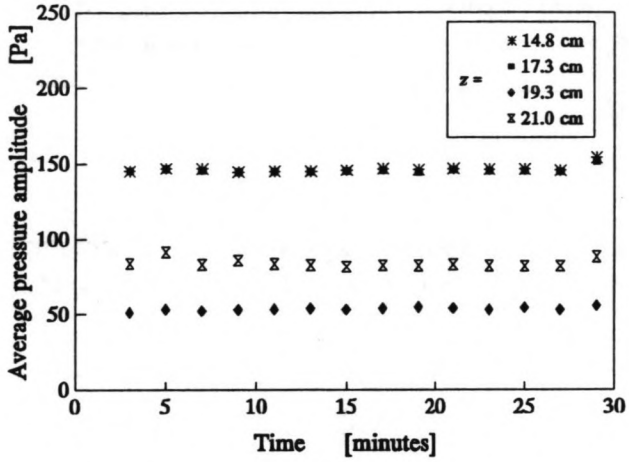

Figure 4.3.17 *Average pressure amplitudes as a function of time (test 3, waves only).*

When a current was generated, the wave height decreased with the average flow rate (figure 4.3.18). For the higher flow rates the wave gauges started to oscillate, so that the accuracy of these measurements decreases a little for higher flow rates. The damping of the waves did not change very much.

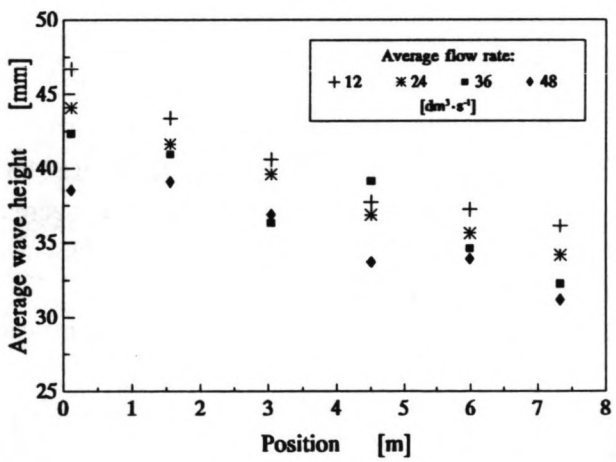

Figure 4.3.18 *Average wave heights measured above the test section for four flow rates (test 3).*

The average velocity and the average velocity amplitudes measured using electromagnetic current meter E013 are shown in figure 4.3.19.

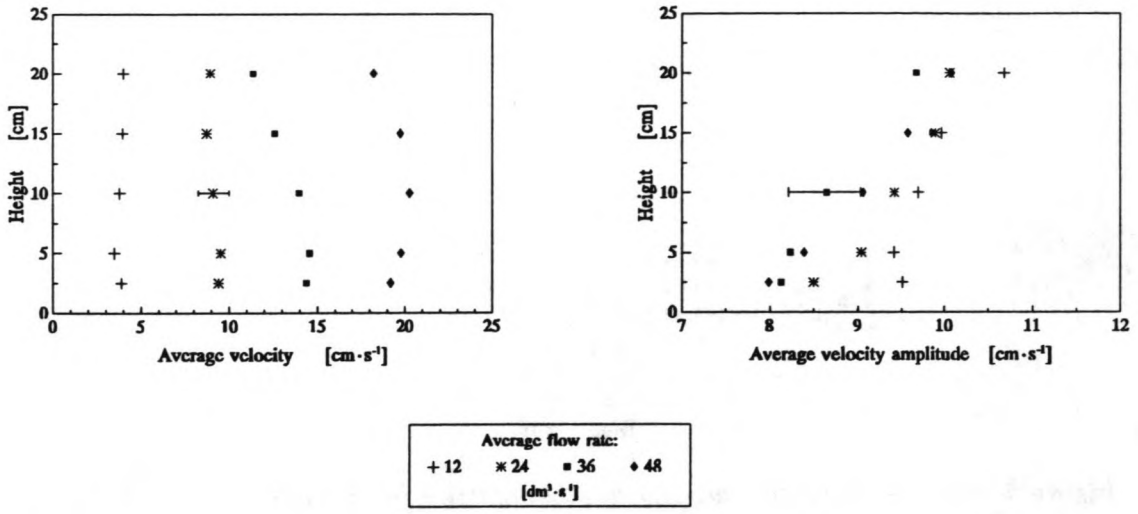

Figure 4.3.19 *Average velocities and average velocity amplitudes during test 3.*

Test 4

In test 4 the wave height was increased again. The average wave height as a function of time is shown in figure 4.3.20. The damping was fairly constant over the measuring period. In this test the moveable plates connecting the test section with the fixed bottom of the flume, were lowered after approximately 7 minutes. Consequently, the wave height at the upstream end of the test section decreased because of the increase in water depth.

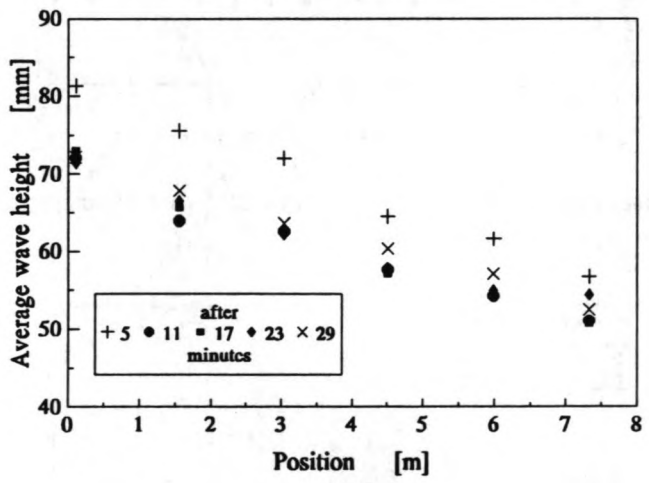

Figure 4.3.20 *Average wave heights during test 4 (waves only).*

The average pore-pressures showed an interesting behaviour as can be seen in figure 4.3.21. The pressures are almost constant over the entire measuring period, except for the pore-pressure measured at z=14.8 cm where a sudden decrease can be observed. The average pressure amplitudes, which are shown in figure 4.3.22, were also almost constant. Comparing these results with the average wave height measured at x=4.51 m, figure 4.3.23, shows no correlation. The sudden decrease in wave height was caused by the lowering of the adjustable plates. This decrease in wave height was also observed in the average pressure amplitudes. The sudden decrease in pore pressure at z=14.8 cm cannot be correlated with a change in wave damping.

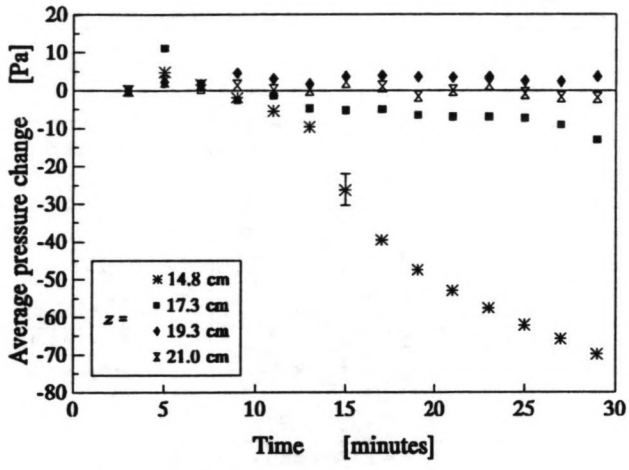

Figure 4.3.21 *Average pressure changes during test 4 (waves only).*

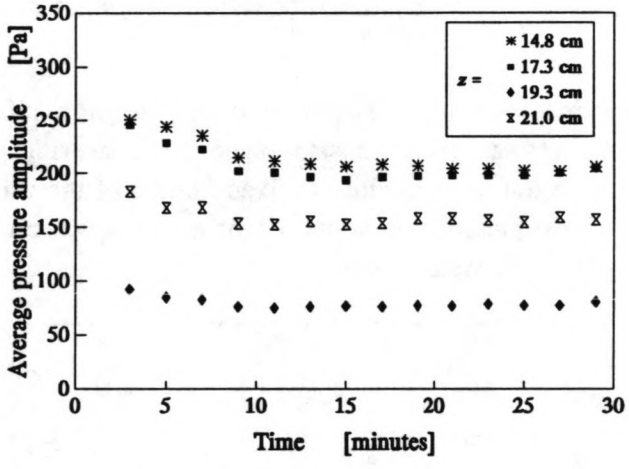

Figure 4.3.22 *Average pressure amplitudes in test 4 (waves only).*

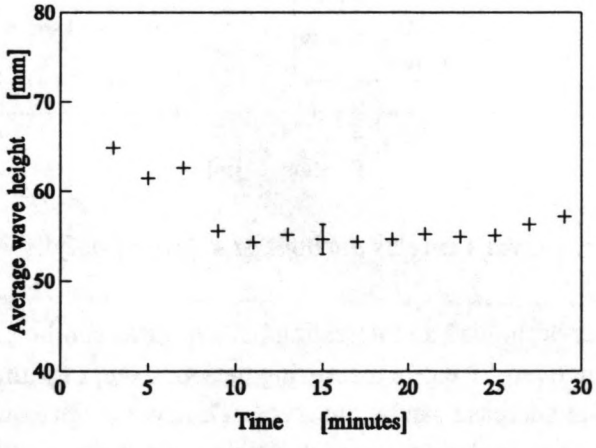

Figure 4.3.23 *Average wave height measured at x=4.51 m in test 4 when only waves were present.*

Finally, a current was generated without changing the settings of the wave generator. Consequently, the average wave height decreased as can be seen in figure 4.3.24. In this test velocity profiles were measured for three settings of the average flow rate, namely 12, 24 and 36 $dm^3 \cdot s^{-1}$. The results of these measurements are shown in figure 4.3.25.

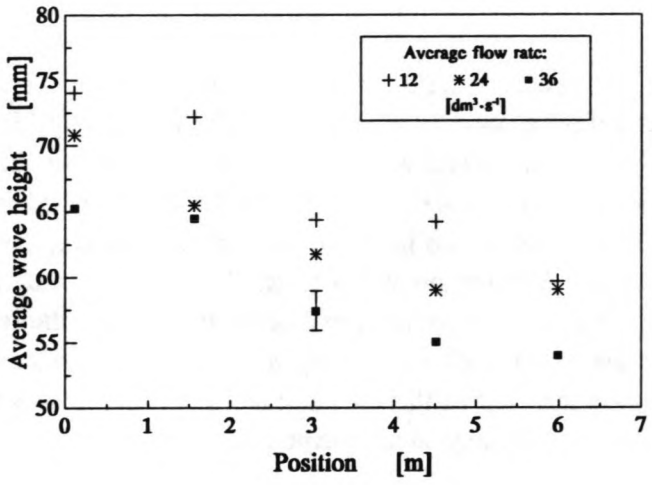

Figure 4.3.24 *Average wave heights measured when both waves and current were present in the flume (test 4).*

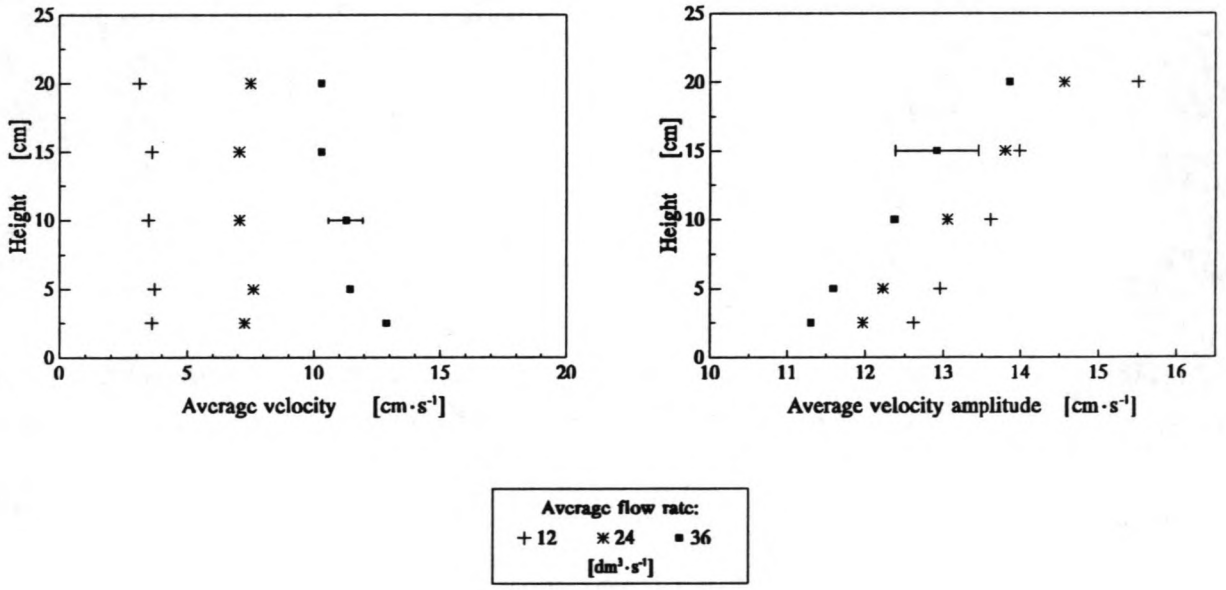

Figure 4.3.25 *Wave-averaged velocities and average velocity amplitudes when both waves and current were present in the flume (test 4).*

At the end of test 4 the suspended sediment concentration in the flume was approximately 0.22 $kg \cdot m^{-3}$. The sudden increase in suspended sediment concentration was not caused by a large resuspension rate of mud from the test section, but was generated in the recirculation pipe. In a later phase of test 3 the fluid mud which was transported in the downstream direction by the current,

reached the outlet beneath the wave damper. The fluid mud and the saline water were fully mixed in the recirculation pipe, and re-entered the flume, which resulted in a very high suspended sediment concentration.

4.3.4 Bed concentrations after the tests

Ten days after the these tests the concentration profiles were measured in two cross-sections. In figure 4.3.26 the concentration profiles at x=3.28 m are shown. The bed is only 11 cm thick and a strange local increase in concentration was found at approximately 5 cm above the bottom of the flume. Similar profiles were measured at x=5.49 m, see figure 4.3.27. The bed is thicker in this cross-section, because fluid mud was transported in the downstream direction at the end of test 4 and some of the mud was trapped by the downstream endwall, which had been a little too high.

These profiles may indicate the lowest level of liquefaction during the tests. After the tests the fluid mud starts to consolidate on top of the non-liquefied layer. The concentration at the interface after consolidation is usually larger than that of the underlying layer, as was already observed by Toorman & Berlamont (1990) in settling column experiments.

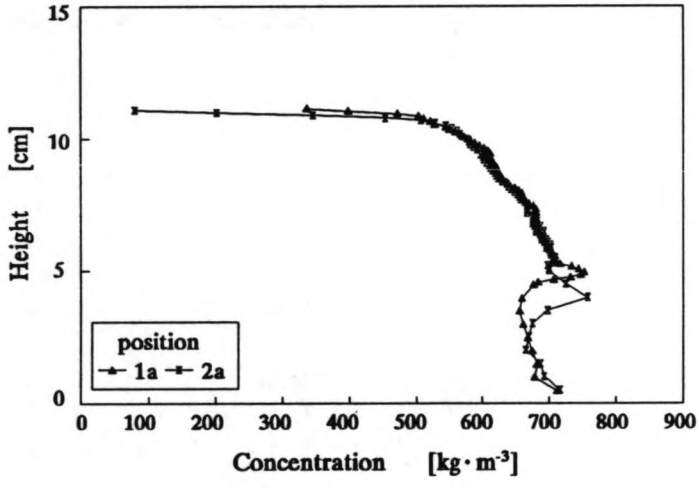

Figure 4.3.26 *Concentration profiles measured at x=3.28 m ten days after the tests. (Position 1a: y=0.40 m; position 2a: y=0.60 m)*

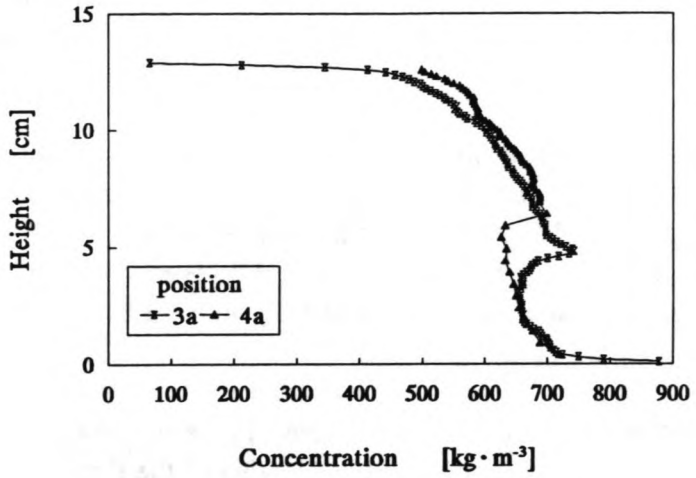

Figure 4.3.27 *Concentration profiles measured at x=5.49 m ten days after the tests. (Position 3a: y=0.40 m; position 4a: y=0.60 m)*

4.4 Conclusions

The following conclusions may be drawn from the results of the second experiment.

- The modification of the test section was successful; the concentration measurements prior to the experiment showed that the bed was rather uniform in the longitudinal as well as the transverse direction. Furthermore, the mud was not trapped in the test section in a later phase of the experiment, for the height of the endwalls of the test section was adjusted during the tests. The removal of the beams and the lowering of the plates could be done easily.

- The velocity profiles measured over the non-liquefied bed agreed very well with a turbulent, logarithmic profile. Furthermore, the turbulence intensities measured with an electromagnetic current meter over the false bottom as well as the intensities measured over a non-liquefied mud bed agree quite well with the empirical relations for the turbulence intensities in open-channel flows according to Nezu and Nakagawa (1993). Consequently, the electromagnetic current meters are suitable for measuring turbulence intensities under similar flow conditions.

- The China Clay started to liquefy almost immediately after the first waves had travelled over the test section. The initial average wave height was approximately 23 mm. In the pilot experiment only waves with a wave height of at least 81 mm were able to generate liquefaction. The concentrations of the bed were similar. However, the consolidation period for the pilot experiment was 22 days whereas for the second experiment a consolidation period of only 9 days was allowed. Consequently, the threshold value at which liquefaction occurs seems to increase with the consolidation period.

- Pressure-induced shear stresses in the bed play an important role in the liquefaction process of China Clay.

- Waves were significantly damped when a layer of fluid mud was present, similar to what was observed in the pilot experiment. The fluid mud was easily transported in the downstream direction by a current.

- The wave-averaged pore-pressures show a transient increase followed by a gradual decrease. Furthermore, there is a phase shift between the reference pressure and the pore-pressures in the bed. In test 2 it was found that the wave damping increased when the pore-pressure amplitude measured at z=14.8 cm decreased (figure 4.3.11). However, a similar decrease in the pore-pressure amplitude measured at z=14.8 cm in test 3 (figure 4.3.21) could not be correlated with an increase in wave damping.

- Concentration profiles measured ten days after the tests showed a sudden increase in concentration at approximately 5 cm above the bottom of the flume followed by a decrease, similar to what was observed in the pilot experiment. If the location of this concentration increment indicates the thickness of the liquefied layer, then the observations through the glass sidewalls cannot be correct, for visual observations during the tests indicated that the maximal thickness of the liquefied layer was only 5 cm.

Chapter 5

The third experiment on China Clay

The third experiment in the wave/current flume was carried out on China Clay from a different lot than the China Clay used in the previous experiments. The characteristics of this slightly different China Clay were described in chapter 2. The experimental set-up was not changed for this experiment. More information on the locations and the specifications of the instruments used and some calibration data are found in appendix E. The preparation of the bed was not ideal (section 5.1) because of some technical problems. An electromagnetic current meter with which velocities could be measured perpendicular to the bottom of the flume and a thermometer were added to the apparatus already described in section 3.3. Furthermore, an additional computer was used to log the data. The experimental program and the results are discussed in sections 5.1 and 5.2, respectively. Finally, the main conclusions of the third experiment on China Clay are summarized in section 5.3.

5.1 Experimental procedure and program

The mixing tank was filled with 3050 dm^3 of tap water, 15.2 kg sodium chloride and 836 kg China Clay. The suspension was mixed for three weeks and pumped into the test section. The concentration of the suspension in the mixing tank was 250 $kg \cdot m^{-3}$. During the filling of the test section substantial leakage past the boards that should separate the fluid in the test section from the fluid in the rest of the flume was observed. Mud was flowing out of the test section and tap water was flowing into the test section. After filling of the test section the initial height of the suspension was 44.5 cm and the concentration appeared to be only 175 $kg \cdot m^{-3}$. This concentration was far to low and it was decided to allow this suspension to consolidate. After a few days of consolidation some of the overlying clear water was replaced by the China Clay suspension which was left in the mixing tank. The concentration was approximately 250 $kg \cdot m^{-3}$ after mixing. During the following consolidation period it was observed that this clay settled much faster than the China Clay used in previous experiments. The experiment could not be started when the thickness of the bed was 20 cm because of some technical problems with the wave height meters. In order to be able to use the pore-pressure transducers during an experiment the bed was resuspended using the mixing device on the measuring carriage on 2 June 1992 and again on 5 June 1992 because of the unsolved problems with the wave gauges at that moment.

On 10 June 1992 the third experiment on China Clay in the wave/current flume was initiated. This experiment also comprised several tests, similar to the experiments already made. Prior to and during every test concentration profiles of the bed were measured using the conductivity probe.

In the first test (test 1) some turbulence characteristics over liquefied and non-liquefied beds were measured. This test was started with measuring velocity profiles and root-mean-square velocities over the bed for three settings of the average flow rate, namely 12, 24 and 36 $dm^3 \cdot s^{-1}$. No waves were present in the flume during these measurements. Subsequently, the average flow rate was reduced to

zero and waves with a constant wave height were generated for approximately half an hour. The wave period was set at 1.5 s. The generation of waves was stopped after a significant layer of fluid-mud was generated and then velocity profiles and root-mean-square velocities were measured for the same settings of the average flow rate. This procedure was also carried out for a larger setting of the wave height (test 2).

The experiment was continued the day after (11 June 1992). During this test (3) velocities in a liquified layer of mud were measured. For this purpose waves were generated for approximately 1 hour to generate a layer of fluid mud. Then an electromagnetic current meter was used to measure velocity amplitudes in the layer of fluid mud.

The final test of this experiment was carried out on 25 June 1992. In this test (test 4) velocities in the fluid mud were measured when both waves and current were present in the flume. The experimental program of the third experiment is summarized in table 5.1.1.

Table 5.1.1 *Experimental program of the third experiment.*

test no.	details
1 (10 June 1992)	* No waves. Measuring velocity profiles and turbulence intensities over a rigid bed for three settings of the flow rate; 12, 24 and 36 $dm^3 \cdot s^{-1}$. Velocity measurements at 2.5, 5, 10, 15 and 20 cm above the bed. * Generation of waves for half an hour resulting in a layer of fluid mud; *average wave height c. 22 mm.* No net current. * No waves. Measuring velocity profiles and turbulence intensities over a partly liquefied bed for three settings of the flow rate; 12, 24 and 36 $dm^3 \cdot s^{-1}$. Velocity measurements at 2.5, 5, 10, 15 and 20 cm above the bed.
2 (10 June 1992)	* No net current. Generation of waves for half an hour; *average wave height c. 38 mm.* * No waves. Measuring velocity profiles and turbulence intensities over a partly liquefied bed for three settings of the flow rate; 12, 24 and 36 $dm^3 \cdot s^{-1}$. Velocity measurements at 2.5, 5, 10, 15 and 20 cm above the bed.
3 (11 June 1992)	* No net current. Generation of waves for an hour resulting in a layer of fluid mud; *average wave height c. 45 mm.* * No net current. Measuring velocity amplitudes in the layer of fluid mud using an electromagnetic current meter.
4 (25 June 1992)	* No net current. Generation of waves for c. four hours; *average wave height c. 90 mm.* * Measuring velocity amplitudes in the bed using an electromagnetic current meter. No net current. * Waves and current. Flow rate 24 $dm^3 \cdot s^{-1}$. Measuring velocities in the fluid-mud layer. Settings wave generator unaltered.

5.2 Results

5.2.1 Concentration measurements prior to test 1

As discussed before, the preparation of the bed was far from ideal. The consequences of the way of preparation can be seen in figure 5.2.1 where the concentration profiles are shown which were measured in a cross-section at x=2.35 m; the bed surface was not horizontal in a transverse direction. Furthermore, the bed was not horizontal in a longitudinal direction, which can be concluded from a comparison of figure 5.2.1 with figure 5.2.2 in which a concentration profile at x=5.82 m is presented. The thickness of the bed was less than 19 cm and consequently one of the pore-pressure transducers which should be inside the bed, may have been just outside the bed. Visual observations were not conclusive in this respect.

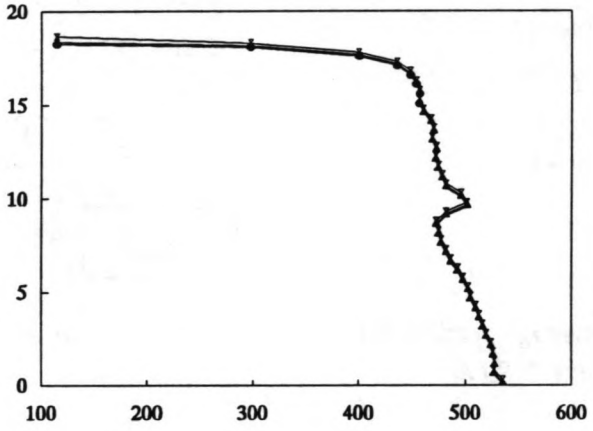

Figure 5.2.1 *Concentration profiles in the bed measured at x=2.35 m prior to test 1. (Position 1: y=0.20 m, position 2: y=0.40 m, position 3: y=0.60 m)*

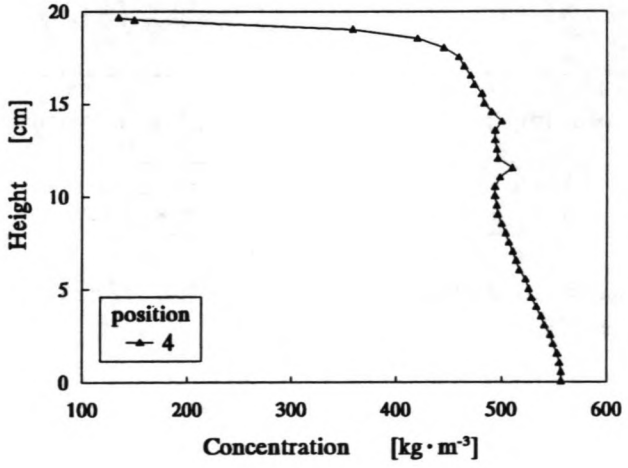

Figure 5.2.2 *Concentration profile in the bed measured at x=5.82, y=0.40 m prior to test 1.*

5.2.2 Test 1

This test was started with the measurement of velocities at five levels over the non-liquefied bed for three settings of the average flow rate. The measurements were made using electromagnetic current meters at several locations in the test section. One current meter was capable of measuring the velocity components in the x-z plane. The results of the measurements of the vertical velocity components (w) are shown in figure 5.2.3. Figures 5.2.4 and 5.2.5 show the velocity components in the longitudinal direction (u) measured at x=2.80 and x=5.13 m, respectively.

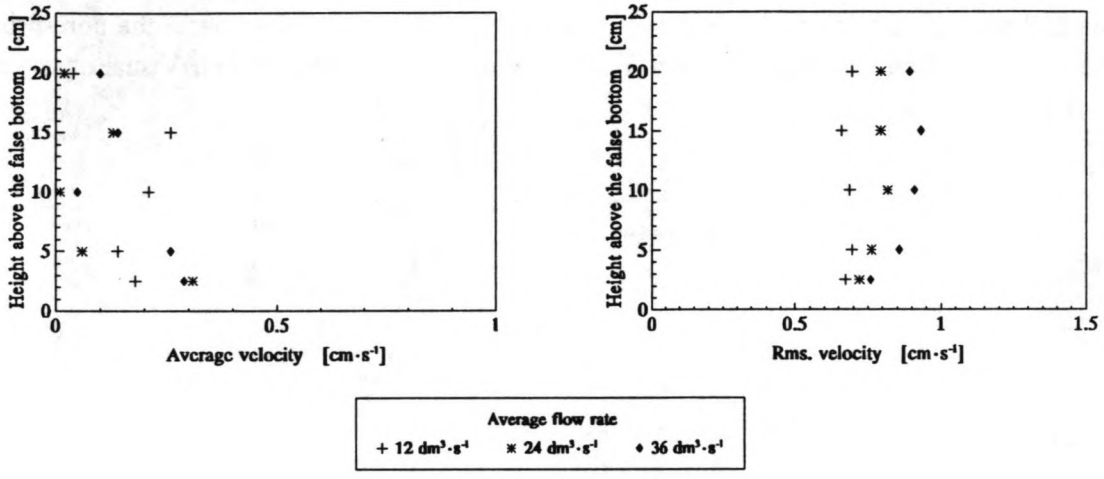

Figure 5.2.3 *Average vertical velocities (w) and rms. velocities measured at x=2.80 m.*

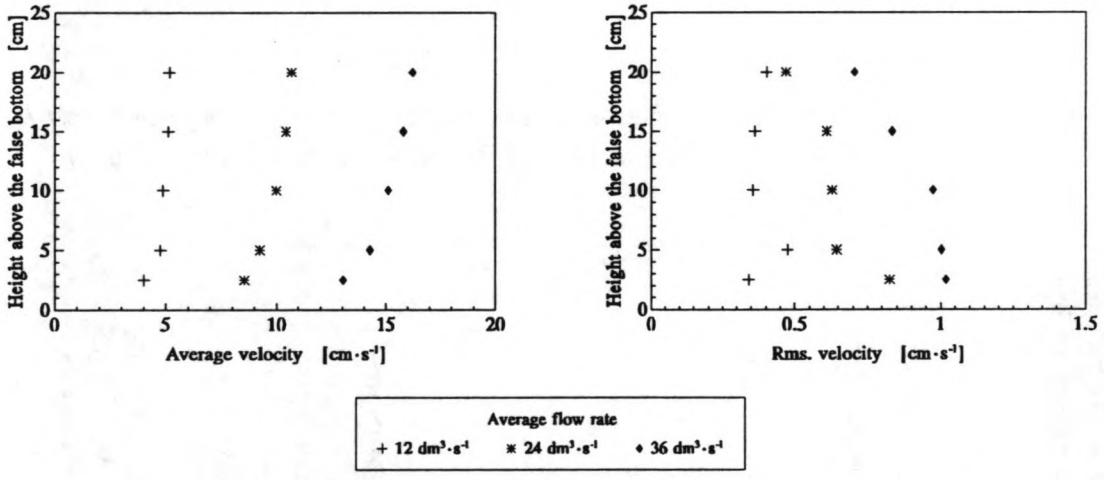

Figure 5.2.4 *Average longitudinal velocities and rms. velocities measured at x=2.80 m.*

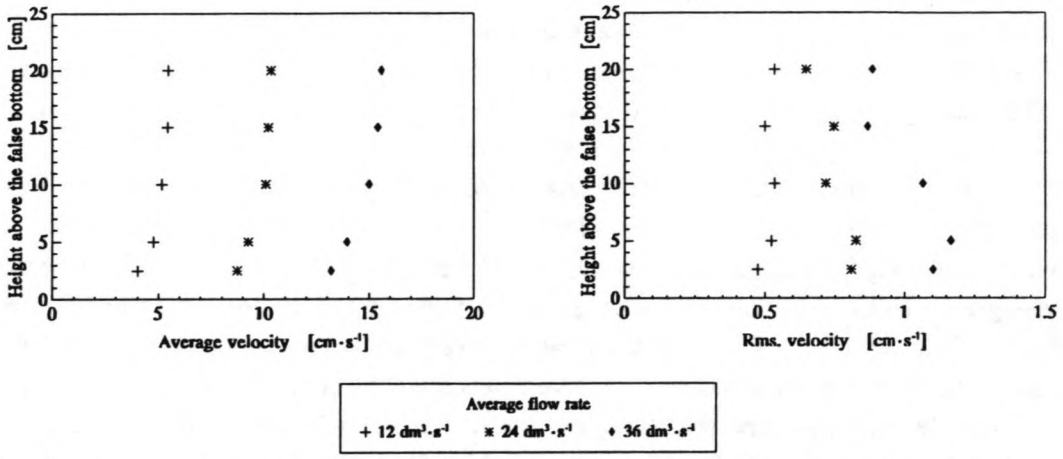

Figure 5.2.5 *Average longitudinal velocities and rms. velocities measured at x=5.13 m.*

These results are similar to the results obtained from the second experiment on China Clay. Assuming a logarithmic velocity profile, friction velocities U_* were estimated applying a least squares approximation on the average velocities measured at 22.5, 25, 30 and 35 cm above the flume bottom for the average flow rates of 24 and 36 $dm^3 \cdot s^{-1}$. These rough estimates were used to check if these relatively inaccurate results agree with the universal expressions for the turbulence intensities in open-channel flows as given in section 5.2.2. Figure 5.2.6 shows the turbulence intensities u' and w' normalized with the friction velocity as a function of the height above the bed normalized with the water depth h. The agreement between the measurements and the expressions for the turbulence intensities according to Nezu is rather good, despite the relatively poor accuracy of the friction velocity and the measured velocities.

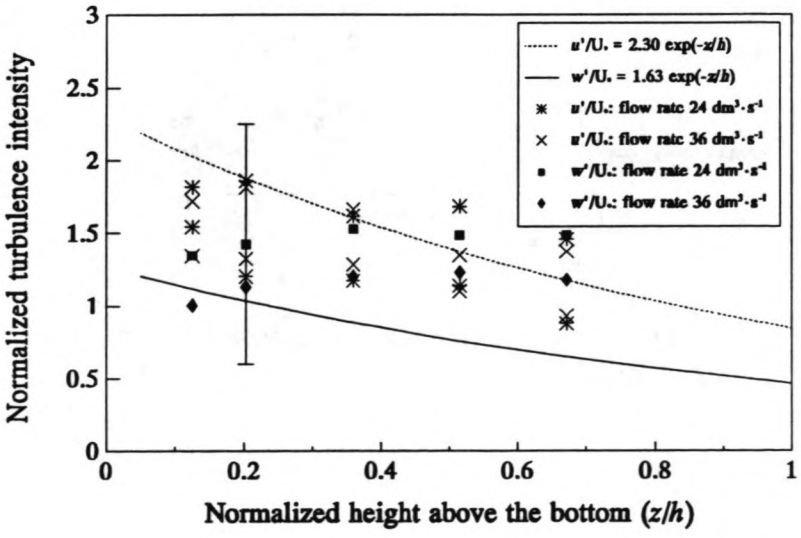

Figure 5.2.6 *Comparison between the measured normalized turbulence intensities and the universal expressions for the turbulence intensity according to Nezu and Nakagawa (1993).*

The bed was cyclicly loaded for the first time directly after measuring the velocity profiles. The wave period was 1.5 s and the average wave height of the incoming waves was approximately 22 mm. As in the second experiment the bed started to liquefy almost immediately after the first waves had travelled over the test section; first a movement was observed in the thin top layer of the bed. Then patches of liquefied mud were formed. The sizes and number of these patches increased with time and at a certain moment the entire surface of the bed seemed to be liquefied. The wave heights and pressures measured are presented later.

After approximately half an hour the wave height was slowly decreased to zero, whereupon a current was generated in the flume. The average flow rate was set at 12 $dm^3 \cdot s^{-1}$. In order to prevent consolidation of the fluid mud, the current was set in a very abrupt way. One minute after the flow rate had been set, velocities were measured at five levels over the bed. The measuring time at every level was 1 minute. Subsequently, the flow rate was increased to 24 and 36 $dm^3 \cdot s^{-1}$ and the same velocity measurements were made for these settings of the flow rate. The relatively short measuring time was chosen in order to minimize the removal of fluid mud (out of the test section), during the measurements. Because of the relatively abrupt changes in the average flow rate a long wave was generated in the flume with a period of approximately one minute. The resulting velocity amplitude was approximately 0.5 $cm \cdot s^{-1}$.

The measurements were used to calculate the average velocities and the root-mean-square values. The effect of the long wave on the root-mean-square fluctuations was filtered out by removing three frequencies from the frequency spectrum of every signal, which was obtained by a Fast Fourier Transformation. The removed frequencies were: 0.0167, 0.0333 and 0.05 Hz. The results are shown in figures 5.2.7, 5.2.8 and 5.2.9.

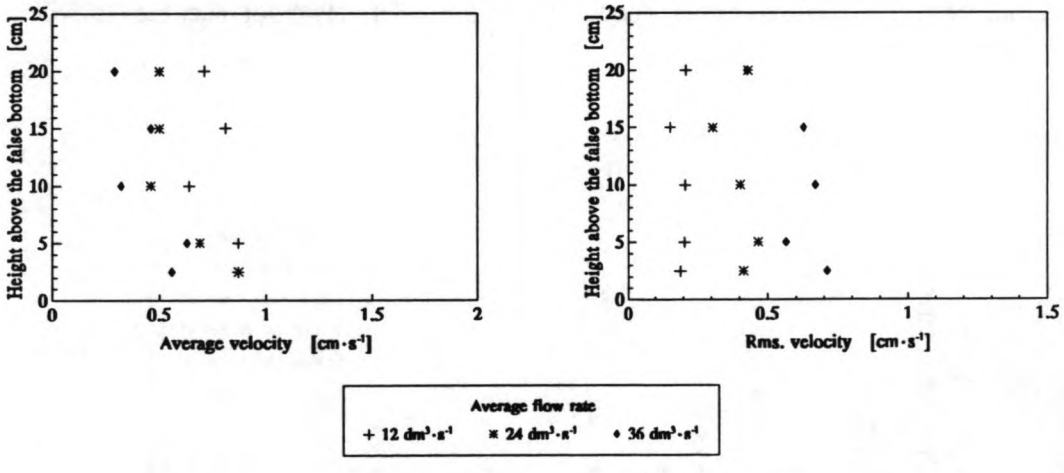

Figure 5.2.7 *Average vertical velocities and rms. velocities measured at x=2.80 m.*

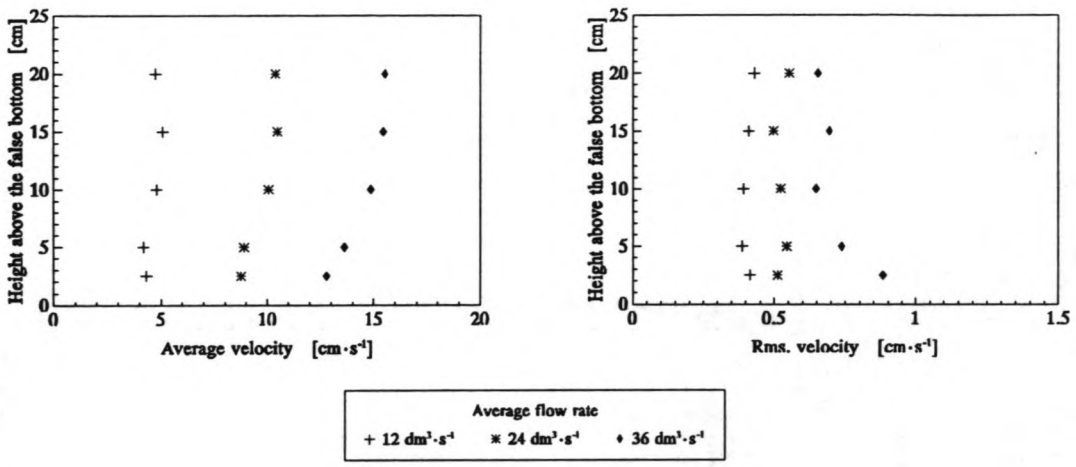

Figure 5.2.8 *Average longitudinal velocities and rms. velocities measured at x=2.80 m.*

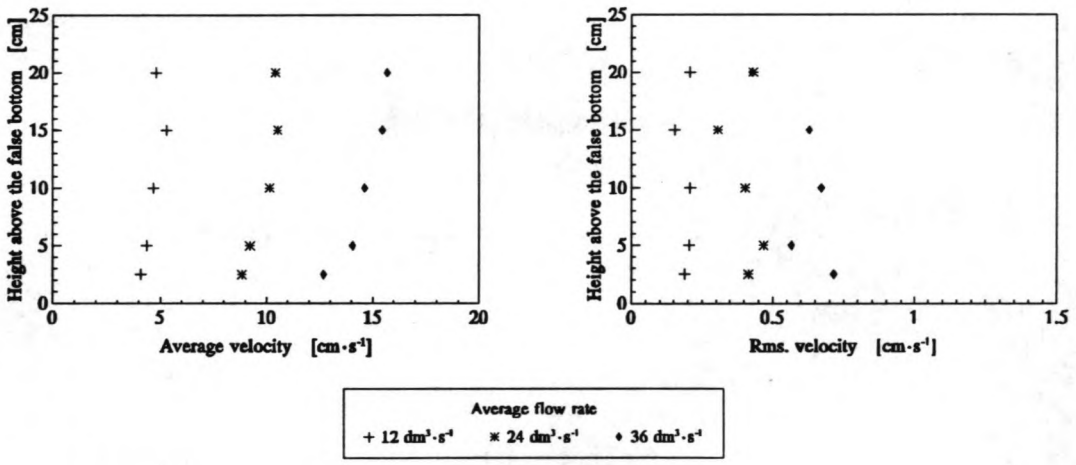

Figure 5.2.9 *Average longitudinal velocities and rms. velocities measured at x=5.13 m.*

The profiles of the velocity components in the longitudinal direction are almost identical to the profiles measured before liquefaction of the bed. However, the turbulence intensities were significantly lower than the intensities measured before liquefaction. This result agrees with the observations made when a dye (potassium permanganate) was added to the water. Due to the movement of the fluid mud the velocity gradient near the bed surface decreased and as a result the turbulence intensities in the overlying water decreased.

The wave-averaged pressures, measured during the waves-only part of test 1, are shown in figure 5.2.10. The cyclic variations in the pressure signals were filtered out using the Fast Fourier Technique. The variations in the pore pressures agree with the results found in experiment 2, keeping in mind that the first part of the measurements was not logged in the second experiment. The pore pressure at z=15.0 cm shows a significant transient decrease followed by a gradual build-up of an excess pore-pressure. A similar trend is observed for the pressures at z=17.5 and z=19.3 cm. However, the pressure change measured at z=19.3 cm is not significant because the maximum error

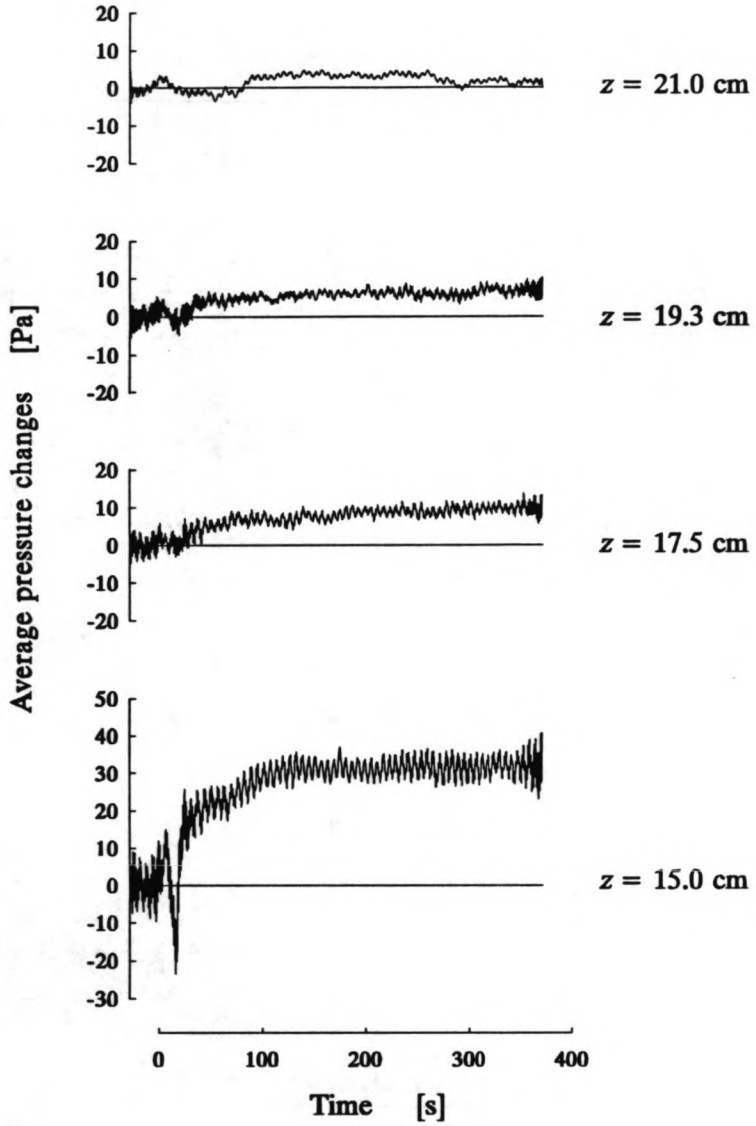

Figure 5.2.10 *Wave-averaged pressure changes during the onset of liquefaction. The bed surface is at $z \approx 19.5$ cm.*

is ± 5 Pa and the position of the transducer relative to the water-mud interface is uncertain. A representative example of the variations in the pressures, recorded approximately 5 minutes after the first waves had travelled over the test section, is shown in figure 5.2.11. No phase shift and little variation in amplitude are observed for this measurement, in contrast to what was found in experiment 2 (figure 4.3.10). The average pressure amplitudes and the average pressure changes during the generation of waves are shown in figures 5.2.12 and 5.2.13, respectively. The average pore-pressure at z=15.0 cm increased during the entire period whereas in the same time the pressure amplitude decreased. The pressure amplitudes and average pressures measured at the other levels were almost constant.

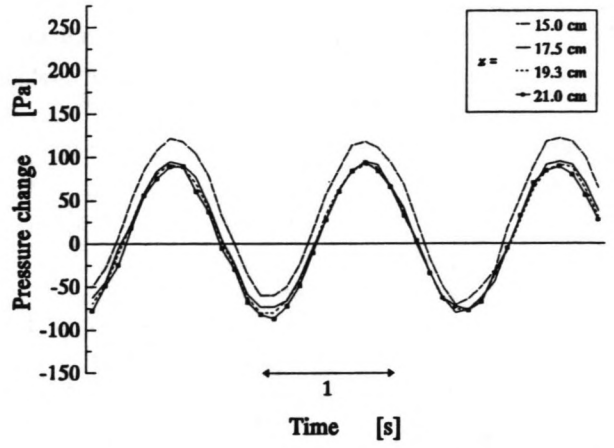

Figure 5.2.11 *Representative example of the unfiltered pressure variations.*

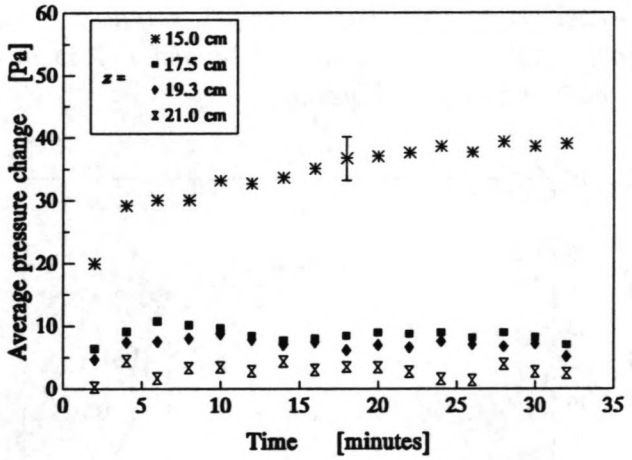

Figure 5.2.12 *Average pressure changes during test 1.*

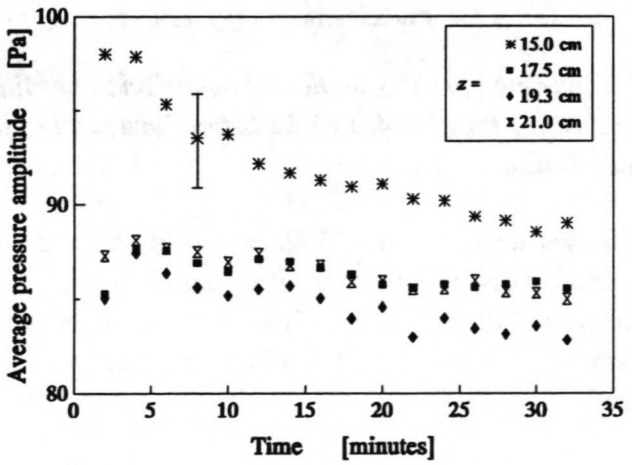

Figure 5.2.13 *Average pressure amplitudes during test 1.*

The average wave heights measured at 6 locations in the test section during this test are shown in figure 5.2.14. As can be seen, the apparent wave damping was not very significant, which was probably caused by a faulty calibration of the wave height meters positioned at x=6.24 and x=7.45 m.

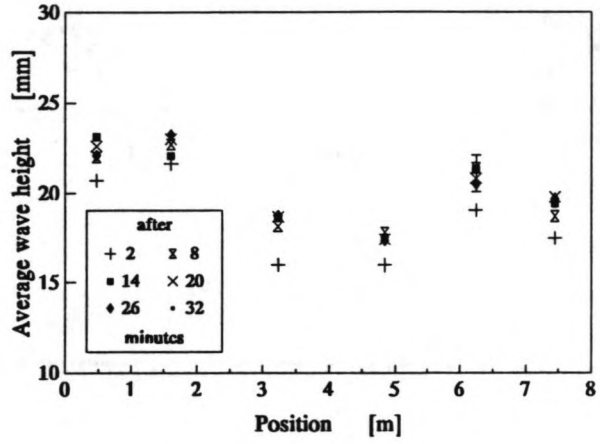

Figure 5.2.14 *Average wave heights during the first half hour of wave action. Wave heights measured at x=6.24 and x=7.45 m may be incorrect because of a faulty calibration.*

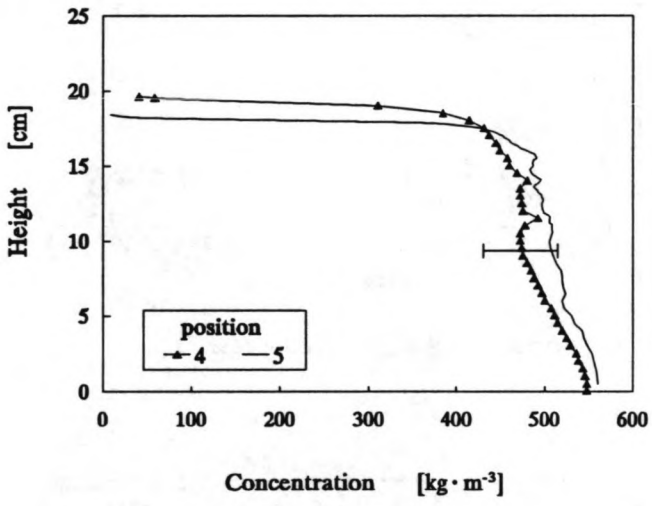

Figure 5.2.15 *Concentration profiles in the bed before and after liquefaction. (y=0.40 m; Position 4: x=5.82 before liquefaction; position 5: x=5.85 after liquefaction)*

A concentration profile was measured at x=5.85 m directly after the velocity measurements. Figure 5.2.15 shows the profile measured at that moment and, for comparison, the profile measured at almost the same location prior to the test. Some of the mud was eroded, which resulted in a smaller thickness of the bed. However, the density structure of the bed was not changed significantly by the wave and/or current action.

5.2.3 Test 2

Test 2 was initiated by generating waves with an average wave height of approximately 38 mm. The wave heights at six locations over the mud compartment are shown in figure 5.2.16. The damping was significant and almost constant over the entire period. An inaccurate calibration of the wave height meters at x=6.24 and x=7.45 m was probably the cause of the increase in wave height at the downstream end of the test section.

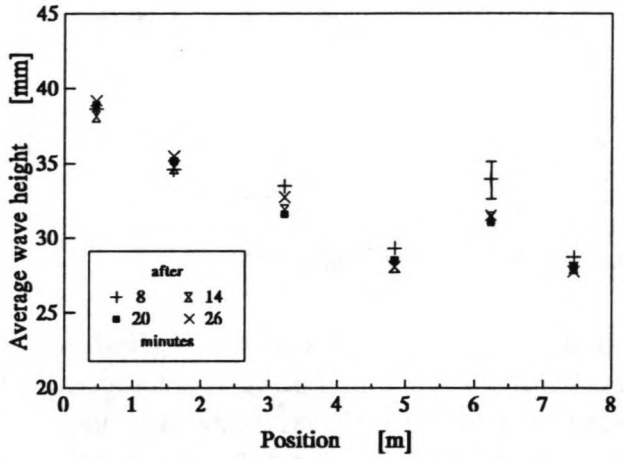

Figure 5.2.16 *Average wave heights during test 2. Wave heights measured at x=6.24 and x=7.45 m may be incorrect because of a faulty calibration.*

The variations in the pressures during this period are shown in figures 5.2.17 and 5.2.18. The changes in average pressures with respect to the pressures measured prior to test 1 are plotted in figure 5.2.17. The excess pore-pressure at 15 cm above the bottom of the flume decreased, whereas the other pressures were almost constant, which is not surprising because the height of the bed was approximately 17.5 cm. The three pressure amplitudes (figure 5.2.18) in the upper part of the vertical were constant, whereas the pressure amplitude at z=15.0 cm tended to decrease.

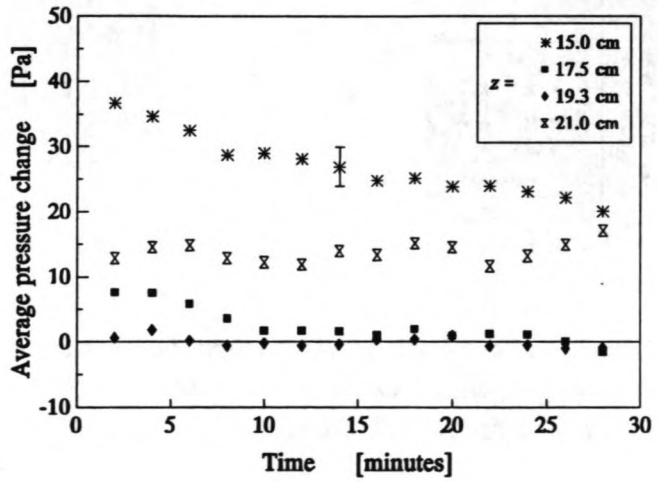

Figure 5.2.17 *Wave-averaged pressure changes during test 2.*

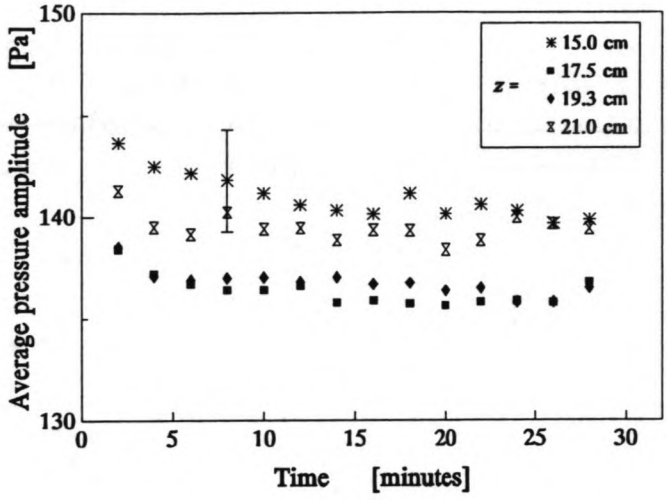

Figure 5.2.18 *Average pressure amplitudes during test 2.*

As in test 1, velocity profiles were measured over the liquefied bed. During the processing of these measurements it was found that these measurements were affected with an unexplained and sometimes dominating noise. The origin of this noise was unknown. Consequently, these measurements are very unreliable and therefore they will not be presented here.

This test was concluded with the generation of waves for half an hour. The average wave height of the incoming waves was about 36 mm. Figure 5.2.19 shows the variation of the average wave height in the test section. A significant and an almost constant wave damping is observed during this period. The peculiar increase of the average wave height at the downstream end of the test section is probably caused by the faulty calibration already mentioned.

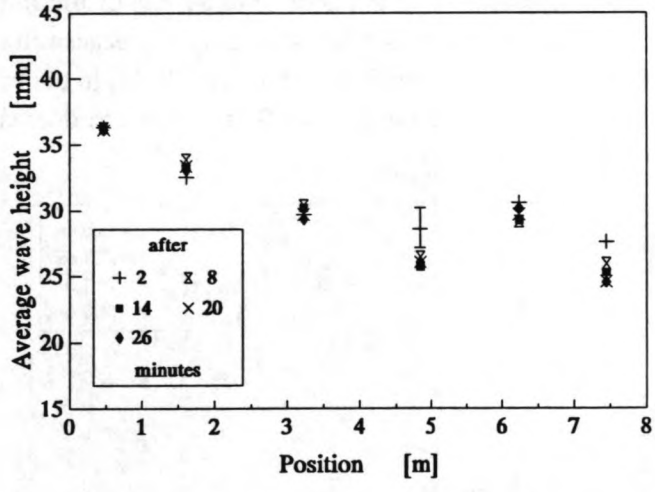

Figure 5.2.19 *Variation of the average wave height during the final part of test 2. Wave heights measured at x=6.24 and x=7.45 m may be incorrect because of a faulty calibration.*

There was almost no change in the wave-averaged pressure changes with respect to the pressures prior to test 1 (figure 5.2.20). The pressures measured at the three lowest levels above the bottom were almost equal to the pressures measured prior to the test. However, the reference pressure at z=21.0 cm seemed to have increased by approximately 30 Pa. This increase is caused by the thermal

drift of the pressure transducer. Measurements showed that the temperature of the water increased by 1 degree centigrade during the test as a result of the dissipation of hydrodynamical energy in the pump. The thermal zero shift and the thermal sensitivity shift of the transducers are ± 0.05% of the range per degree centigrade and ± 0.2% of the reading per degree centigrade, respectively. The range of the reference pressure transducer was 350 mbar and the range of the other transducers was 75 mbar. (1 mbar ≡ 100 Pa) Consequently, the maximal drift of the reference transducer during the test was approximately 27.5 Pa (reading c. 5 kPa) and for the other transducers approximately 9.75 Pa (reading 3 kPa). The average pressure amplitude measured at 15 cm above the bottom tends to decrease (figure 5.2.21) whereas the pressure amplitudes measured at the other levels seem to be fairly constant. The height of the bed at the end of this test was approximately 17.0 cm.

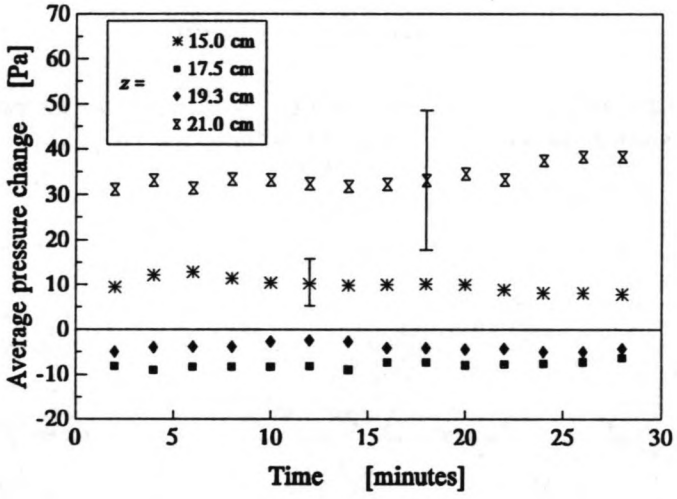

Figure 5.2.20 *Wave-averaged pressure changes during test 2.*

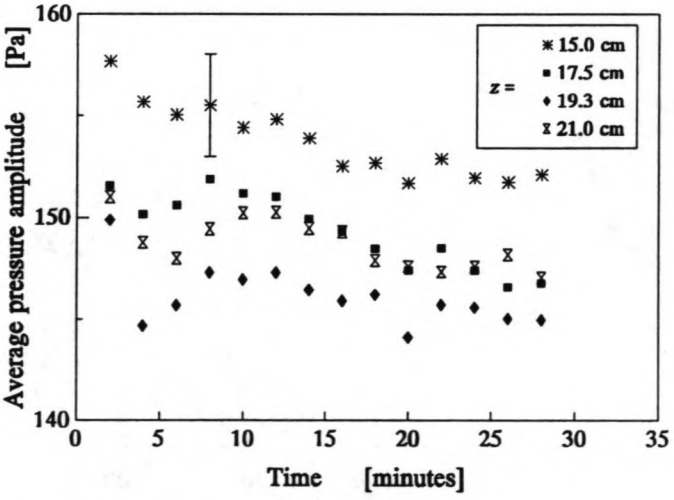

Figure 5.2.21 *Average pressure amplitudes during test 2.*

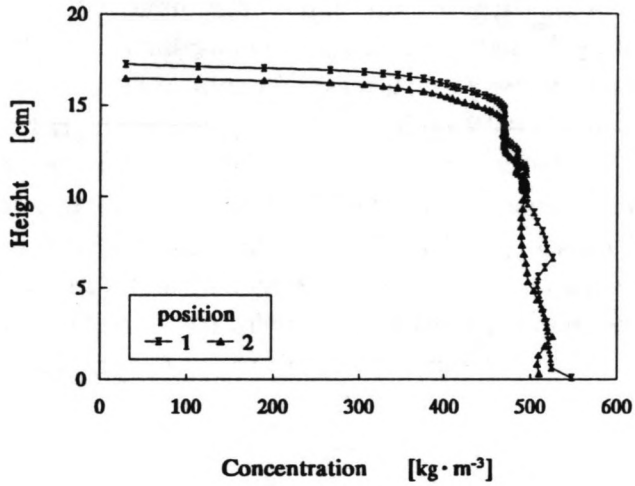

Figure 5.2.22 *Concentration profiles in the bed measured prior to test 3. (y=0.40 m, position 1: x=2.31 m, position 2 : x=5.65 m)*

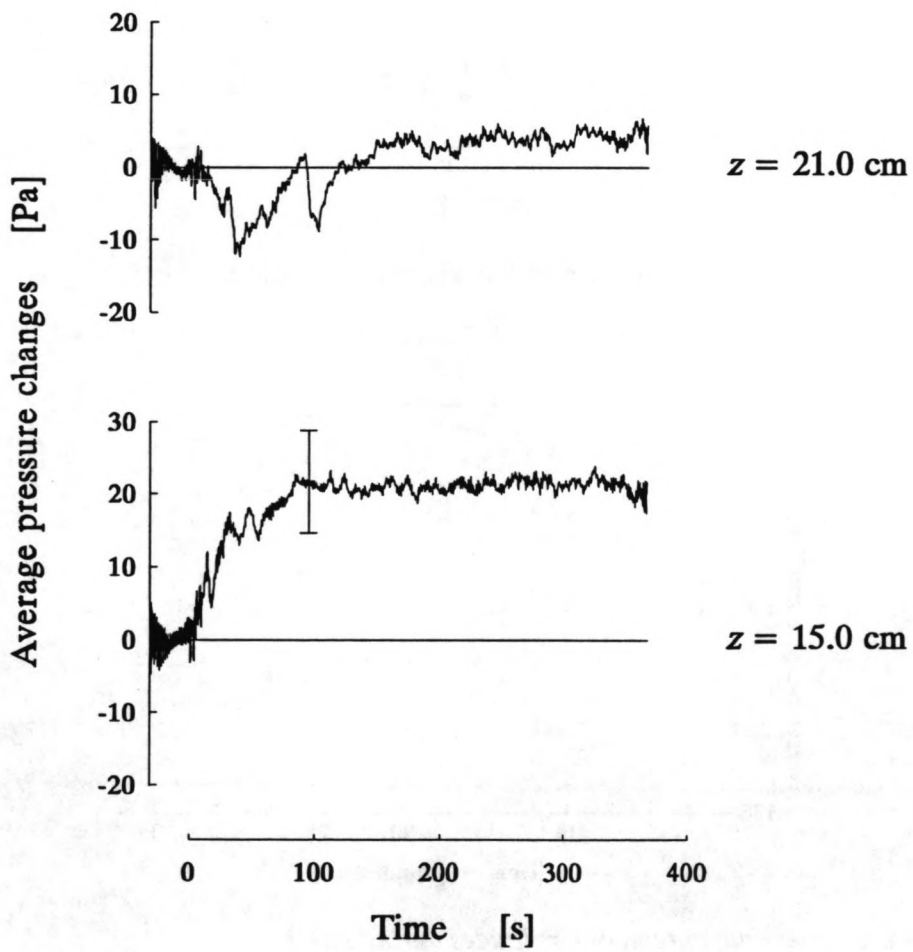

Figure 5.2.23 *Wave-averaged pressure changes at the beginning of test 3.*

5.2.4 Test 3

Concentration profiles were measured at two positions in the bed. The results are shown in figure 5.2.22. The average height of the bed was approximately 17.0 cm. As a result, only one pressure transducer was positioned in the mud.

The objective of this test was to measure velocities in the fluid-mud layer by means of an electromagnetic current meter. For this purpose the wave generator was set to a constant value of the wave height and the wave period was 1.5 s. The average wave height of the incoming waves was approximately 45 mm. As in test 1 the bed started to liquefy as soon as the first waves had travelled over the mud compartment. The variations in wave-averaged pressures measured at z=21.0 and z=15.0 cm are shown in figure 5.2.23. Here the pore pressure again shows a gradual build-up. This excess pore-pressure remained during test 3, as can be seen in figure 5.2.24. The average pressure amplitudes are shown in figure 5.2.25. Again, a gradual decrease in pressure amplitude was observed at z=15.0 cm.

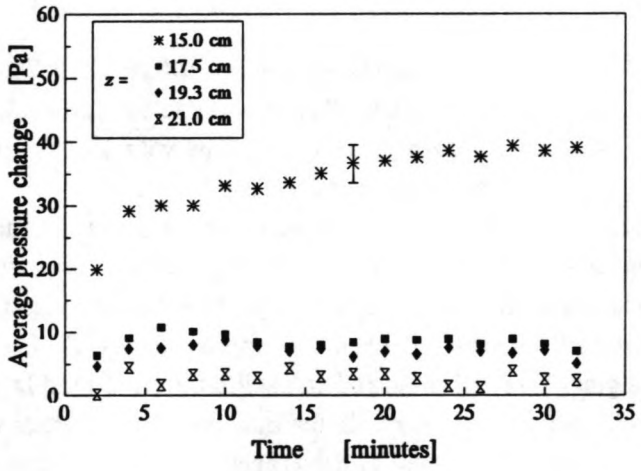

Figure 5.2.24 *Wave averaged pressure changes during test 3.*

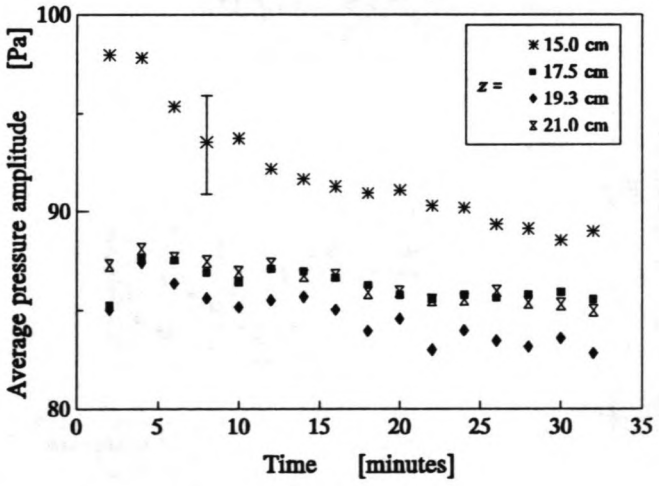

Figure 5.2.25 *Averaged pressure amplitudes during test 3.*

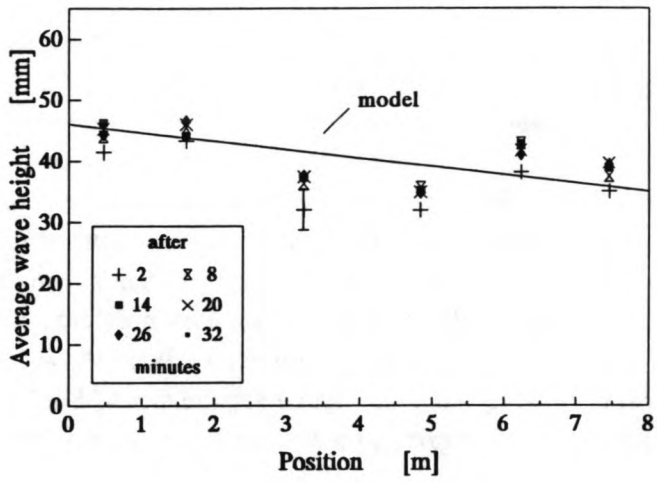

Figure 5.2.26 *Averaged wave heights during test 3 and model result.*

The results of the wave height measurements are shown in figure 5.2.26. This graph also shows the wave height as a function of the distance travelled over the test section calculated according to the modified model of Gade (1958) described in appendix G. The values of the parameters used for this calculation are discussed later. The agreement is fairly good.

An electromagnetic current meter was used to measure velocities in the fluid mud layer after approximately 40 minutes. It was already found that an electromagnetic current meter could be used to measure velocities in a layer of mud (appendix D). The current meter was positioned at the downstream end of the test section, where the bed was approximately 17.5 cm thick at that moment. Visual observations at the glass sidewall indicated an oscillating fluid-mud layer of about 4 cm thick. The electromagnetic current meter was lowered in the mud and the velocities were measured at every measuring point for approximately 2 minutes. The averaged velocity amplitudes calculated from those measurements are shown in figure 5.2.27. These measurements clearly reveal that there was a much thicker oscillating layer of fluid mud. This measurement confirms the visual observations made in previous experiments on China Clay which indicated that a significant boundary layer was present at

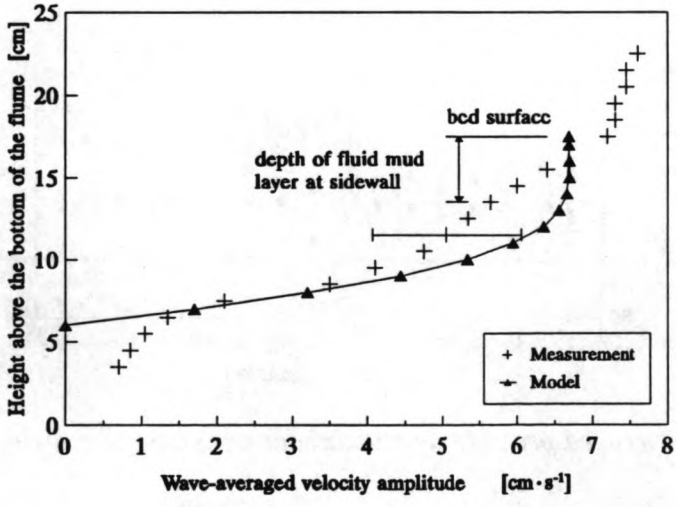

Figure 5.2.27 *Wave-averaged velocity amplitudes in and above a partly liquefied bed. (standard deviation:±0.35 cm·s^{-1})*

the sidewall.

The velocity amplitudes calculated using the model described in appendix G are also shown in figure 5.2.27. The input parameters used for this calculation and also for the calculation of the wave damping were: $\bar{h}_1 = 0.115$ m, $\bar{h}_0 = 0.440$ m, $\eta_0 = 0.02$ m, $\rho_2 = 1316$ kg·m^{-3} and $\nu_2 = 2.66 \cdot 10^{-3}$ m^2·s^{-1} (De Wit, 1992a). The calculated and measured velocity amplitudes correspond reasonably well.

5.2.5 Test 4

On 23 June 1993 velocities were measured in a layer of fluid mud when both waves and current were present. Prior to this test concentration profiles were measured (figure 5.2.28). The average concentration was very high so that it was difficult to generate a fluid-mud layer of sufficient thickness.

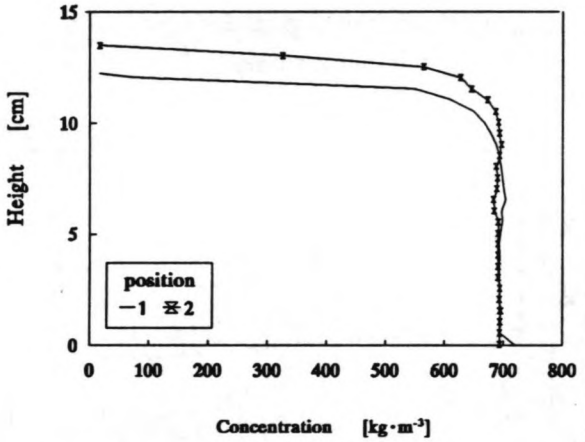

Figure 5.2.28 *Concentration profile measured prior to test 4. (y=0.20 m, position 1: x=3.68 m, position 2: x=5.68 m)*

Waves were generated for approximately 4 hours to generate a fluid mud layer. The average wave heights measured in the test section are shown in figure 5.2.29. Then a current meter was lowered in the fluid-mud layer and at the same time a conductivity probe was used to measure concentrations in the vicinity of the velocity gauge. Initially only waves were present in the flume. The results of the averaged velocity amplitudes are shown in figure 5.2.30 and the concentration profile measured at the same time, is shown in figure 5.2.31.

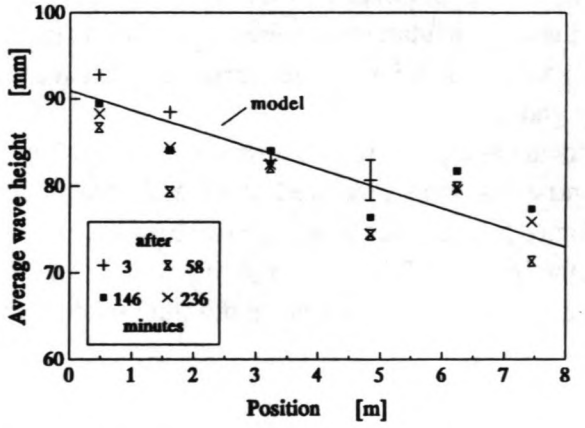

Figure 5.2.29 *Average wave heights during the first part of test 4 and model result.*

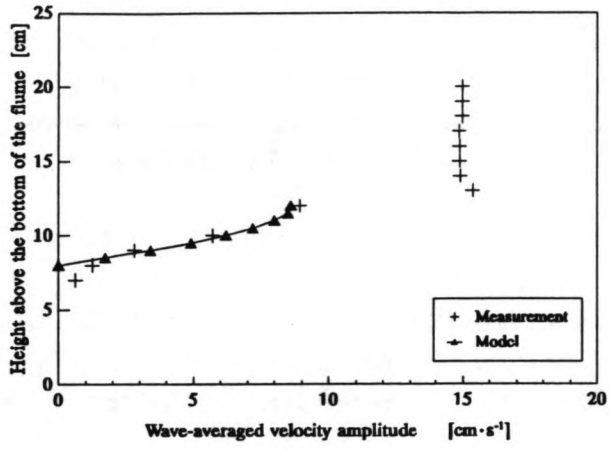

Figure 5.2.30 *Wave-averaged velocity amplitudes over and in the partly liquefied bed. (waves only)*

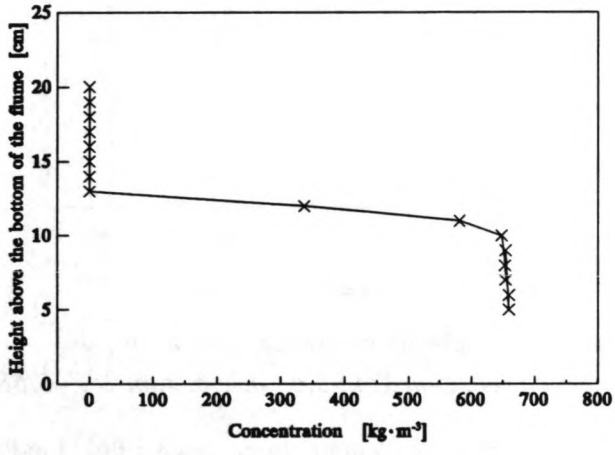

Figure 5.2.31 *Concentration profile (waves only).*

The measured velocity amplitudes show a similar trend as in test 3 (figure 5.2.27) and the concentration profile clearly indicates that the electromagnetic current meter was in the fluid-mud layer when the measurements were made. In figures 5.2.29 and 5.2.30 also the wave attenuation and velocity amplitudes calculated using the model as described in appendix G are shown. The input parameters used for these calculations were: $\rho_2 = 1316$ kg·m^{-3}, $\nu_2 = 2.66 \cdot 10^{-3}$ m^2·s^{-1}, $\bar{h}_1 = 0.04$ m, $\bar{h}_0 = 0.41$ m and $\eta_0 = 0.045$ m. The agreement between the calculations and the measurements is also fairly good.

After these measurements the pump was turned on and an average flow rate of 24 dm^3·s^{-1} was set. Then velocities and concentrations were measured at several levels. The wave-averaged velocity amplitudes are shown in figure 5.2.32. The average velocities are shown in figure 5.2.33 and the concentration profile is shown in figure 5.2.34. Comparing figures 5.2.33 and 5.2.34 clearly shows a significant average velocity caused by the current in the fluid mud layer at z=12 cm.

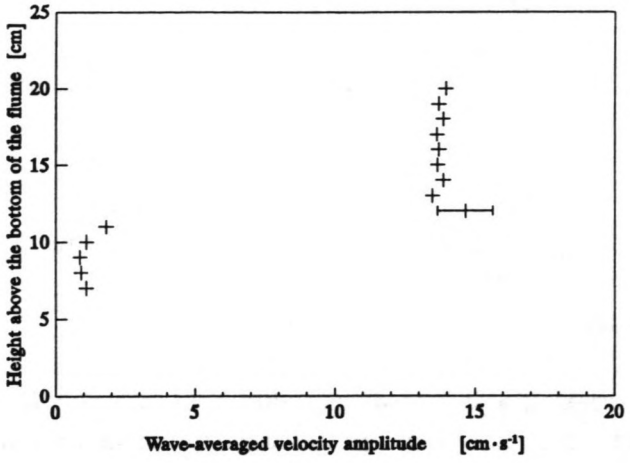

Figure 5.2.32 *Wave-averaged velocity amplitudes when waves and current were present.*

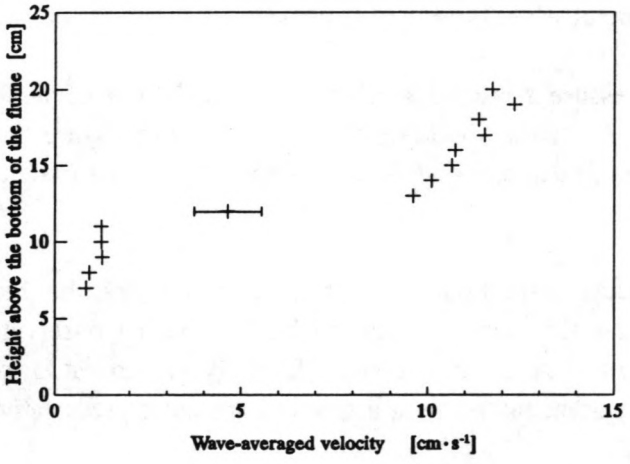

Figure 5.2.33 *Average velocities when waves and current were present.*

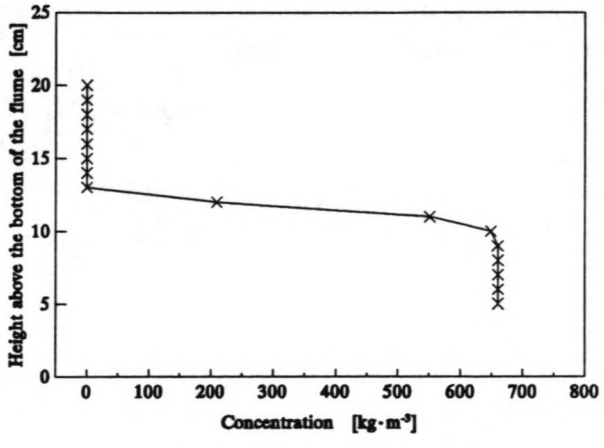

Figure 5.2.34 *Concentration profile when waves and current were present.*

5.3 Conclusions

The following conclusions may be drawn from the results of the third experiment.

- The velocity measurements over the non-liquefied bed confirmed that the electro magnetic current meters can be used to measure turbulence intensities. Even the relatively small fluctuations of the vertical velocity components (w) can be measured well. The results obtained agree with the empirical relations for the turbulence intensities in open-channel flows according to Nezu and Nagawaka (1993).

- Fluid mud was generated almost immediately after the first waves had travelled over the test section, which result was similar to that obtained in the second experiment.

- The root-mean-square velocities measured above the non-liquefied bed are larger than the those measured above a liquefied bed under almost similar flow conditions. This quantitative result confirms the visual observations made when the water was dyed; the turbulence intensities decrease to some extent when fluid mud is present.

- In test 1 the pore-pressure measured at 15 cm above the bottom of the flume showed a transient decrease followed by a gradual build-up of an excess pore-pressure. Furthermore, the average pore-pressure amplitude decreases while the average pore-pressure is increasing. A similar trend was found in test 2.

- Velocity measurements in the liquefied-mud layer showed that the thickness of the fluid-mud layer is much greater than expected on the basis of visual observations made at the glass sidewall of the flume. A thick boundary layer is present at a sidewall. Consequently, observations or measurements made at a sidewall are not representative of the actual physical processes in the bed.

- Velocities in the fluid mud calculated using the modified model of Gade (appendix A) correspond fairly well with the velocities measured in the fluid mud. The calculated wave damping corresponds also with that in the measurements. The assumption of the fluid mud to be a viscous fluid seems to be justified by these results.

Chapter 6

General conclusions

In all of the experiments on China Clay it was observed that a layer of fluid mud was formed as soon as the wave height exceeded a certain threshold value. This value increased with the consolidation period of the China Clay. In table 6.1 the consolidation periods and the wave heights at which liquefaction occurred are listed for the different experiments.

Table 6.1 *Consolidation periods and wave heights at which liquefaction occurred.*

Experiment no.	date	consolidation period [days]	wave height at which liquefaction occurred [mm]
I	June 1991	22	c. 81
II	December 1991	9	c. 23
III	June 1992	6	c. 21

Although the assumption of China Clay being a poro-elastic material is not quite appropriate, the calculated (Spierenburg, 1989) pressure-induced shear stresses in a finite layer of a poro-elastic material are of the same order of magnitude as the yield stresses. Consequently, these shear stresses may play an important role in the liquefaction process of China Clay.

The wave height was significantly damped as soon as a layer of fluid mud was generated. The damping was only little influenced by a current.

The good agreement between the measured turbulence intensities and the calculated intensities according to Nezu and Nakagawa (1993) for an open-channel flow indicate that an electromagnetic current meter is suitable for measuring turbulence intensities for flow conditions as encountered during the experiments on China Clay.

The velocity measurements made with such an electromagnetic current meter clearly showed that the turbulence intensities decreased in a stationary current when a layer of fluid mud was present, which corresponded with the visual observations made using a dye.

Fluid mud was transported very easily by a current and hardly any mud was entrained into the water layer during this process.

Usually visual observations and pressure measurements are made at a transparent sidewall of a set-up. However, from the measurements made with an electromagnetic current meter it was found that observations or measurements made at a sidewall are not representative of the actual physical processes away from the sidewalls. Only measurements carried out far from a wall give a quantitative description of the processes inside the bed.

Pore-pressure measurements showed a transient decrease in average pressure, possibly caused by the breakdown of the aggregate structure, succeeded by a gradual build up of an excess pore pressure so as to compensate for the reduced effective stress.

The measured wave damping and velocity amplitudes in the fluid mud correspond well with calculated results using the modified model of Gade (1958). This result seems to validate that the rheological properties of fluid China Clay can be modelled as a Newtonian fluid for this purpose.

Appendix A

Wave and current characteristics of the set-up

A number of tests were carried out to measure wave and current characteristics of the flume. During these tests a temporary cement false-bottom was placed over the test section. The measuring procedures and the results of these tests will be described next. In section A.1 the measured wave characteristics will be discussed. At the downstream end of the flume a special wave damper was installed (see figure 3.1.6). The performance of this wave damper was also determined. The procedure and the results of these tests will be presented in section A.2. Section A.3 is concerned with the current characteristics of the set-up, which were determined in stationary tests. Finally, in section A.4 the results will be presented of measurements made when both waves and current were present in the flume.

A.1 Wave decay

Four wave height meters were installed at an equal mutual distance in order to measure wave characteristics. The locations of the wave gauges are shown in figure A.1.1. The wave height meters were numbered 1 to 4 in the downstream direction and calibrated as described by De Wit (1992b).

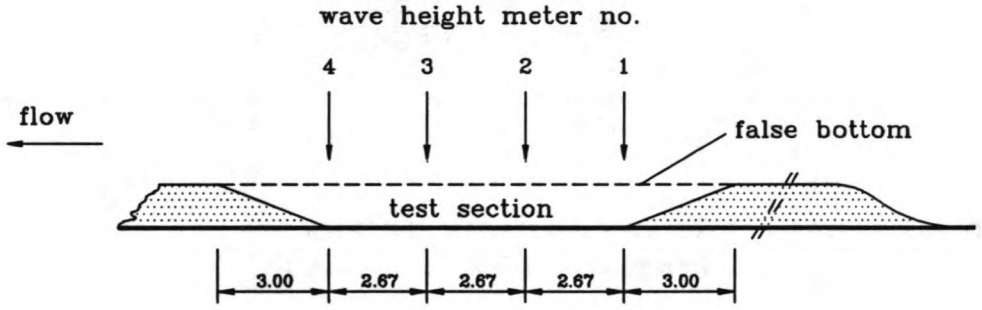

Figure A.1.1 *Configuration in which wave characteristics were measured. (Dimensions in metre)*

The water depth over the closed test section was 30 cm and regular waves were generated with a constant wave period of 1.49 ± 0.05 s. The measurements were recorded on a Hewlet Packard 7404A pen-recorder. The wave height was increased step by step ranging from 1 cm to 11 cm. Three representative measurements made at three different wave heights are shown in figures A.1.1, A.1.2 and A.1.3. The accuracy of the average wave height is ± 2%.

From these measurements it can be observed that over the whole range of generated wave heights the wave shape is almost sinusoidal. Furthermore, comparing the recordings of the four wave height meters shows that the wave shape does not change significantly and that there is no significant wave damping when the waves propagate over the test section.

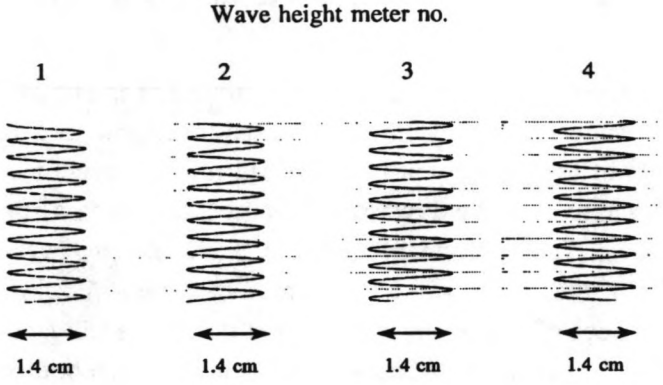

Figure A.1.2 *Wave profiles recorded over the closed test section. Average wave height: 1.40 ± 0.03 cm*

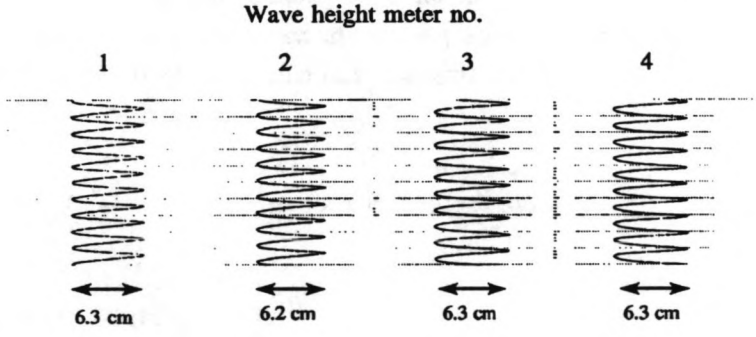

Figure A.1.3 *Wave profiles recorded over the closed test section. Average wave height: 6.3 ± 0.1 cm*

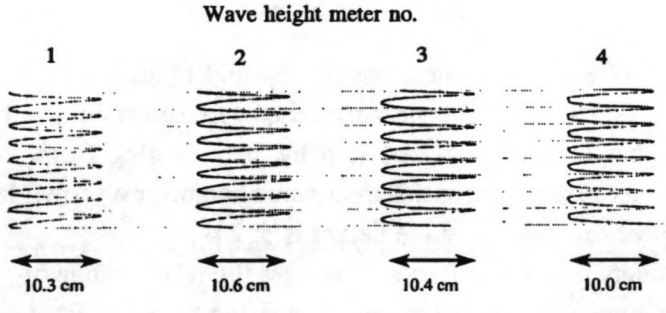

Figure A.1.4 *Wave profiles measured over the closed test section. Average wave height: 10.3 ± 0.2 cm*

A.2 Wave reflection

Part of the generated waves will be reflected by the non-ideal wave damper and in a lesser amount by changes in water depth. In order to test the performance of the wave damper several measurements were carried out. The measurements were used to estimate the incident and reflected waves in the flume. The results were used to calculate an estimate of the reflection coefficient of the wave damper.

The measured surface elevation at a certain location is a superposition of the surface elevation of the incident and reflected wave, η_i and η_r, respectively. A general description of non-damping waves propagating along the x coordinate direction is

$$\left.\begin{aligned} \eta_i &= a_i \cos(kx - \omega t + \epsilon_i) \\ \eta_r &= a_r \cos(kx + \omega t + \epsilon_r) \end{aligned}\right\} \qquad \text{(A.2.1)}$$

where k is the wave number, ω is the angular frequency and ϵ_i and ϵ_r are the phase angles of the incident and reflected waves.

When two surface elevations, η_1 and η_2, are simultaneously recorded at two adjacent positions x_1 and $x_2 = x_1 + \Delta l$, respectively, the measured surface elevation will be (Goda, 1976)

$$\left.\begin{aligned} \eta_1 &= (\eta_i + \eta_r)_{x=x_1} = A_1 \cos\omega t + B_1 \sin\omega t \\ \eta_2 &= (\eta_i + \eta_r)_{x=x_2} = A_2 \cos\omega t + B_1 \sin\omega t \end{aligned}\right\} \qquad \text{(A.2.2)}$$

where

$$\left.\begin{aligned} A_1 &= a_i \cos\phi_i + a_r \cos\phi_r \\ B_1 &= a_i \sin\phi_i - a_r \sin\phi_r \\ A_2 &= a_i \cos(k\Delta l + \phi_i) + a_r \cos(k\Delta l + \phi_r) \\ B_2 &= a_i \sin(k\Delta l + \phi_i) - a_r \sin(k\Delta l + \phi_r) \end{aligned}\right\} \qquad \text{(A.2.3)}$$

$$\left.\begin{aligned} \phi_i &= kx_1 + \epsilon_i \\ \phi_r &= kx_1 + \epsilon_r \end{aligned}\right\} \qquad \text{(A.2.4)}$$

Substituting equation A.2.1 in equation A.2.2 yields

$$a_i = \frac{1}{2|\sin k\Delta l|}\sqrt{(A_2 - A_1\cos k\Delta l - B_1\sin k\Delta l)^2 + (B_2 + A_1\sin k\Delta l - B_1\cos k\Delta l)^2} \quad \text{(A.2.5)}$$

$$a_r = \frac{1}{2|\sin k\Delta l|}\sqrt{(A_2 - A_1\cos k\Delta l + B_1\sin k\Delta l)^2 + (B_2 - A_1\sin k\Delta l - B_1\cos k\Delta l)^2} \quad \text{(A.2.6)}$$

When regular wave profiles measured in flume are analyzed using a Fourier transform, it is possible to estimate the value of the amplitudes A_1, B_1, A_2 and B_2 for the fundamental frequency as well as for higher harmonics, for actual wave profiles contain some higher harmonics. Substituting these values in equations A.2.5 and A.2.6 and using linear short-wave theory yields an estimation of a_i and a_r. Next the reflection coefficient R can be calculated using

$$R = \sqrt{\frac{a_r^2}{a_i^2}} \quad \text{(A.2.7)}$$

The described procedure of estimating the reflection coefficient of an object is valid for one incoming and one reflected wave. However, the reflected waves in a closed, laboratory flume will be reflected again by the wave paddle and consequently waves may travel many times between a reflective model structure and the wave paddle. However, this phenomenon is neglected.

Above the closed test section two pairs of wave height meters, A and B, were installed. The intervals between the wave height meters of pair A and pair B were 2.94 and 1.76 m, respectively. The wave generator was set at a constant wave height and period (1.49 s) and after 15 minutes wave records were simultaneously taken of the four wave height meters. The water depth was 30 cm. The measurements were recorded on a personal computer with a sample rate of 53.3 Hz. Measurements were made for four different settings of the wave height.

The measurements were analyzed using a Fast Fourier Transformation technic and the coefficients A_1, A_2, B_1 and B_2 were determined for the basic frequency. Finally, the reflection coefficient was calculated from equation A.2.7. The calculated reflection coefficients are listed for several wave heights in table A.2.1. It can be seen that the performance of this fairly simple wave damper was quite good. The assumption made that no multiple reflected waves were present in the flume appeared to be reasonable, for the measured reflection coefficients were quite low.

Table A.2.1 *Calculated reflection coefficients for various wave heights.*

average wave height [mm]	R*) (measurement A) [%]	R*) (measurement B) [%]
25.0 ± 0.5	5	3
52.0 ± 0.6	5	5
76.0 ± 0.6	4	3
102 ± 1	3	3

*) Standard deviation of the reflection coefficient is ± 3%.

A.3 Current characteristics

Electromagnetic current meters were used to measure velocity profiles in order to learn more about the flow characteristics over the closed test section. The maximum error of these current meters is 0.5 $cm \cdot s^{-1}$ for flow velocities smaller than 20 $cm \cdot s^{-1}$. Although the electromagnetic current meters are capable of measuring the velocity components in the longitudinal and transverse direction, only the velocity components in the longitudinal direction were measured. See for further information on the electromagnetic current meters De Wit (1992b).

First preliminary measurements were carried out in order to assess if the flow in the flume was symmetrical with respect to the centre-line of the flume. These measurements were made at location *a* at six positions in the cross-section of the flume (figure A.3.1) for three different settings of the flow rate. The measurements were logged on a personal computer with a sample rate of 10 Hz. During these measurements no waves were present in the flume.

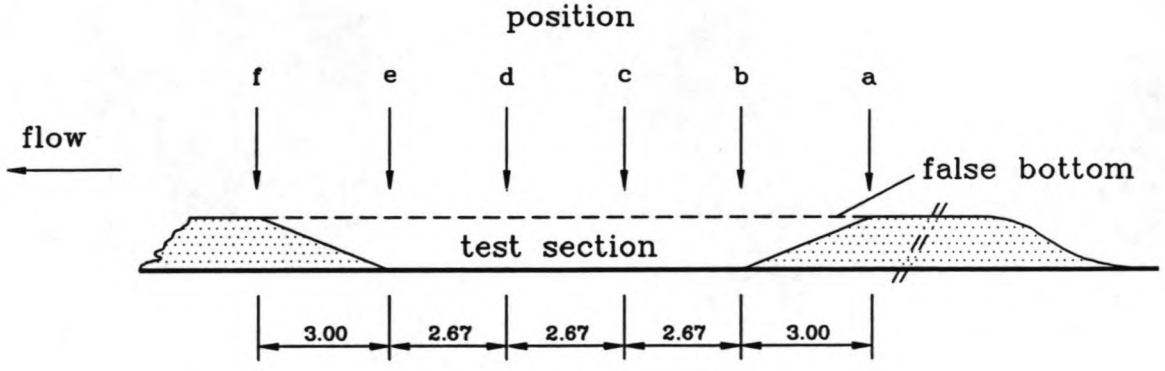

Figure A.3.1 *Locations at which velocity profiles were measured. (Dimensions in metre)*

Some results of these measurements are presented in figure A.3.2. These graphs show three minute averages of the velocities in the longitudinal direction of the flume measured at several heights above the bottom and at several positions in the cross-section. The sidewall of the flume that is used as a reference in figure A.3.2 and also in figures A.3.3 - A.3.5 is the side wall at the right hand side when looking in the downstream direction of the flume. As can be seen the steady-state flow is fairly

symmetrical for the different flow velocities.

Knowing that the flow was symmetrical, additional tests were carried out to measure more accurately the flow characteristics over the test section. For this purpose the velocity profiles were measured in six cross-sections at four different locations for three settings of the average flow velocity. The positions of the different cross-sections are shown in figure A.3.1. The results of these measurements are shown in figures A.3.3, A.3.4 and A.3.5. The presented velocity values are the longitudinal velocities and they are averaged over three minutes.

Comparing the measurements made at position *a* down to position *f* it can be observed that in the lower part of the water column (2 to 5 cm above the bottom) the velocity gradient is increasing in the downstream direction, which is caused by increasing influence of bottom friction. However, the average velocity at 2 cm above the false bottom is fairly constant. Furthermore, the influence of the sidewall friction on the flow velocity gets increasingly noticeable in the upper part of the vertical at positions close to the sidewall when moving in the downstream direction.

Although the electromagnetic current meters are not well suited to measure turbulence characteristics, the measurements were also used to calculate the turbulence intensities. Only the measurements made in the centre of each cross-section were used for this analysis. The sample time was 22.16 ms ($\approx$ 45 Hz) and the average was taken over 6000 samples ($\approx$ 133 s). The turbulence intensities (root-mean-square velocities) in the longitudinal direction are shown in figure A.3.6 for three different settings of the average flow rate.

Finally, the root-mean-square velocities measured at the three upstream positions (*a*, *b*, *c*) and the three downstream positions (*d*, *e*, *f*) were averaged for every setting of the flow rate. These average variations of the relative turbulence intensities versus the dimensionless height are shown in figures A.3.7 and A.3.8 for three settings of the flow rate. See section 4.3.2 for the explanation of the symbols. Figure A.3.7 shows the average relative variations measured at the positions *a*, *b*, and *c* and the average relative variations measured at the positions *d*, *e* and *f* are shown in figure A.3.8.

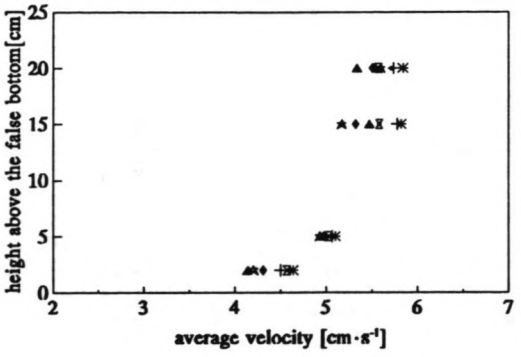

a)

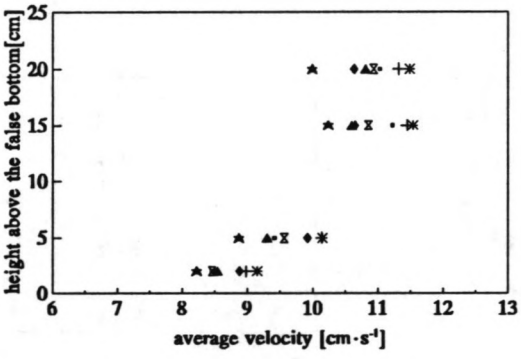

b)

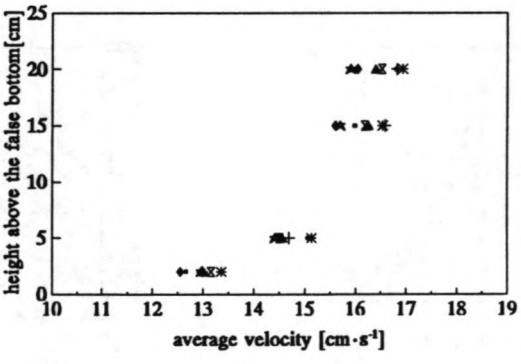

c)

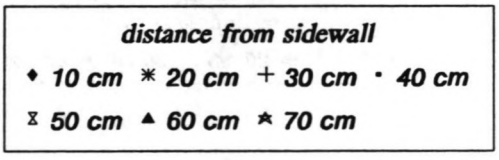

Figure A.3.2 *Velocity profiles measured at 7 positions in location a for three different settings of the flow rate (a, b, c). The width of the flume was 80 cm.*

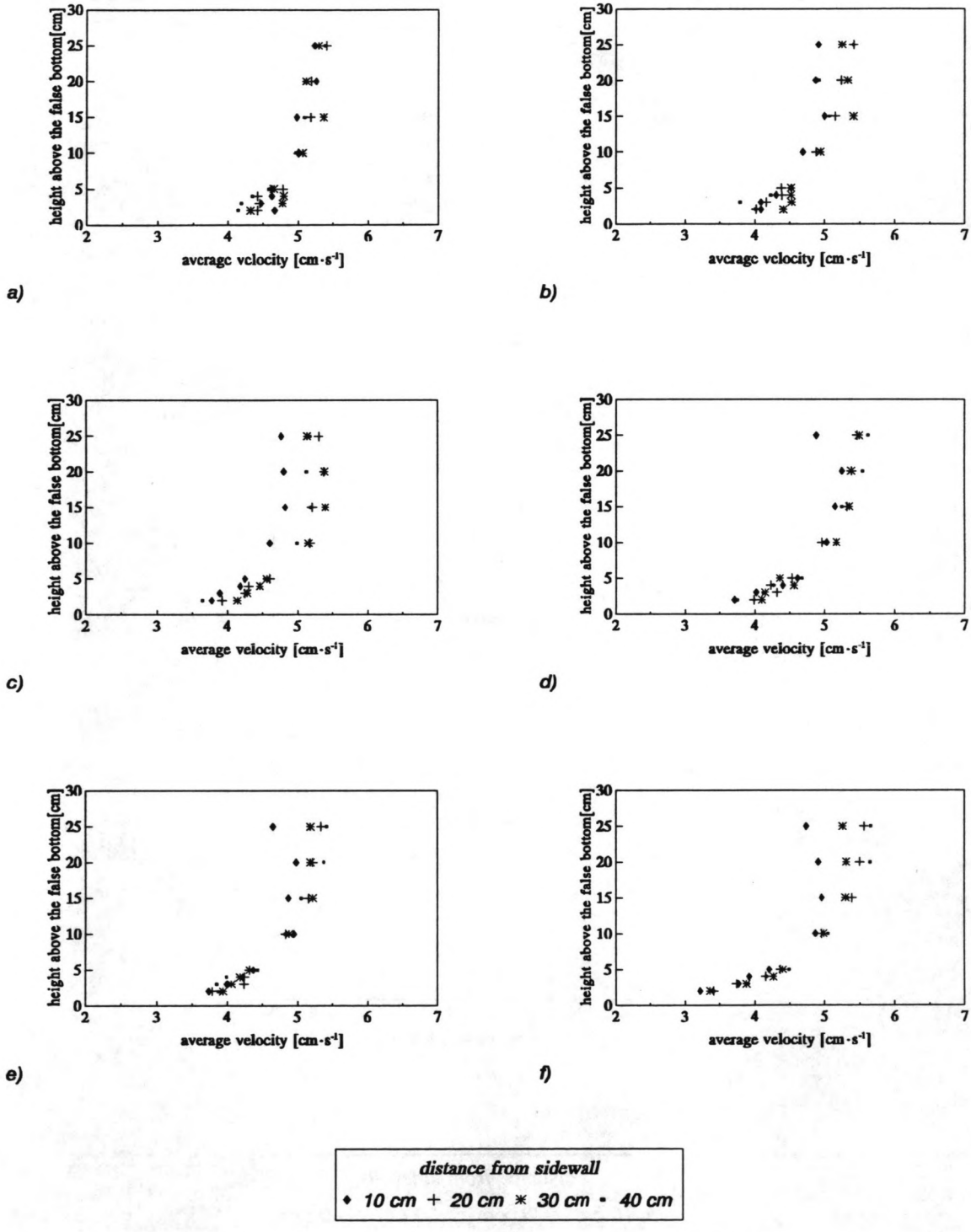

Figure A.3.3 *Velocity profiles measured at 4 positions in cross-sections a) - f). Flow rate: 12 $dm^3 \cdot s^{-1}$. The width of the flume was 80 cm.*

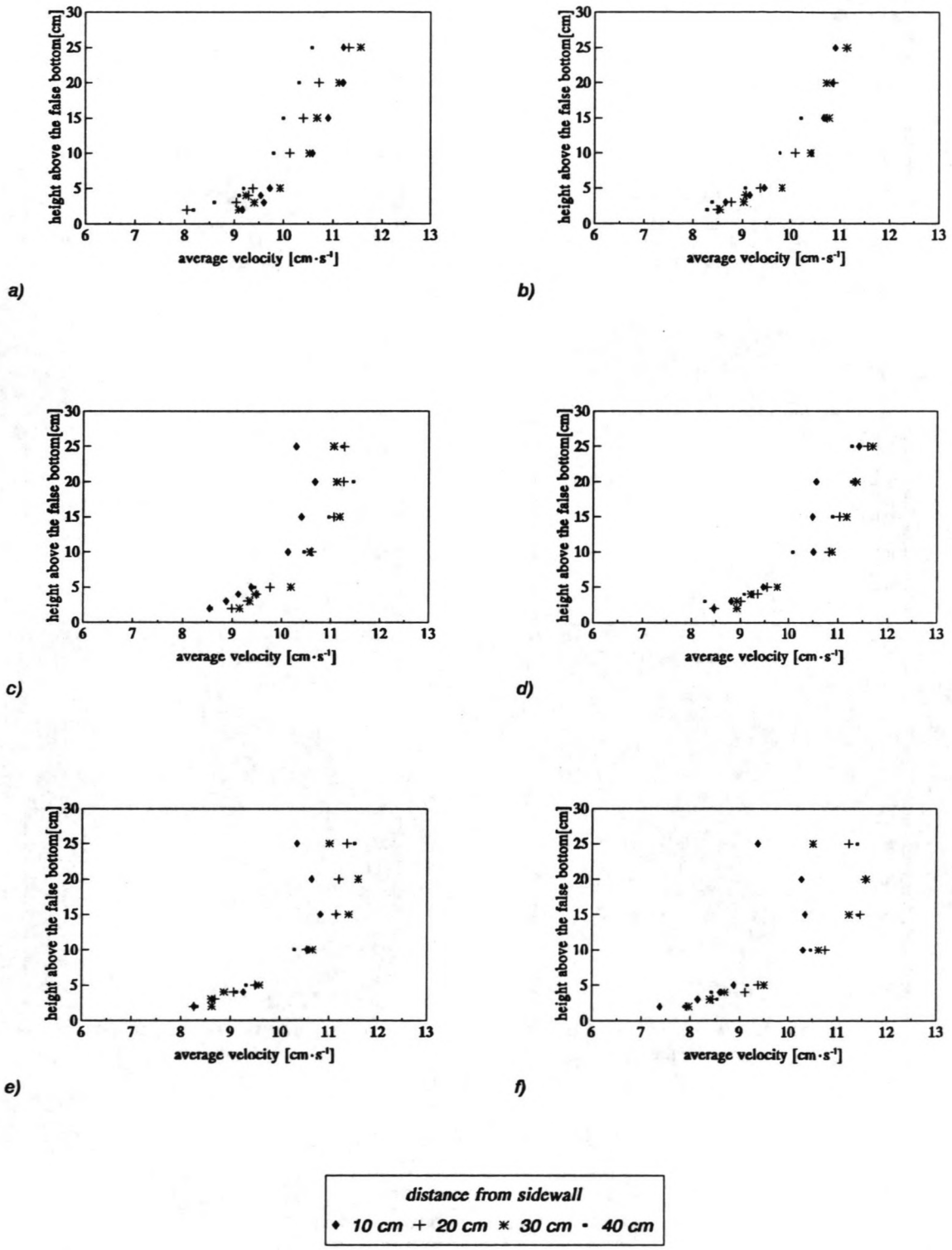

Figure A.3.4 *Velocity profiles measured at 4 positions in cross-sections a) - f). Flow rate: 24 $dm^3 \cdot s^{-1}$. The width of the flume was 80 cm.*

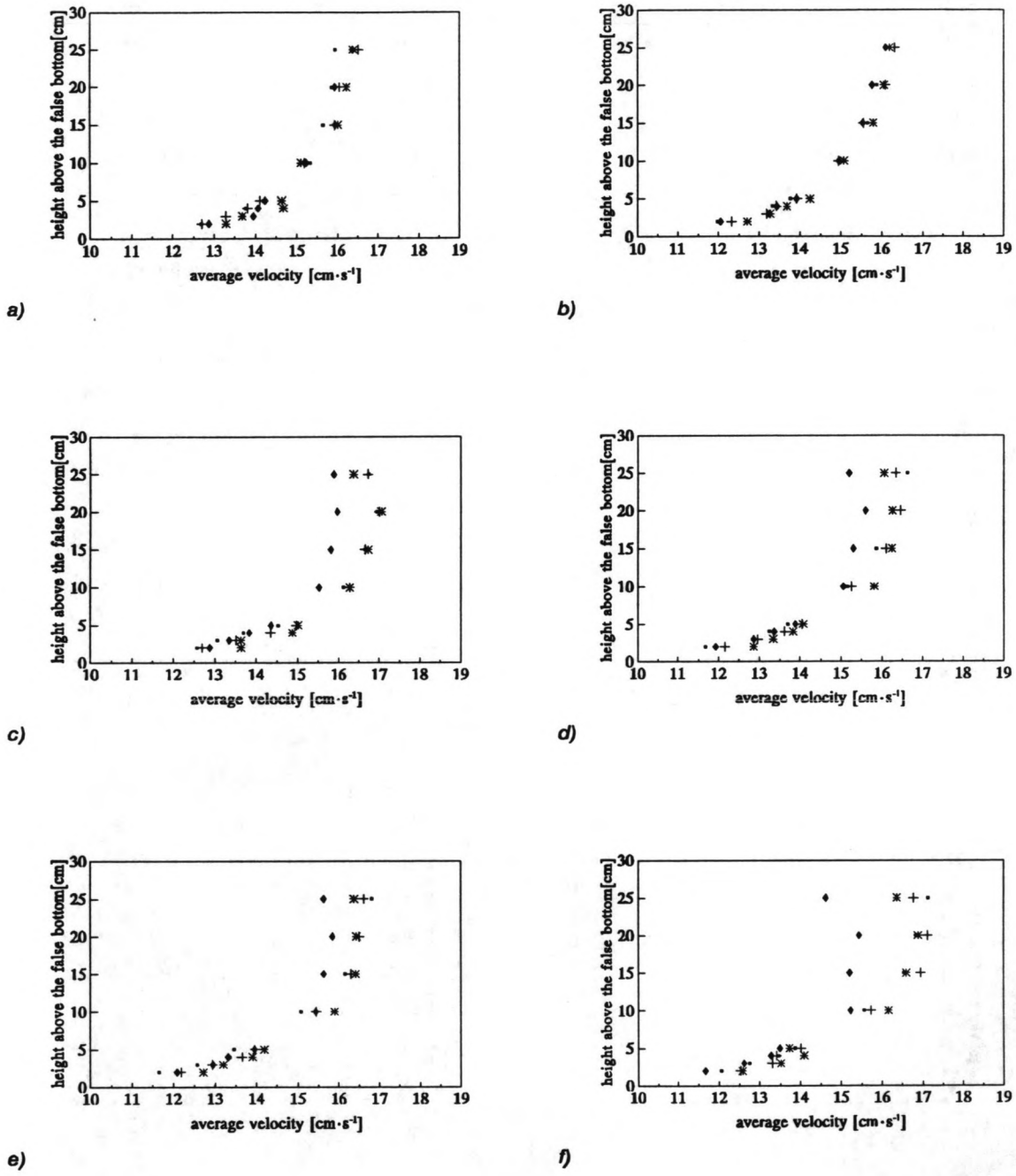

Figure A.3.5 *Velocity profiles measured at 4 positions in cross-sections a) - f). Flow rate: 36 $dm^3 \cdot s^{-1}$. The width of the flume was 80 cm.*

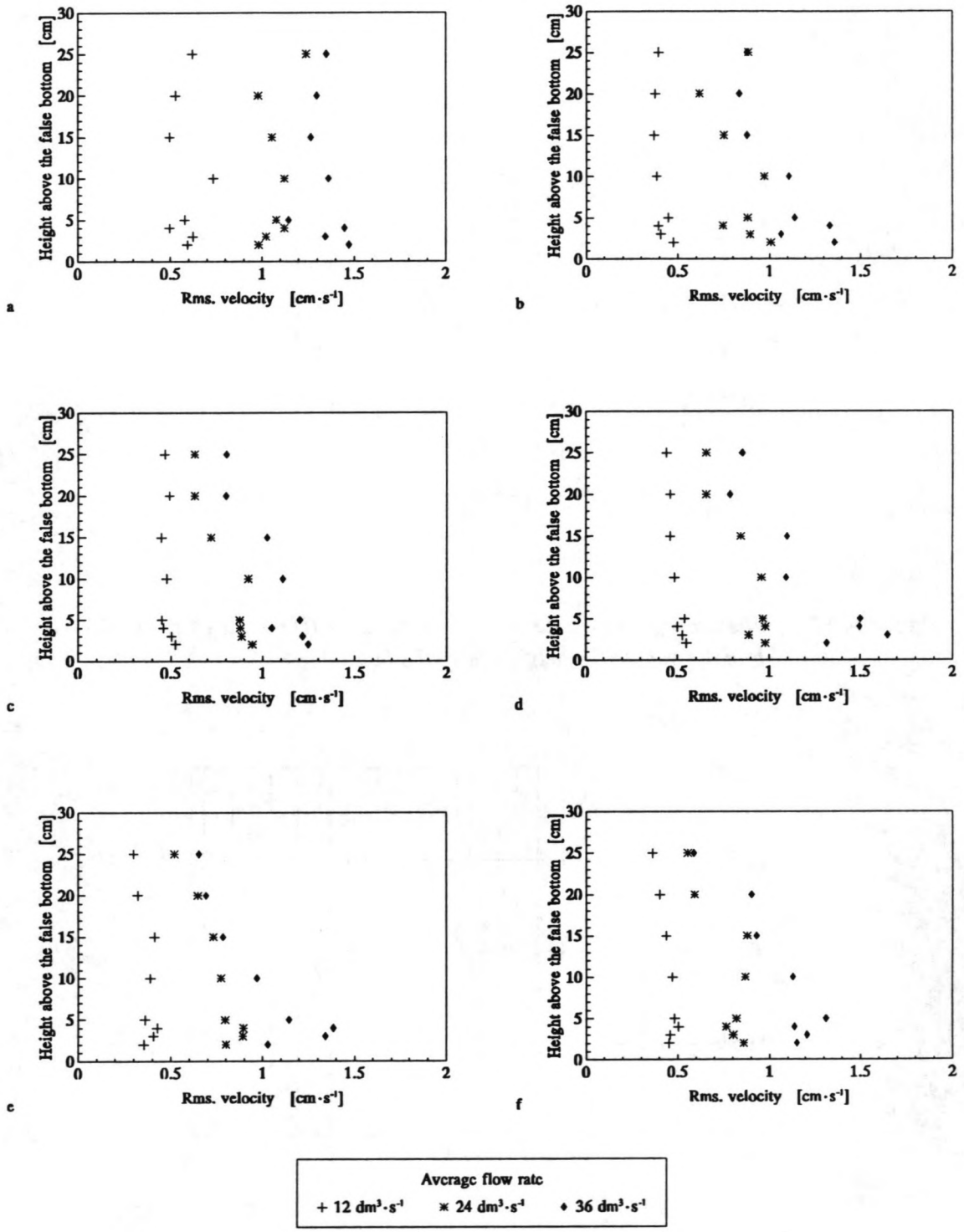

Figure A.3.6 *Root-mean-square velocities in the longitudinal direction in six cross-sections a) - f) for several settings of the average flow rate.*

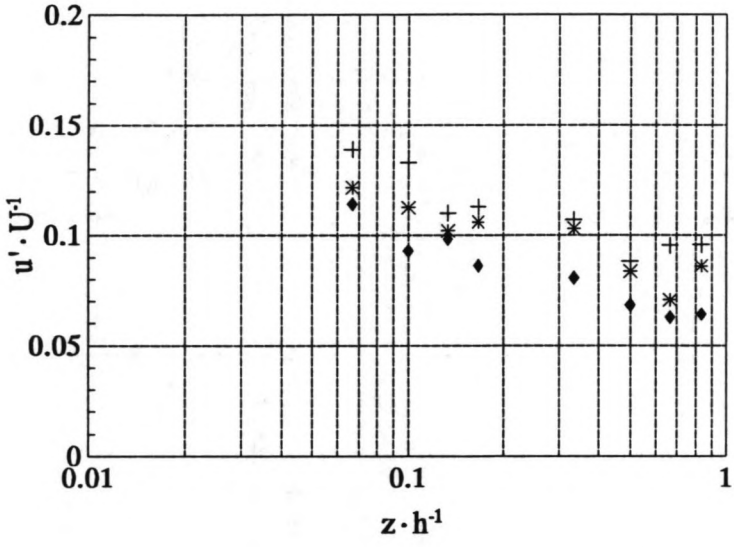

Figure A.3.7 *The averages of the turbulence intensities u'/U measured at positions a, b and c versus the height above the bed.*

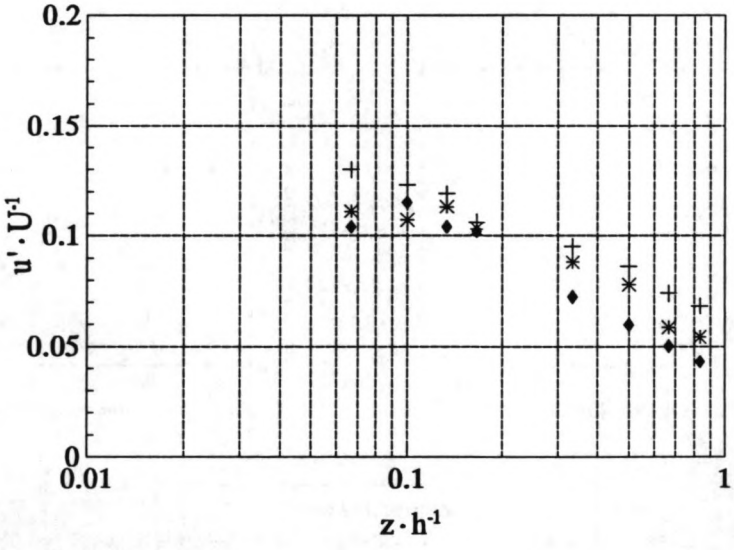

Figure A.3.8 *The averages of the turbulence intensities u'/U measured at positions d, e and f versus the height above the bed.*

A.4 Wave/current characteristics

The objective of the final experiments over the closed test section was to determine flow characteristics when both waves and current were present in the flume. For this purpose an electromagnetic current meter and a wave height meter were installed in the centre of the test section (x=7.0 m, y=0.40 m). The settings of the generator were fixed to preselected values and then the generator was initiated. The pump was also started and a current was generated in the flume. As soon as a quasi-steady state had formed, velocities were measured at eight levels above the bottom for three settings of the average flow rate, namely 12, 24 and 36 $dm^3 \cdot s^{-1}$. This procedure was also used for three other settings of the wave generator. The measurements were logged on a personal computer with a sample rate of 33.3 Hz and every measurement lasted 75 s.

The average velocities and the average velocity amplitudes as a function of the height above the false bottom are shown in the next figures. In each figure the results are presented for one setting of the wave generator. The average wave heights measured during the experiments are printed in table A.4.1.

Table A.4.1 *Average wave heights*

setting wave generator	Average wave height*) [mm]				
1	31		22.2 ± 0.4	19.4 ± 0.6	
2	53		37.3 ± 0.4	31.2 ± 0.6	
3	78	57.1 ± 1.0	52.4 ± 1.5	50.9 ± 1.8	
4	96	67.7 ± 1.2	63.8 ± 1.6		
	0[1)]	12[2)]	24[2)]	36[2)]	average flow rate [$dm^3 \cdot s^{-1}$]

*) Water depth: 30 cm.
1) Determined using an analogue recorder, maximal error in average wave height: ± 5%
2) The accuracy is shown as standard deviation.

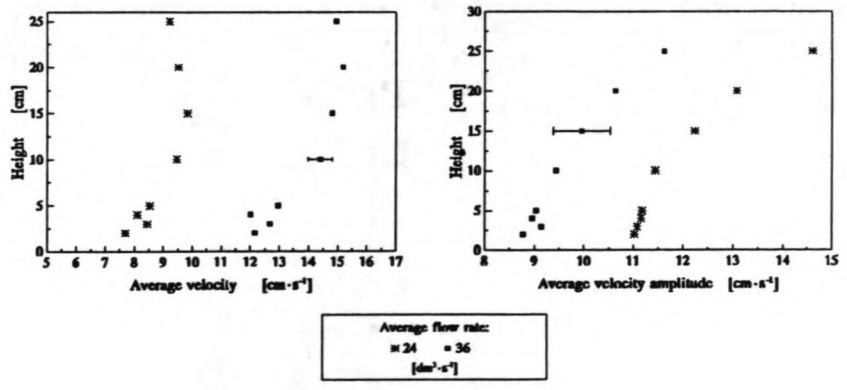

Figure A.4.1 *Wave-averaged velocities and average velocity amplitudes. (wave generator setting 1)*

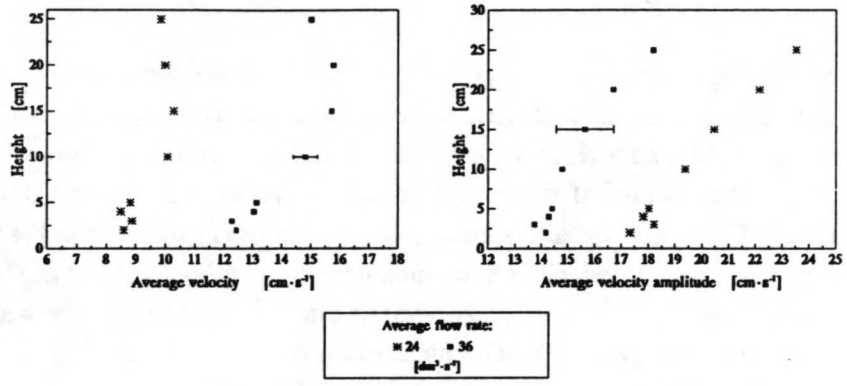

Figure A.4.2 *Wave-averaged velocities and average velocity amplitudes. (wave generator setting 2)*

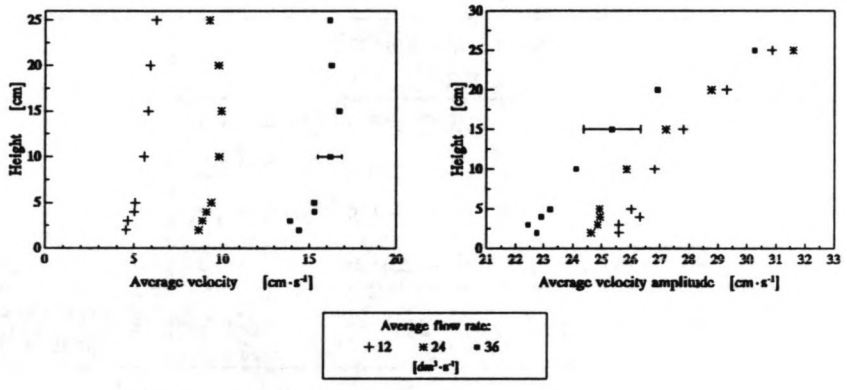

Figure A.4.3 *Wave-averaged velocities and average velocity amplitudes. (wave generator setting 3)*

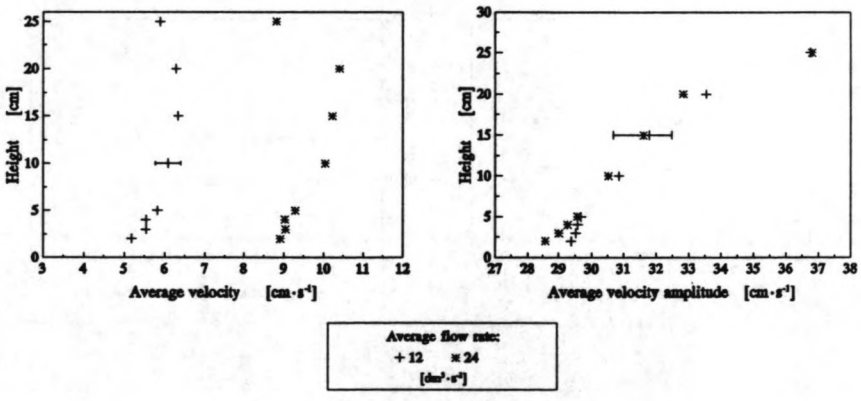

Figure A.4.4 *Wave-averaged velocities and average velocity amplitudes. (wave generator setting 4)*

Appendix B

Additional information on the pilot experiment

In the pilot experiment 6 wave height meters, 3 electromagnetic current meters, 3 optical concentration meters and 1 pressure meter were used. The signals generated by these instruments were recorded on a personal computer using a data-acquisition system. In table B.1 an outline is given of the exact location, the number and the channel on which the signal of every instrument was recorded. The original recording files, as they were recorded during the experiment, can be found on tape no. 1 under session no. 1 entitled "Pilot Experiment". This backup was made using the Interpreter TapeXchange TX120 tape backup system with Txplus Software version 5.14.

The calibration measurements of the wave height meters for the ranges 5, 10 and 20 cm are saved under the directories "CALWHM\RANGE05", "..\RANGE10" and "..\RANGE20", respectively. The filename of each measurement contains the position of the gauge relative to the mean water level; every filename starts with "CWHM" (Calibration Wave Height Meter) followed by "U" or "D", which refers to the change in position of the gauge with respect to the mean water level: U for Upward and D for Downward. The remaining digits indicate the vertical displacement in millimetres.

The measurements from which the zero-flow drift of the electromagnetic current meters was determined are saved under directory "DRIFTEMS". Measurements of only the X-channel were made in quiescent water prior to and after the experiment and were saved as "EMSNIL.LOG" and "EMSEND.LOG", respectively.

The measurements of the tests, as described in section 4.3, are saved under directory "TESTS" as "TEST?.LOG", where ? refers to 1, 2, 3, 4, 5, 6 or 7. The selected ranges of the wave height meters during the tests were as follows; tests 1 - 3: range 5 cm, test 4: range 10 cm, tests 5 - 7: range 20 cm.

Table B.1 *Additional information on the instruments used during the pilot experiment.*

Instrument	number	location on flume[1] [m]	signal recorded on channel no.
wave height meter	1	3.00	1
wave height meter	2	4.58	2
wave height meter	3	6.04	3
wave height meter	4	7.84	4
wave height meter	5	9.60	5
wave height meter	6	10.99	6
concentration meter	0591	0.00	7
concentration meter	2	7.50	8
concentration meter	0194	14.60	9
Height[2]			10
e.m. current meter	E005	3.33	11
e.m. current meter	E013	7.00	12
e.m. current meter	E015	11.25	13
pore-pressure meter[3]		7.15	14

[1] Maximal error: $\pm$ 0.01 m, instruments installed at $y = 0.40$ m. See section 4.4.1 for the definition of the coordinate system.
[2] 0.1 Volt $\propto$ 0.01 m, 0.0 Volt $\sim$ 0.20 m above the bottom of the flume
[3] Range 150 mbar, installed at 0.15 m above the bottom of the flume

Appendix C

Additional information on the second experiment

Three additional pressure meters were used in the second experiment on China Clay. In table C.2 some additional specifications are given on the location, the number and the channel on which the signal of each instrument was recorded.

The original measurements can be found on tape no. 1 under session number 2 entitled "Second experiment on China Clay". The calibration measurements of the wave height meters and the measurements from which the zero-flow drift of the electromagnetic current meters is determined are saved under a separate directory. The naming of these directories is similar to those of the pilot experiment. The measurements made during the four tests as described in section 5.2, are saved in the directories TEST1, TEST2, TEST3 and TEST4. Three subdirectories can be found in directory TEST1, namely VEL05, VEL10 and VEL15 which refer to the three settings of the average flow rate; 12, 24 and 36 $dm^3 \cdot s^{-1}$, respectively. The files saved in these subdirectories have the following format: **VEL??.LOG, where ** refers to the average velocity (05, 10 or 15 $cm \cdot s^{-1}$) and ?? refers to the height (dimension: cm) above the bottom at which the measurement was made minus 20 cm.

Table C.1 *Measuring positions during tests 2, 3 and 4.*

Position number	Height above the bottom of the flume [cm]
1	22.5
2	25.0
3	30.0
4	35.0
5	40.0

The filenames in the directories TEST2, TEST3 and TEST4 have a different format, because during these tests measurements were made at five positions in the water column (table C.1). The format of the filenames is as follows:

*TEST@.LOG: where * refers to the test number and @ refers to the position number. During this measurement only waves were present in the flume;

T*VEL??@.LOG: where * refers to the test number, ?? refers to the average velocity (dimension $cm \cdot s^{-1}$) and @ refers to the position number. During these measurements waves and current were present in the flume.

The data-acquisition set was also calibrated prior to the experiments. The numerical results of this calibration are listed in table C.3. The selected ranges of the wave height meters during the tests were: test 2, range 5 cm and tests 3 and 4, range 10 cm. The optical concentration meters were calibrated during the tests using the data listed in table C.4.

Table C.2 *Additional information on the instruments used during the second experiment on China clay.*

Instrument	number of gauge	number of main amplifier	location on flume[1] [m]	signal recorded on channel no.
wave height meter	75G045	MS76003	0.11	1
wave height meter	75G046	MS76004	1.56	2
wave height meter	76GP070	MS76007	3.04	3
wave height meter	78AP92	MS76008	4.51	4
wave height meter	78AP93	MS76006	5.99	5
wave height meter	A74-032	MS76010	7.33	6
e.m. current meter	E005	E005	0.95	7
e.m. current meter	E013	E013	3.65	8
e.m. current meter	E015	E015	6.70	9
concentration meter	-	2	-2.05	10
concentration meter	-	0591	3.98	11
concentration meter	-	0194	7.66	12
pressure meter[2]	5937	7457/91/2	5.03	13
pressure meter[3]	5938	7461/91/2	5.03	14
pressure meter[4]	5939	7466/91/2	5.03	15
pressure meter[5]	5075	5443/90-2	5.03	16

[1] Maximal error: $\pm$ 0.01 m, instruments installed at y = 0.40 m, except for the pressure transducers. See section 5.1 for the definition of the coordinate system.
[2] Range: 0-75 mbar ($\sim$ 0-10 Vdc), installed at 14.8 cm above the bottom of the flume.
[3] Range: 0-75 mbar ($\sim$ 0-10 Vdc), installed at 17.3 cm above the bottom of the flume.
[4] Range: 0-75 mbar ($\sim$ 0-10 Vdc), installed at 19.3 cm above the bottom of the flume.
[5] Range: 0-350 mbar ($\sim$ 0-10 Vdc), installed at 21.0 cm above the bottom of the flume.

Table C.3 *Calibration data-acquisition set.*

Input voltage [V]	Number returned by data-acquisition set	Input voltage [V]	Number returned by data-acquisition set
-8.08	-1696	0.24	51
-6.08	-1276	2.14	450
-4.11	-862	4.13	869
-2.13	-446	6.10	1283
-0.24	-51	8.11	1703

Table C.4 *Calibration data used for the optical concentration meters during test 2.*

Number 2		Number 0591		Number 0194	
concentration [kg·m^{-3}]	output voltage [V]	concentration [kg·m^{-3}]	output voltage [V]	concentration [kg·m^{-3}]	output voltage [V]
0.080	1.38	0.124	2.04	0.068	1.07
0.137	2.24	0.136	2.19	0.175	2.27
0.234	3.37	0.254	3.93	0.219	3.25
0.350	5.07	0.287	4.48	0.377	5.16
0.724	9.76	0.694	9.68	0.666	9.17

Appendix D

Velocity measurements in mud

After the second experiment on China Clay towing tests were carried out to assess the feasibility of an electromagnetic current meter for measuring velocities in a mud layer. In these tests an electromagnetic current meter (E015), fixed on a measuring rod, was installed on a measuring carriage placed on top of the flume. The velocity of this measuring carriage could be varied. The flume was filled with saline tap water (salinity 5‰) and a non-liquefied China Clay bed of approximately 10 cm thick. The concentration profile measured prior to the tests using a conductivity probe is shown in figure D.1. The water depth was 24 cm. The signal of the electromagnetic current meter was logged on a personal computer. The sample frequency was 100 Hz and 6000 samples were logged in each test. The velocity of the measuring carriage was set to a constant value and the probe was positioned at approximately 12 cm from the water-mud interface. Approximately 15 seconds after the measuring carriage was initiated the data logging was started. In the tests the velocity of the measuring carriage was varied. The probe was also positioned on the water-mud interface and in the mud at approximately 2 cm above the bottom of the flume.

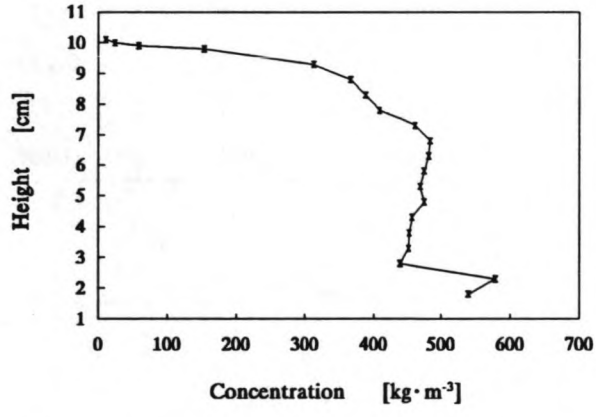

Figure D.1 *Concentration profile of the bed prior to the towing tests.*

The velocity of the carriage was determined by measuring the time needed to cover a certain distance. This distance ranged from 1 to 2 m. The calibration supplied with the electromagnetic current meter was used to calculate the one-minute averaged velocities. The results of these measurements are listed in table D.1.

These measurements show that a electromagnetic current meter can be used to measure velocities in the bed without a recalibration of the instrument. The maximal error, according to the supplier, should be ± 0.5 $cm \cdot s^{-1}$ for velocities smaller than 20 $cm \cdot s^{-1}$. The maximal standard deviation found for the average velocity determined with the electromagnetic current meter was 0.4 $cm \cdot s^{-1}$. This relatively large error was probably caused by the oscillations of the probe caused by the electric drive and the movement of the carriage over the flume.

Table D.1 *Results of the velocity measurements in mud.*

Position probe	velocity carriage[1] [cm·s^{-1}]	velocity EMC[2] [cm·s^{-1}]
12 cm above water-mud interface	-3.4	-3.2
	3.3	3.2
at water-mud interface	-3.3	-3.4
	3.4	3.3
10 cm below the water-mud interface, 2 cm above the bottom of the flume	-3.4	-3.5
	3.4	3.1
	-7.9	-7.3
12 cm above water-mud interface	-7.7	-7.8
	7.7	7.6

[1] Standard deviation: 0.1 cm·s^{-1}
[2] Standard deviation: 0.4 cm·s^{-1}

Appendix E

Additional information on the third experiment

In the third experiment one additional electromagnetic current meter was installed. This current meter was capable of measuring velocities perpendicular to the flume bottom. Furthermore, a Fluke thermometer was used to measure the temperature changes of the fluid and an additional computer was used to log the data. The signals generated by the instruments which were fixed, such as the wave height meters, the pressure meters and the thermometer, and the signals from the optical concentration meters were continuously logged on computer 1. Computer 2 was used to record the signals of those instruments which were traversed in the water column, i.e. the velocity and concentration meters. The measurements made at a certain position were saved in single files. In tables E.1 and E.3 specifications are given on the exact location, the number and the channel on which the signal of every instrument was recorded for the computers used. The original measurements, can be found on tape no. 1 under session entitled "Third experiment on China Clay". The calibration measurements of the wave height meters and the measurements from which the zero-flow drift of the electromagnetic current meters is determined are saved under separate directories. The naming of these directories is identical with those of the pilot experiment. The data-acquisition sets were also calibrated prior to the experiments. The numerical results of this calibration for both sets are listed in tables E.2 and E.4. The measurements of the tests, as described in section 6.2, are saved under the directories "TEST@", where @ denotes the number of the test.

Four sub-directories containing the measurements of the sub-tests will be found in directory TEST1. During these sub-tests measurements were made at five positions in the water column, similar to the measurements made in experiment 2 (table D.1). The format used for these measurements was as follows. The measurements made when only waves were present in the flume are entitled "WAVE?P#.LOG", where ? denotes the setting of the wave generator (1, 2 or 3) and # denotes the position of the traversable instruments in the water column. The measurements made when both waves and current were present in the flume are saved as "**GOL?P#.LOG". Here ** indicates the average velocity in the flume during the measurement (05, 10 or 15 cm·s-*1*). The other variables have the same meaning as already described.

The measurements made in order to determine the velocity profile in the fluid mud are saved in directory TEST2. The file names of every single measurement were "P1EMS&&&.LOG". Here &&& denotes the displacement (dimension: mm) of the electromagnetic current meter in vertical direction relative to position 1.

The profile measurements made in test 3 are saved in sub-directories "WAVE" and "WAVE_CUR". In sub-directory "WAVE" the measurements made when only waves were present are saved and in sub-directory "WAVE_CUR" the measurements when both waves and current were present. The files are entitled "PROF%%.LOG", where %% denotes the vertical displacement (dimension: cm) of the electromagnetic current meter and conductivity meter with respect to the point located at 20 cm above the bottom of the flume. The optical concentration meters were calibrated during test 1 using the data listed in table E.5.

Table E.1 *Additional information on the instruments used during the second experiment on China clay (computer 1).*

Instrument	number of gauge	number of main amplifier	location on flume[1] [m]	signal recorded on channel no.
wave height meter	A74-032	MS76003	0.47	1
wave height meter	A74-033	MS76004	1.61	2
wave height meter	75B046	MS76007	3.23	3
wave height meter	76BP070	MS76008	4.84	4
wave height meter	78AP92	MS76006	6.24	5
wave height meter	78AP94	MS76010	7.45	6
pressure meter[2]	5937	7457/91/2		7
pressure meter[3]	5938	7461/91/2		8
pressure meter[4]	5939	7466/91/2		9
pressure meter[5]	5075	5443/90-2		10
concentration meter	-	2	0.21	11
concentration meter	-	0194	4.22	12
concentration meter	-	0591	7.81	13
thermometer	-	-		14

[1] Maximal error: ± 0.01 m, instruments installed at $y = 0.40$ m, except for the pressure transducers. See section 5.1 for the definition of the coordinate system.
[2] Range: 0-75 mbar (~ 0-10 Vdc), installed at 15.0 cm above the bottom of the flume.
[3] Range: 0-75 mbar (~ 0-10 Vdc), installed at 17.5 cm above the bottom of the flume.
[4] Range: 0-75 mbar (~ 0-10 Vdc), installed at 19.3 cm above the bottom of the flume.
[5] Range: 0-350 mbar (~ 0-10 Vdc), installed at 21.0 cm above the bottom of the flume.

Table E.2 *Calibration data-acquisition set (computer 1).*

Input voltage [V]	Number returned by data-acquisition set	Input voltage [V]	Number returned by data-acquisition set
-9.41	-1976	2.01	425
-7.94	-1666	3.97	835
-5.96	-1251	5.01	1053
-5.02	-1054	7.94	1666
-3.97	-833	9.42	1976
-2.02	-426		

Table E.3 *Additional information on the instruments used during the second experiment on China clay (computer 2).*

Instrument	number of gauge	number of main amplifier	location on flume[1] [m]	signal recorded on channel no.
current meter[2]	E005	E005	0.95	1
current meter[2]	E013	E013	2.80	2
current meter[2]	E015	E015	6.99	3
current meter[2]	E075	E075	5.13	4
current meter[3]	E075	E075	5.13	5
concentration meter	-	2	0.21	6
concentration meter	-	0194	4.22	7
concentration meter	-	0591	7.81	8

[1] Maximal error: ± 0.01 m, instruments installed at $y = 0.40$ m.
[2] X channel
[3] Y channel

Table E.4 *Calibration data-acquisition set (computer 2).*

Input voltage [V]	Number returned by data-acquisition set	Input voltage [V]	Number returned by data-acquisition set
-7.99	-1680	0.26	55
-6.09	-1281	2.12	446
-4.26	-896	4.26	895
-2.12	-446	6.09	1281
-0.26	-54	7.99	1680

Table E.5 *Calibration data used for the optical concentration meters during test 1.*

Number 2		Number 0591		Number 0194	
concentration [kg·m^{-3}]	output voltage [V]	concentration [kg·m^{-3}]	output voltage [V]	concentration [kg·m^{-3}]	output voltage [V]
0.018	0.21	$6.0 \cdot 10^{-4}$	0.18	0.061	0.62
0.0604	0.54	0.0244	0.33	0.087	0.78
		0.0582	0.61		

Appendix F

Response of a non-rigid bed to progressive waves
(a literature review)

In several coastal waters it is often observed that the characteristics of waves travelling over a horizontal bed change as a result of the interaction between the bed and the waves. These changes are dependent on the type of bottom material. Over a rigid bed, for instance, waves may be dampened due to the bottom friction or percolation losses. However, when waves are travelling over a non-rigid bed, such as fluid mud, deflections in the bed are induced and due to the internal friction within the bed, wave energy is dissipated and waves attenuate. In the Gulf of Mexico, for example, there is a location known as the Mud Hole, where the bed mainly consists of fluid mud. At this site the wave damping is so strong that fishing boats use it as an emergency harbour during storms (Dalrymple and Liu, 1978).

Various researchers have investigated the interaction between a non-rigid bed and waves using several constitutive equations to describe the mechanical characteristics of the non-rigid bed (Suhayda, 1984). Basically five rheological models were used to model the interaction. A description of these models and the consequences for the response to water waves will be discussed in the next sections.

F.1 Waves over an ideal elastic bed

The general stress-strain relationship for an ideal, isotropic elastic material is given by the isotropic Hooke's law (Malvern, 1969)

$$T_{ij} = \lambda E_{kk}\delta_{ij} + 2\mu E_{ij} \tag{F.1.1}$$

where T_{ij} are the components of the stress tensor of Cauchy, λ and μ are the Lamé elastic constants, δ_{ij} is the Kronecker delta and E_{ij} are the components of the strain tensor

$$E_{ij} = \frac{1}{2}\left[\frac{\partial \varsigma_i}{\partial x_j} + \frac{\partial \varsigma_j}{\partial x_i}\right]. \tag{F.2.2}$$

Here ς_i is the displacement in the x_i direction.
The strain in terms of stress can be easily found by putting $i=j$ in equation F.1.1 and resubstituting the result in equation F.1.1. This yields

$$E_{ij} = -\frac{\lambda\delta_{ij}}{2\mu(3\lambda+2\mu)}T_{kk} + \frac{1}{2\mu}T_{ij} \tag{F.1.3}$$

or

$$E_{ij} = -\frac{\nu}{E} T_{kk}\delta_{ij} + \frac{1+\nu}{E} T_{ij} \tag{F.1.4}$$

using the more familiar Young's modulus E and Poisson's ratio ν. The relation between the Lamé elastic constants and these constants is:

$$\mu = G = \frac{E}{2(1+\nu)}, \qquad \lambda = \frac{\nu E}{(1+\nu)(1-2\nu)} \tag{F.1.5}$$

where G is the shear modulus.
Equation F.1.4 is equivalent to the following equations in a more common notation for a Cartesian coordinate system:

$$\left.\begin{aligned} \epsilon_x &= \frac{1}{E}[\sigma_x - \nu(\sigma_y + \sigma_z)] & \gamma_{yz} &= \frac{1}{G}\tau_{yz} \\ \epsilon_y &= \frac{1}{E}[\sigma_y - \nu(\sigma_z + \sigma_x)] & \gamma_{zx} &= \frac{1}{G}\tau_{zx} \\ \epsilon_z &= \frac{1}{E}[\sigma_z - \nu(\sigma_x + \sigma_y)] & \gamma_{xy} &= \frac{1}{G}\tau_{xy} \end{aligned}\right\} \tag{F.1.6}$$

where

$$T = \begin{bmatrix} \sigma_x & \tau_{xy} & \tau_{xz} \\ \tau_{yx} & \sigma_y & \tau_{yz} \\ \tau_{zx} & \tau_{zy} & \sigma_z \end{bmatrix} \quad \text{and} \quad E = \begin{bmatrix} \epsilon_x & \frac{1}{2}\gamma_{xy} & \frac{1}{2}\gamma_{xz} \\ \frac{1}{2}\gamma_{yx} & \epsilon_y & \frac{1}{2}\gamma_{yz} \\ \frac{1}{2}\gamma_{zx} & \frac{1}{2}\gamma_{zy} & \epsilon_z \end{bmatrix} \tag{F.1.7}$$

Equation F.1.4 may be simplified by using the deviatoric stress T'_{ij} and the deviatoric strain E'_{ij}. In a Cartesian coordinate system the deviatoric stress and strain are

$$T'_{ij} = T_{ij} - \frac{1}{3} T_{kk}\delta_{ij} \tag{F.1.8}$$

$$E'_{ij} = E_{ij} - \frac{1}{3} E_{kk}\delta_{ij} \tag{F.1.9}$$

Substituting these equations in equation F.1.4 a simple form for the isotropic Hooke's law is found,

$$T'_{ij} = 2GE'_{ij} \quad \text{and} \quad p = -Ke, \tag{F.1.10}$$

where $p = -\frac{1}{3}T_{kk}$ is the mean pressure, $e = E_{kk}$ is the volume strain and K is the bulk modulus.

The bulk modulus K is related to the previously defined elastic constants in the following way

$$K = \lambda + \frac{2}{3}G = \frac{E}{3(1-2\nu)}. \tag{F.1.11}$$

Mallard and Dalrymple (1977) studied the propagation of water waves over an ideal elastic, 2-D, non-porous, soft marine soil of infinite depth. A linear analytic solution was presented for sinusoidal water waves assuming a constant water depth and a nearly equal density of the soil and the water. This solution demonstrates that for a fixed wave frequency the wave number increases as the shear modulus of the soil decreases for a constant water depth. Furthermore, the variation of the bottom pressure, i.e. the pressure at the water-soil interface, for a deformable bed is greater than that predicted by rigid bottom theory and increases as the shear modulus decreases.

Under the assumptions that only the pressure is continuous across the soil-water interface and that there are no tangential stresses at the soil-water interface, Mallard and Dalrymple (1977) also found relations for the normal horizontal and vertical stresses in the bed (σ_x and σ_y, respectively) and the shear stress (τ_{xy}),

$$\sigma_x = -N(1+ky)\,e^{ky}\cos(kx-\omega t) \tag{F.1.12}$$

$$\sigma_y = -N(1-ky)\,e^{ky}\cos(kx-\omega t) \tag{F.1.13}$$

$$\tau_{xy} = -Ne^{ky}\sin(kx-\omega t) \tag{F.1.14}$$

where

$$N = \frac{\rho g a}{\cosh kh}\left[\frac{G'}{G'-\tanh kh}\right], \tag{F.1.15}$$

$$G' = \frac{Gk^2}{\rho\omega^2(1-\nu)} \tag{F.1.16}$$

and k is the wave number, ω is the angular wave frequency, g the gravitational acceleration, a the wave amplitude, h the mean water depth and ρ is the density of the soil. The positive x axis is in the direction of the wave propagation and the positive y axis is up from the soil- water interface. The deviatoric shear stress τ_{max} can be calculated according to Mohr's stress analysis (Malvern, 1969)

$$\tau_{max} = \sqrt{\tau_{xy}^2 + \frac{1}{4}(\sigma_x-\sigma_y)^2} \tag{F.1.17}$$

Substituting from equations F.1.12 - F.1.14, equation F.1.17 yields for the maximal shear stress, due to the streamwise variation of the pressure, in an isotropic, ideal elastic material,

$$\tau_{max} = \pm N e^{ky} \sqrt{\sin^2(kx-\omega t) + (ky)^2 \cos^2(kx-\omega t)} \quad . \tag{F.1.18}$$

Equation F.1.18 can be used to make a first estimation of the maximum shear stresses in a non-liquefied mud bed under wave action. Although mud is not an ideal elastic solid, the estimation of the maximum wave-induced shear stress at some depth could be used to predict the onset of liquefaction of mud: when the shear stress exceeds the soil yield strength at a certain depth, failure may occur and consequently the bed may be liquefied.

De Wit and Kranenburg (1993) calculated the deviatoric shear stresses in a semi-infinite isotropic linear-elastic solid for a sinusoidal pressure distribution ($p = \hat{p}\sin(kx)$). Their calculation was based on Boussinesq's solution for a vertical point source (Timoshenko, 1951) and proposed

$$\tau_{max} = \hat{p} ky\, e^{ky} \tag{F.1.19}$$

where $\hat{p}$ is the pressure amplitude at the upper bed surface generated by progressive waves as calculated using linear short-wave theory

$$\hat{p} = \frac{\rho g a}{\cosh kh} \tag{F.1.20}$$

The total shear stress at a certain depth in the bed is the sum of the pressure-induced shear stresses and the shear stresses on the bed induced by the oscillatory flow. The latter can be calculated from viscous flow theory for laminar flow or from an empirical equation for turbulent flow. For laminar flow the shear stress on the bed is calculated by

$$\tau_{lam} = \eta \frac{\partial u(y,t)}{\partial y} \tag{F.1.21}$$

where η is the dynamic viscosity and $u(y,t)$ the horizontal velocity component as a function of y and time t. An empirical relation for the maximum shear stress for turbulent oscillatory flow is given by Tolman (1990)

$$\tau_{turb} = \frac{1}{2}\rho f_w u_0^2 \tag{F.1.22}$$

where f_w is a friction factor and u_0 the maximum horizontal velocity component just outside the boundary layer. Using linear wave theory it is found that the horizontal velocity component is

$$u(y,t) = \omega a \frac{\cosh ky}{\sinh kh} \sin(\omega t - kx) \tag{F.1.23}$$

A relation for f_w is also given by Tolman (1990), namely

$$\frac{1}{4\sqrt{f_w}} + \log\left[\frac{1}{4\sqrt{f_w}}\right] = -0.08 + \log\left[\frac{a_0}{r}\right] \tag{F.1.24}$$

where a_0 is the maximal horizontal displacement of the water particles just outside the boundary layer and r is the bottom roughness.
Calculating the flow induced shear stress τ_{flow} on a mud bed with bottom roughness 0.001 m for waves with a wave height of 0.05 m and wave period of 1.5 s and a water depth of 0.3 m gives $\tau_{flow} \approx 0.1$ Pa. Calculating the maximal pressure-induced shear stress according to De Wit and Kranenburg (1992) for the same wave characteristics 0.01 m below the water-mud interface it is found that $\tau_{max} \approx 4.7$ Pa. A soft marine mud has a shear modulus of approximately 200 psf (1 psf $\approx$ 47.9 Pa, Weast 1973) according to Mallard and Dalrymple (1977). Assuming a Poisson's ratio of 0.5 and the same wave characteristics it is found that $\tau_{max} \approx$ 170 Pa at 0.01 m below the water-mud interface. These calculations clearly show that the flow induced shear stresses on the bed surface are very small in comparison with the pressure induced shear stresses in the bed. These pressure induced shear stresses are large when compared with the yield strength of a mud. Rheological measurements on suspensions of Kaolinite, for instance, show that the characteristic yield strength of remoulded suspensions with a concentration of approximately 500 $kg \cdot m^{-3}$ is in the order of 5 Pa (Chou, 1989 and De Wit, 1992a). Consequently, the pressure induced shear stresses for the above mentioned wave characteristics are larger than the yield strength and as a result fluid mud may be generated.

The damping of waves over a muddy bed cannot be modelled with an elastic model, because no energy is dissipated in an ideal elastic bed.

However, Foda (1989) showed that gravity waves over an elastic bed with inhomogeneous properties representing some vertical stratifaction profile, would lose energy in a viscous sublayer on the bed due to sideband oscillations. These sidebands are contaminated with small-amplitude, short elastic shear waves that will interact with the viscous boundary layer at the bed-water interface and thus dissipating significant wave energy in the boundary layer.

F.2 Waves over a poro-elastic bed

The response of a poro-elastic bed to water waves is a combination of the mechanical effects of the fluid and the solid; a fluid flow is induced in the porous medium and the porous medium itself is forced to deform. Biot accomplished the fundamental description of the deformation of such an completely saturated porous medium and is commonly known as Biot's theory of (linear) consolidation (Verruijt, 1992). This theory has been studied extensively.

Yamamoto et al. (1978) treated analytically the response of a porous elastic bed to water waves and obtained the exact solution for the pore-water pressure and the displacements of the porous medium. They showed that the bed response was strongly dependent on the permeability and the stiffness of the porous medium, and the compressibility of the pore fluid. However, the soil and water wave dynamics were not included in their model. The analyses of the response of a inhomogeneous bed was made by Yamamoto (1981).

The effect of the intergranular Coulomb friction on the response of a poro-elastic soil was studied by Yamamoto et al. (1983). A Froude-Mach similitude law was established from the nonlinear Coulomb-damped poro-elastic theory. From theoretical and experimental results it was found that the response of clay beds to water waves was highly nonlinear. Furthermore, the Coulomb friction is the main wave damping mechanism compared to other damping mechanisms. Yamamoto and Takahashi (1985) examined quantitatively the wave damping by wave-soil interactions. Various damping mechanisms were considered, namely energy loss by the bottom turbulence layer, energy loss by the percolation of water through the sediments and and energy loss by the Coulomb friction between the

grains. An explicit form of the dispersion relation was derived for a normally consolidated, depth varying, poro-elastic bed. It was also concluded that the main energy dissipation mechanism by soft soils, e.g. clays and silts, is the Coulomb friction. This mechanism is highly nonlinear due to the dynamic softening behaviour of these soils and as a result waves with a large wave height damp much quicker than small waves. However, the attenuation of waves over very soft, fluid-like muds was found to become nearly independent of the wave height (Feng, 1993). The motion of the soil modifies the wavelength; for soils softer than a critical bed rigidity the wavelength may be increased by up to 15% for fixed wave frequencies.

Recently, Huang and Song (1993) obtained the general solution of linear waves over a horizontal bed of infinite thickness and defined five nondimensional parameters as controlling physical factors. Mei & Foda (1981) and Mei (1982) showed that a Stokes-like boundary layer may exist near the surface of the solid. Outside the boundary layer the fluid and the solid skeleton move together according to the laws of classical elasticity for a single fase. However, in the boundary layer a significant relative movement is found between the two phases.

Spierenburg (1987) calculated analytically and numerically the response of a relatively thin layer of poro-elastic material to water waves. The calculations were made for poro-elastic layer over a completely rough and perfectly smooth base.

Next the general solution will be given for the response of a poro-elastic bed to water waves as obtained by Yamamoto et al. (1978). The basic assumptions are that (1) the soil has linear, reversible, isotropic, non-retarded elastic properties (Hooke's law), (2) the movement of the fluid obeys Darcy's law and (3) the bed is loaded by simple two-dimensional harmonic waves. The coordinate system is defined in following way; the x axis is taken on the bed surface and the positive direction of the z axis is taken vertically downward from the bed surface.

From Terzaghi's principle of effective stress together with Hooke's law, the equations of equilibrium in x and z direction are

$$G\nabla^2 u_s + \frac{G}{1-2\nu}\frac{\partial e}{\partial x} = \frac{\partial p}{\partial x} \tag{F.2.1}$$

$$G\nabla^2 w_s + \frac{G}{1-2\nu}\frac{\partial e}{\partial z} = \frac{\partial p}{\partial z} \tag{F.2.2}$$

where u_s is the x component of the soil displacement, w_s is the z component of the soil displacement, p is the excess pore pressure and e is the volume strain for the two-dimensional problem

$$e = \frac{\partial u_s}{\partial x} + \frac{\partial w_s}{\partial z}. \tag{F.2.3}$$

The continuity or storage equation is given by

$$\frac{k}{\gamma}\nabla^2 p = n\beta'\frac{\partial p}{\partial t} + \frac{\partial e}{\partial t} \tag{F.2.4}$$

where n is the porosity, t is the time, γ the specific weight of the fluid, k the permeability of the solid matrix and β' is the compressibility of the pore fluid. This pore fluid usually consists of two phases, namely liquid and air. Due to a very small amount of air the compressibility changes drastically and

it can be related to the degree of saturation S and the absolute water pore-water pressure P_0

$$\beta' = \frac{1}{K} + \frac{1-S}{P_0} \tag{F.2.5}$$

where K is the bulk modulus of elasticity of the pore water.
Defining a dimensionless elastic parameter m

$$m = \frac{1}{1-2\nu} = \frac{K + \frac{1}{3}G}{G} \tag{F.2.6}$$

the consolidation coefficient c

$$c = \frac{k}{\gamma}(m+1)G \tag{F.2.7}$$

and the dimensionless parameter θ

$$\theta = n\beta' G \tag{F.2.8}$$

the basic equations can be rewritten as

$$c\nabla^2 p = \theta(1+m)\frac{\partial p}{\partial t} + (1+m)G\frac{\partial e}{\partial t} \tag{F.2.9}$$

$$G\nabla^2 u_s + mG\frac{\partial e}{\partial x} = \frac{\partial p}{\partial x} \tag{F.2.10}$$

$$G\nabla^2 w_s + mG\frac{\partial e}{\partial z} = \frac{\partial p}{\partial z} \tag{F.2.11}$$

The total stresses are related to the strains by Hooke's law as

$$\left.\begin{aligned} \sigma_x &= 2G\frac{\partial u_s}{\partial x} + (m-1)Ge + p \\ \sigma_y &= 2G\frac{\partial w_s}{\partial z} + (m-1)Ge + p \\ \tau_{xz} &= G\left[\frac{\partial u_s}{\partial z} + \frac{\partial w_s}{\partial x}\right] \end{aligned}\right\} \tag{F.2.12}$$

At two levels boundary conditions have to be specified for a finite poro-elastic layer over a stiff impermeable base. At the bed surface it is assumed that sinusoidal pressure fluctuations are present for a two-dimensional, progressive, harmonic surface-wave with angular frequency ω and wave number k. Furthermore, the shear stress at the surface of the bed are negligibly small and there are no vertical effective stresses.

As the base is supposed to be stiff and impermeable, the boundary conditions are that there are no vertical displacements and the pressure gradient normal to the base is zero. The final boundary condition depends on the contact between the poro-elastic layer and the base. For a perfectly smooth interface, the shear stress τ_{xz} is zero and horizontal displacements are possible. However, no slip conditions are valid for a completely rough base, i.e. no horizontal displacements are possible along the base.

Hence the boundary conditions are:
at the bed surface

$$\left.\begin{aligned} p &= p_0 \exp[i(\mathrm{k}x - \omega t)] \\ \sigma_z &= 0 \\ \tau_{xz} &= 0 \end{aligned}\right\} \qquad \text{(F.2.13)}$$

at the base

$$\left.\begin{aligned} w_s &= 0 \\ \frac{\partial p}{\partial z} &= 0 \\ \tau_{xx} &= 0 \qquad \text{(perfectly smooth base)} \\ u_s &= 0 \qquad \text{(completely rough base)} \end{aligned}\right\} \qquad \text{(F.2.14)}$$

Spierenburg (1987) calculated the general solution for an incompressible pore fluid ($\beta' = 0$) by supposing the following response of the displacements and pore pressure:

$$\left.\begin{aligned} p &= \mathrm{A} \exp(\alpha z) \exp[i(\omega t - \mathrm{k}x)] \\ u_s &= \mathrm{B} \exp(\alpha z) \exp[i(\omega t - \mathrm{k}x)] \\ w_s &= \mathrm{C} \exp(\alpha z) \exp[i(\omega t - \mathrm{k}x)] \end{aligned}\right\} \qquad \text{(F.2.15)}$$

Substituting this solution in equations F.2.9 - F.2.11 gives a set of three homogenous, linear equations in A, B and C, namely

$$\left.\begin{aligned} -i\mathrm{k}\,\mathrm{A} + G[\alpha^2 - (m+1)\mathrm{k}^2]\,\mathrm{B} - i\alpha\mathrm{k}mG\,\mathrm{C} &= 0 \\ \alpha\,\mathrm{A} - i\alpha\mathrm{k}mG\,\mathrm{B} + G[(m+1)\alpha^2 - \mathrm{k}^2]\,\mathrm{C} &= 0 \\ c(\alpha^2 - \mathrm{k}^2)\,\mathrm{A} + (m+1)G\omega\,\mathrm{k}\,\mathrm{B} + i(m+1)G\alpha\omega\,\mathrm{C} &= 0 \end{aligned}\right\} \qquad \text{(F.2.16)}$$

The general solution of this set of equations can be found by equating the determinant to zero. The determinant *Det* is

$$Det = (m+1)\,G(\alpha^2 - \mathrm{k}^2)^2\left(-i\omega + c(\alpha^2 - \mathrm{k}^2)\right) \qquad \text{(F.2.17)}$$

and consequently the eigenvalues are

$$\alpha_1 = \pm k,\ \alpha_2^2 = k^2\left[1 + i\frac{\omega}{ck^2}\right]. \tag{F.2.18}$$

Finally, the general solution for the response of a poro-elastic bed to surface waves can be obtained:

$$p = \left[A_1\exp(kz) + A_4\exp(-kz) + A_3\exp(\alpha_2 z) + A_6\exp(-\alpha_2 z)\right]\exp(i(\omega t - kx)) \tag{F.2.19}$$

$$\begin{aligned} u_s = \Big\{ & B_1\exp(kz) + B_4\exp(-kz) + \\ & \frac{i}{2Gk}\{A_1 kz\exp(kz) - A_4 kz\exp(-kz)\} + \\ & \frac{ck}{(m+1)G\omega}\{A_3\exp(\alpha_2 z) + A_6\exp(-\alpha_2 z)\}\Big\}\exp\left(i(\omega t - kx)\right) \end{aligned} \tag{F.2.20}$$

$$\begin{aligned} w_s = \Big\{ & \{B_1\exp(kz) - B_4\exp(-kz)\}i + \\ & \frac{1}{2Gk}\{A_1\exp(kz) - A_4\exp(-kz)\} - \\ & \frac{1}{2Gk}\{A_1 kz\exp(kz) + A_4 kz\exp(-kz)\} + \\ & \frac{ic\alpha}{(m+1)G\omega}\{A_3\exp(\alpha_2 z) - A_6\exp(-\alpha_2 z)\}\Big\}\exp\left(i(\omega t - kx)\right) \end{aligned} \tag{F.2.21}$$

where

$$\alpha_2 = k\sqrt{1 + i\frac{\omega}{ck^2}} \qquad \mathrm{Re}(\alpha) > 0 \tag{F.2.22}$$

The solution for the wave response of a poro-elastic bed over a perfectly smooth base or over a completely rough base is found by taking the general solution together with the appropriate boundary conditions resulting in a set of six linear equations. Spierenburg (1987) calculated numerically the response of a relatively thin poro-elastic layer. The results are shown in figure F.2.1 for a layer with a relatively thickness of kD=1.5 and a Poisson ration of 1/3 over both a smooth and a rough base. Note that the deviatoric stress at the surface of the finite bed which is not equal to zero as opposed to the deviatoric stress at the surface of a semi-infinite bed.

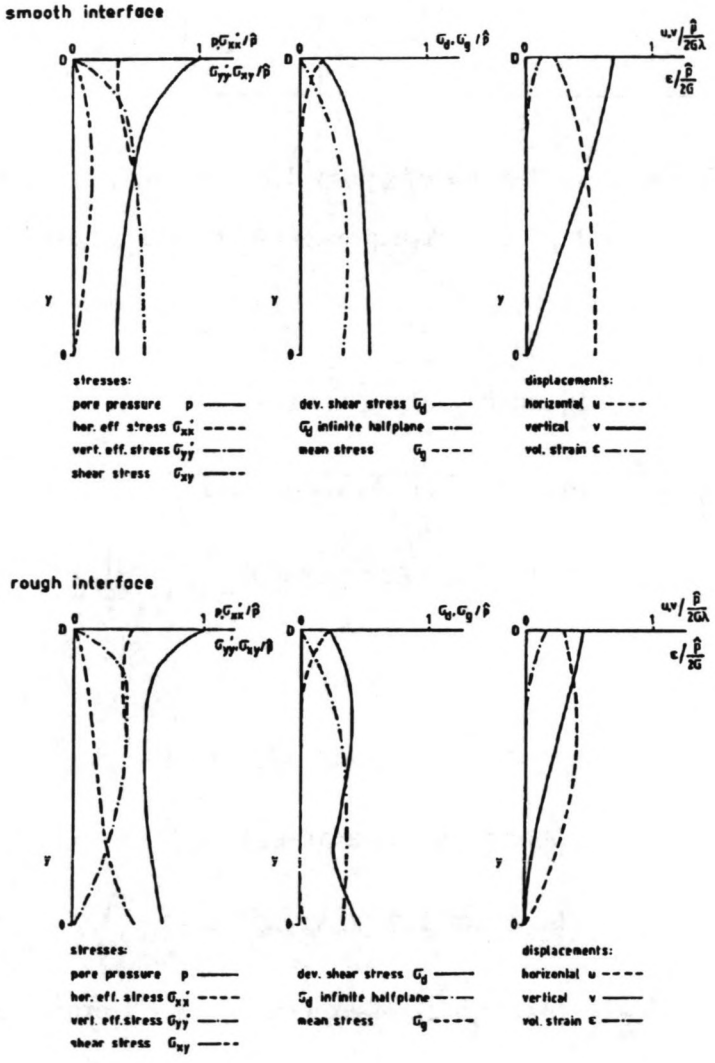

Figure F.2.1 *Response of a finite poro-elastic bed to waves (Spierenburg, 1987). (y=D is the top of the bed)*

F.3 Waves over a Newtonian fluid bed

The constitutive equation for a Newtonian or viscous fluid relates the rate of deformation to the applied stress and is generalized in the form (Malvern, 1969)

$$T'_{ij} = 2\eta D'_{ij} \tag{F.3.1}$$

where

$$D_{ij} = \frac{1}{2}\left[\frac{\partial u_i}{\partial x_j} + \frac{\partial u_j}{\partial x_i}\right] \qquad \text{(F.3.2)}$$

Here T and D are the stress tensor and rate of deformation tensor, i,j are subscripts, u_i is the velocity in the x_i direction and η the dynamic viscosity. The prime indicates the deviatoric part of the tensor. Under the assumption of incompressibility it is found that $D'_{ij} = D_{ij}$.

For a stationary flow of an ideal Newtonian fluid past a flat boundary equation F.3.1 can be simplified to the form $\tau = \eta\, dv/dy = \eta\dot{\gamma}$ where τ is the shear stress, z is the coordinate perpendicular to the direction of the flow at speed $v(z)$ and $\dot{\gamma}$ is the shear rate.

Gade (1958) was one of the first researchers who studied theoretically and experimentally the effects of a viscous, impermeable bottom on surface waves in shallow water. He formulated a two-layer mathematical model in which an inviscid fluid was laying over a viscous fluid of greater density. A boundary layer approximation was used for both layers. It was found that the wave height of a harmonic wave decays exponentionally with the travelled distance. Furthermore, the rate of decay has a maximum value when

$$D\sqrt{\frac{\omega}{2\eta}} \approx 1.2 \qquad \text{(F.3.3)}$$

where D denotes the thickness of the lower viscid layer. A modification of Gade's model is described in appendix A, where no boundary approximation is used for the upper inviscid layer.

Another extension of Gade's model was made by Dalrymple and Liu (1978) who developed a model for any depth of the upper and lower layers. Also the viscosity of the upper layer was included. Similar results were obtained; a maximum attenuation rate is found when the lower layer is approximately 30% thicker than the corresponding boundary thickness $\sqrt{\omega/(2\eta_2)}$, where η_2 is the kinematic viscosity of the lower layer. Furthermore, the conclusion was drawn that the principal mechanism of energy transfer to the lower layer is the pressure of the surface waves working on the lower fluid, not the interfacial shear stress in the upper fluid. This model was used by Shibayama et al. (1986) to estimate the rate of mud mass transport under wave action. Comparison of experimental and theoretical results showed that the mass transport could be modelled under the assumption that the mud behaves similar to a viscous fluid. However, the measured attenuation of waves was greater than the wave attenuation rate predicted by the model.

The response of a viscous bed to nonlinear, cnoidal waves was studied by Jiang et al. (1990). A two-layer viscous model modified with three laminar boundary layers; one boundary layer in the upper fluid near the interface, one in the lower fluid near the interface and one near the rigid bottom. A first-order analytical solution was obtained for the velocity distributions and for the wave damping under the assumption of non-linear, progressing shallow-water waves. It was found that the attenuation of nonlinear shallow-water waves over a viscous bed is larger than the attenuation of sinusoidal waves.

F.4 Waves over a viscoplastic bed

A viscoplastic or Bingham material is able to sustain a shear stress (solid like), but when the stress intensity reaches a critical value (yield condition, τ_y) the material will start to flow with viscous stresses proportional to the excess of the stress intensity over the yield-stress intensity. The general form of the constitutive law for a viscoplastic material in three dimensional, incompressible flows is (Malvern, 1969)

$$2\eta_B D_{ij} = \begin{cases} 0 & \text{for} \quad F < 0 \\ F T'_{ij} & \text{for} \quad F \geq 0 \end{cases} \tag{F.4.1}$$

where

$$F = 1 - \frac{\tau_y}{\sqrt{J'_2}}, \tag{F.4.2}$$

η_B denotes the Bingham viscosity, which is analogous to the Newtonian dynamic viscosity and J'_2 is the second invariant of the stress deviator ($J'_2 = \frac{1}{2} T'_{ij} T'_{ij}$). Equation F.4.1 is in fact the viscoplastic analogue of the constitutive equation of a Newtonian fluid, as the constitutive equation for a Newtonian fluid is $2\eta D'_{ij} = T'_{ij}$ and can be rewritten as

$$\begin{aligned} D_{ij} &= 0 && \text{for} \quad F < 0 \\ T'_{ij} &= \left[2\eta_B + \frac{\tau_y}{\sqrt{\Pi_D}} \right] D_{ij} && \text{for} \quad F \geq 0 \end{aligned} \tag{F.4.3}$$

where Π_D is the second invariant of the rate of deformation tensor ($\Pi_D = \frac{1}{2} D_{ij} D_{ij}$ for $D_{kk} = 0$). In the case of a one-dimensional simple shear flow, equation F.4.3 reduces to

$$\begin{aligned} \frac{\partial u}{\partial z} &= 0 && \text{for} \quad |\tau| < \tau_y \\ \tau &= \tau_y \operatorname{sgn}\left[\frac{\partial u}{\partial z} \right] + \eta_B \frac{\partial u}{\partial z} && \text{for} \quad |\tau| \geq \tau_y \quad . \end{aligned} \tag{F.4.4}$$

The mathematical model due to Dalrymple and Liu (1978) was modified by Sakakiyama and Bijker (1989) who introduced an apparent viscosity η_a to model the Bingham behaviour of mud on the analogy of the viscosity of a Newtonian fluid defined as

$$\tau = \eta_a \frac{\partial u}{\partial z} = \tau_y + \eta_B \frac{\partial u}{\partial z}. \tag{F.4.5}$$

However, the behaviour of the mud is still assumed viscous by this definition of the apparent

viscosity. Furthermore, the fact that the yield stress τ_y and the shear rate $\partial u/\partial z$ should have the same sign is ignored (Feng, 1993).

Liu and Mei (1989) studied the motion in a thin layer of mud induced by a solitary wave propagating in a much thicker layer of overlying water. The mud was modelled as a Bingham plastic and interfacial friction was included in the model. The mass transport and the wave damping were strongly affected by this friction.

The interaction between a relatively thick layer of mud modelled as a Bingham plastic fluid with long gravity waves in the overlying layer of clear water was theoretically studied by Liu and Mei (1993a,b).

F.5 Waves over a viscoelastic bed

Several viscoelastic models are described in literature (Kuiken and Merk, 1978) that describe behaviour between the extremes of a viscous fluid and an elastic solid. Basically there are two linear viscoelastic elements, namely the Kelvin - or Voigt element and the Maxwell element. These elements are based on the analogy with a spring-dashpot system and are described as follows:

Voigt model: $$T'_{ij} = 2GE'_{ij} + 2\mu\dot{E}'_{ij} \tag{F.5.1}$$

Maxwell model: $$\dot{E}'_{ij} = \frac{1}{2G}\dot{T}'_{ij} + \frac{1}{2\mu}T'_{ij} \tag{F.5.2}$$

where $\dot{E}'_{ij} \equiv \frac{dE'_{ij}}{dt}$ and $\dot{T}'_{ij} \equiv \frac{dT'_{ij}}{dt}$

For a simple shear with shear stress τ and strain γ, these equations can be expressed in the form:

Voigt model: $$\tau = G\gamma + \mu\dot{\gamma} \tag{F.5.3}$$

Maxwell model: $$\tau = \mu\dot{\gamma} - \frac{\mu}{G}\dot{\tau} \tag{F.5.4}$$

The Voigt model is represented in figure F.5.1 as a parallel combination of a spring and a dashpot. In this configuration the strain is equal for both elements. However, the total stress is the sum of the stresses in spring and dashpot. At a constant strain equation F.5.3 reduces to $\tau = G\gamma$, i.e. to the relationship of a Hookean solid. This model therefore shows a viscoelastic solid-like behaviour.

The Maxwell model is a serial combination of a spring and a dashpot and consequently the elements undergo the same shear stress, see figure F.5.1. However, the total strain is a summation of the strains of both elements. Equation F.5.4 shows that the stress depends on the rate of strain. Consequently, the Maxwell model describes the behaviour of a viscoelastic fluid. At constant stress equation F.5.4 reduces to the relationship for a Newtonian fluid $\tau = \mu\dot{\gamma}$.

Using these basic mechanical elements it is very easy to build more complex models, such as the multi-element generalized Kelvin-Voigt or Maxwell model or the four-element Burgers model. For reasons of brevity, these models will not be described in this report. For more information about these models see Kuiken and Merk (1978), for instance.

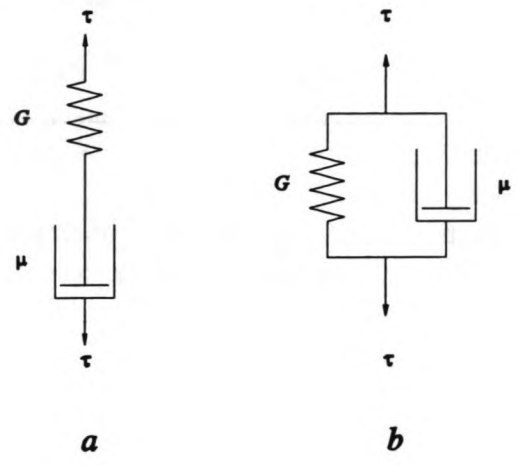

Figure F.5.1 Mechanical representation of the Maxwell (a) and the Kelvin model (b).

The response of a viscoelastic bed with a finite thickness to surface waves in an overlaying inviscid fluid was studied independently by MacPherson (1980) and Hsiao & Shemdin (1980). A dispersion relation was derived on the basis of small-amplitude wave theory and modelling the bed as a Voigt body. The results obtained by MacPherson showed that the amount of wave damping is largely dependent on the viscosity and elastic parameters in the bed. He also compared the amount of energy dissipation by the various mechanisms, such as bottom friction, percolation in a permeable bed and the formation of a laminar boundary layer. The energy dissipation in a viscous bed was found to be one order of magnitude greater than the dissipation in a viscoelastic bed. The theoretical dissipation rates found by Hsiao and Shemdin (1980) were favourably compared with field measurements.

Suhayda (1984) presented a simplified technique for making engineering predictions on the interaction between surface waves and a muddy bottom. This technique was based on an empirical, nonlinear stress-strain and damping-strain soil model. Wave attenuation, soil shear stress and shear strain profiles can be roughly calculated with this technique.

Although the Voigt and the Maxwell elements are both used to model the behaviour of mud, it was suggested by Maa and Mehta (1988) that the Voigt element is a better selection for modelling soft mud bed responses. This conclusion was based on the fact that the mud studied showed no creep phenomena, which is characteristic of the Maxwell model. Furthermore, the mud showed a reasonably linear response for small strains and the mud showed an ability to resist a shear force.

Motion in a soft mud bed, wave-induced shear stress and wave attenuation under small amplitude waves were calculated by Maa and Mehta (1987,1990). A linearized, multilayered hydrodynamic model was developed in which the mud properties were modelled as a simple linear viscoelastic solid (Voigt element). The overlaying water layer was modelled as a viscous fluid. The calculated results were compared with experimental results and showed acceptable agreement. A similar model was developed by Shibayama et al. (1989).

Chou (1989) developed a model which simulates the wave-bottom interaction by considering water as a viscous fluid and the mud as a three-layered viscoelastic medium. The thickness of the upper two layers of the bed were determined as part of the solution through an iterative technique. The results showed that the wave damping and also the depth of fluidization increased with the wave height.

A second order hydrodynamic model was developed by Feng (1993) to examine wave-mud interactions. The properties of the mud were modelled using a three-parameter viscoelastic model; the mechanical representation is a spring in series with a Voigt element. The overlying water layer was considered to be viscid. This model has no restriction for the wave heights because second order kinematic and dynamic boundary conditions were considered. The forcing waves may be nonlinear.

An extension of MacPherson's model (1980) was presented by Cueva (1993), who considered also the continuity of the shear stress through the water-mud interface taking into account a thin boundary layer upon the interface. An analytical approach was given to gain insight into the response of a mud bed, modelled as a Voigt body, to surface water waves.

Appendix G

Waves over a viscous bed: a modification of the model due to Gade (1958)

Gade (1958) discussed the effects of a nonrigid, viscous bottom on plane surface waves in shallow water. A mathematical model was built assuming two separated layers resting on a rigid, horizontal base. The upper layer was treated as a frictionless fluid and the lower layer was assumed to be a homogeneous fluid with a constant viscosity and a higher density than the overlaying layer. Boundary layer approximations were used for both layers. This model was extended to deeper water and the results were used to calculate velocities in a layer of fluid mud and wave damping rates in the China Clay experiments. A summary of this modified model will be given next.

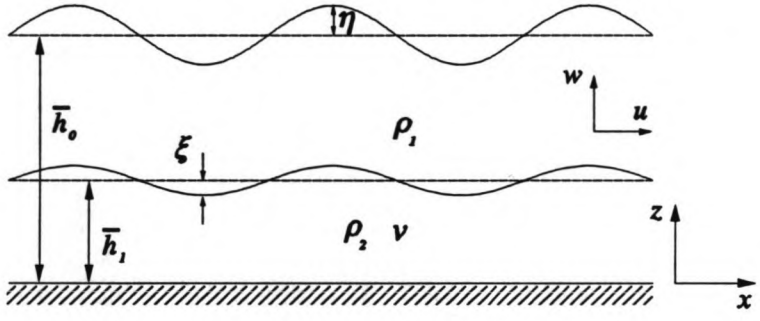

Figure G.1 *Schematic presentation of the model and the various parameters.*

Consider two overlaying fluid layers; the upper layer is inviscid and the lower layer is viscous (kinematic viscosity ν) and is resting on a rigid, completely rough, horizontal base. The latter layer is homogeneous and relatively thin (thickness h_1) and it is assumed that the pressure distribution in this layer is quasi-hydrostatic (boundary approximation). The density (ρ_1) of the upper layer is lower than the density (ρ_2) of the lower layer. Net water velocities are assumed to be zero, and the problem is linearized. There are no horizontal velocities at the base (no-slip condition). The positive x-axis is on the rigid horizontal base in the direction of the propagating waves. The z-axis is positive up from the horizontal base. A schematic diagram is shown in figure G.1.

The equations of motion are
for the upper layer

$$\begin{aligned} \frac{\partial u_1}{\partial t} + \frac{1}{\rho_1}\frac{\partial p_1}{\partial x} &= 0 \\ \frac{\partial w_1}{\partial t} + \frac{1}{\rho_1}\frac{\partial p_1}{\partial z} &= -g \end{aligned} \qquad \text{(G.1)}$$

and for the lower layer

$$\frac{\partial u_2}{\partial t} + \frac{1}{\rho_2}\frac{\partial p_2}{\partial x} = \nu\frac{\partial^2 u_2}{\partial z^2}$$
$$\frac{1}{\rho_2}\frac{\partial p_2}{\partial z} = -g \qquad \text{(G.2)}$$

where u_i is the horizontal velocity, w_i is the vertical velocity, p_i is the pressure and the subscripts $i=1, 2$ indicate the upper (1) and lower (2) layers.

The conservation of mass (continuity) equations for the upper and lower layers are

$$\frac{\partial u_i}{\partial x} + \frac{\partial w_i}{\partial z} = 0 \qquad \text{(G.3)}$$

The boundary conditions are
at the free surface $(z=h_0)$:

$$w_1 = \frac{\partial h_0}{\partial t} \qquad \text{(kinematic boundary condition)} \qquad \text{(G.4)}$$

$$p = 0 \qquad \text{(dynamic boundary condition)} \qquad \text{(G.5)}$$

at the water-bed interface $(z=h_1)$:

$$w_1 = \frac{\partial h_1}{\partial t} \qquad \text{(G.6)}$$

$$w_2 = \frac{\partial h_1}{\partial t} \qquad \text{(G.7)}$$

$$\frac{\partial u_2}{\partial z} = 0 \qquad \text{(no shear stress)} \qquad \text{(G.8)}$$

$$p\Big|_{\text{layer 1}} = p\Big|_{\text{layer 2}} \qquad \text{(G.9)}$$

at the base $(z=0)$:

$$u_2 = 0 \qquad \text{(no-slip condition)} \qquad \text{(G.10)}$$

$$w_2 = 0 \qquad \text{(G.11)}$$

Waves propagate in the positive x direction. The free surface displacement is denoted by $\eta(x,t)$ and

the displacement of the interface between the two liquids is denoted by $\xi(x,t)$.
These displacements are given by $\eta(x,t) = \eta_0 \exp\left(i(\mathrm{k}x - \omega t)\right)$ and $\xi(x,t) = \xi_0 \exp\left(i(\mathrm{k}x - \omega t)\right)$, where ω is the real angular wave frequency and k is the complex wave number. The solutions for u_i, w_i and p_i are assumed separable and periodical in time. They can be expressed as

$$\left.\begin{aligned} u_i &= \hat{u}_i(z)\,\mathrm{e}^{i(\mathrm{k}x - \omega t)} \\ w_i &= \hat{w}_i(z)\,\mathrm{e}^{i(\mathrm{k}x - \omega t)} \\ p_1 &= \hat{p}_1(z)\,\mathrm{e}^{i(\mathrm{k}x - \omega t)} + \rho_1 g\left(\bar{h}_0 - z\right) \\ p_2 &= \hat{p}_2(z)\,\mathrm{e}^{i(\mathrm{k}x - \omega t)} + \rho_2 g\left(\bar{h}_0 - \bar{h}_1\right) + \rho_2 g\left(\bar{h}_1 - z\right) \end{aligned}\right\} \qquad \text{(G.12)}$$

where $\bar{h}_0$ denotes the mean total depth and $\bar{h}_1$ the mean depth of the lower layer.

Substituting the general solution G.12 in the governing equations leads to a set of five equations with five unknown coefficients, namely

$$\left.\begin{aligned} \cosh(\mathrm{k}a)\,\mathrm{A} + \sinh(\mathrm{k}a)\,\mathrm{B} + i\omega\eta_0 &= 0 \\ i\frac{\omega}{\mathrm{k}}\sinh(\mathrm{k}a)\,\mathrm{A} + i\frac{\omega}{\mathrm{k}}\cosh(\mathrm{k}a)\,\mathrm{B} - g\eta_0 &= 0 \\ \frac{i}{\omega}(\rho_2 - \rho_1)g\,\mathrm{A} + i\frac{\omega}{\mathrm{k}}\rho_1\,\mathrm{B} - \rho_2\frac{\omega}{\mathrm{K}}\mathrm{D} &= 0 \\ \cosh(\lambda h_1)\,\mathrm{C} + \mathrm{D} &= 0 \\ \mathrm{A} + \frac{i\mathrm{k}}{\lambda}\sinh(\lambda h_1)\,\mathrm{C} + i\mathrm{k}h_1\,\mathrm{D} &= 0 \end{aligned}\right\} \qquad \text{(G.13)}$$

where $\lambda = \pm(1-i)\sqrt{\frac{\omega}{2\nu}}$ and $a = \bar{h}_0 - \bar{h}_1$.

The nontrivial solution is found by equating the determinant *Det* of the set of equations G.13 to zero, which yields an equation in which k is the only unknown variable:

$$\begin{aligned} Det = &\left[-1 + \frac{\varrho_2 - \varrho_1}{\varrho_2}\frac{g\mathrm{k}}{\omega^2}\left[\mathrm{k}h_1 - \frac{\mathrm{k}}{\lambda}\tanh(\lambda h_1)\right]\right]\left[\frac{g\mathrm{k}}{\omega^2}\tanh(\mathrm{k}a) - 1\right] - \\ &\frac{\varrho_1}{\varrho_2}\left[\mathrm{k}h_1 - \frac{\mathrm{k}}{\lambda}\tanh(\lambda h_1)\right]\left[\frac{g\mathrm{k}}{\omega^2} - \tanh(\mathrm{k}a)\right] = 0. \end{aligned} \qquad \text{(G.14)}$$

Equation G.14 comprises in fact two equations because the wave number k is a complex variable. The other coefficients (A, B, C, D) can be calculated as soon as the value for k is determined and subsequently the horizontal and vertical velocities can be calculated. This was done for some of the experiments made. The equations were solved using MAPLE version 4.2, a system for symbolic mathematical computation, which is a product of the University of Waterloo, Canada.

References

Carter, D.L., Heilman, M.D. and Gonzales, C.L., (1965), *Ethylene glycol monoethyl ether for determining surface area of silicate minerals*, Soil Science, Vol. 100, No. 5, pp. 356-360.

Chou, H.-T., (1989), *Rheological response of cohesive sediments to water waves*, Dissertation, University of California at Berkeley, USA.

Coles, D., (1956), *The law of the wake in the turbulent boundary layer*, Journal of Fluid Mechanics, Vol. 1, pp. 191-226.

Cornelissen, J.M. et al., (1993), *Experiments with surface waves on natural mud*, Cohesive Sediments Report 40, Delft Hydraulics and Rijkswaterstaat, The Netherlands.

Cueva, I.P., (1993), *On the response of a muddy bottom to surface water waves*, Journal of Hydraulic Research, Vol. 31, No. 5, pp. 681-696.

Dacon, (1990a), *DACON Data-acquisition software vers. 1.2*, Delft University of Technology, Hydromechanics Laboratory, The Netherlands.

Dacon, (1990a), *DACON Program listings vers. 1.2*, Delft University of Technology, Hydromechanics Laboratory, The Netherlands.

Dalrymple, R.A. and Liu, P.L.-F., (1978), *Waves over soft muds: a two-layer fluid model*, Journal of Physical Oceanography, Vol. 8, November 1978, pp. 1121-1131.

DCW, (1973), Original design drawings of the wave generator made by the TH Delft Centrale Werkplaats, drawing no. B-2-038, pp. 1-109.

De Wit, P.J., (1992a), *Rheological measurements on artificial muds*, report no. 9-92, Delft University of Technology, The Netherlands.

De Wit, P.J., (1992b), *Instruments used in the research on cohesive sediments*, report no. 8-92, Delft University of Technology, The Netherlands.

De Wit, P.J. and Kranenburg, C., (1993), *Liquefaction and erosion of China Clay due to waves and current*, Proceedings of the 23th International Conference on Coastal Engineering, Vol. 3, pp.2937-2948.

Feng, J., (1992), *Laboratory experiments on cohesive soil bed fluidization by water waves*, Thesis, Report UFL/COEL-92/005, University of Florida, Gainesville, USA.

Feng, J., (1993), *Bottom mud transport due to water waves*, Dissertation, Report UFL/COEL-TR/090, University of Florida, Gainesville, USA.

Foda, M.A., (1989), *Sideband damping to water waves over a soft bed*, Journal of Fluid Mechanics, Vol. 201, pp. 189-201.

Gade, H.G., (1958), *Effect of a nonrigid, impermeable bottom on plane surface waves in shallow water*, Journal of Marine Research, Vol. 16, No. 2, pp. 61-82.

Hendrix, W.P. and Orr, C., (1970), *Automatic sedimentation size analysis instrument*, Proceedings of the 2nd conference on Particle Size Analysis, Bradford Sept. 1970, eds.: M.J. Groves and J.L. Wyatt-Sargent, pp. 133-146.

Hsiao, S.V. and Shemdin, O.H., (1980), *Interaction of ocean waves with a soft bottom*, Journal of Physical Oceanography, Vol. 10, April 1980, pp. 605-610.

Huang, L.H. and Song, C.H., (1993), *Dynamic response of poroelastic bed to water waves*, Journal of Hydraulic Engineering, Vol. 119, No. 9, September 1993, pp. 1003-1020.

Jiang, L., Kioka, W. and Ishida, A., (1990), *Viscous damping of cnoidal waves over a fluid-mud seabed*, Journal of Waterway, Port, Coastal, and Ocean Engineering, Vol. 116, No. 4, July/August 1990, pp. 470-491.

Kuiken, G.D.C. and Merk, H.J., (1978), *Rheology of fluids*, parts A, B and C, in Dutch, Delft University of Technology, The Netherlands.

Liu, K.-F. and Mei, C.C., (1989), *Effects of wave-induced friction on a muddy seabed modelled as a Bingham-plastic fluid*, Journal of Coastal Research, Vol. 5, No. 4, Fall 1989, pp. 777-789.

Liu, K.-F. and Mei, C.C., (1993a), *Long waves in shallow water over a layer of Bingham-plastic fluid-mud - I. Physical aspects*, International Journal of Engineering Science, Vol. 31, No. 1, pp. 125-144.

Liu, K.-F. and Mei, C.C., (1993b), *Long waves in shallow water over a layer of Bingham-plastic fluid-mud - II. Mathematical derivation of long wave equations*, International Journal of Engineering Science, Vol. 31, No. 1, pp. 145-155.

Maa, P.-Y., (1986), *Erosion of soft muds by waves*, Technical report no. UFL/COEL-TR/059, Coastal & Oceanographic Engineering Department, University of Florida, Gainesville, USA.

Maa, P.-Y and Mehta, A.J., (1987), *Mud erosion by waves: a laboratory study*, Continental Shelf Research, Vol. 7, Nos 11/12, pp 1269-1284.

Maa, P.-Y and Mehta, A.J., (1988), *Soft mud properties: Voigt model*, Journal of Waterway, Port, Coastal and Ocean Engineering, Vol. 114, No. 6, November 1988, pp. 765-770.

Maa, P.-Y and Mehta, A.J., (1990), *Soft mud response to water waves*, Journal of Waterway, Port, Coastal and Ocean Engineering, Vol. 116, No. 5, September/October 1990, pp. 634-650.

MacPherson, H., (1980), *The attenuation of water waves over a non-rigid bed*, Journal of Fluid Mechanics, Vol. 97, part 4, pp. 721-742.

Mallard, W.W. and Dalrymple, R.A., (1977), *Water waves propagating over a deformable bottom*, Proceedings of the 9th Annual Offshore Technology Conference, Vol. 3, pp. 141-146.

Malvern, L.E., (1969), *Introduction to the mechanics of a continuous medium*, Prentice-Hall, Inc.

Mei, C.C. and Foda, A., (1981), *Wave-induced responses in fluid-filled poro-elastic solid with a free surface - a boundary layer theory*, Geophysical Journal of the Royal astronomical Society, Vol. 66, pp. 597-631.

Mei, C.C., (1982), *Analytical theories for the interaction of offshore structures with a poro-elastic sea-bed*, Proceedings BOSS' 82 Conference, pp. 358-370.

Nezu, I. and Nakagawa, H., (1993), *Turbulence in open-channel flows*, IAHR Monograph Series, A.A. Balkema Publishers, ISBN 90 5410 118 0.

Sakakiyama, T. and Bijker, E.W., (1989), *Mass transport velocity in mud layer due to progressive waves*, Journal of Waterway, Port, Coastal, and Ocean Engineering, Vol. 115, No. 5, September 1989, pp. 614-633.

Shibayama, T., Takikawa, H. and Horikawa, K., (1986), *Mud mass transport due to waves*, Coastal Enigineering in Japan, Vol. 29, pp. 151-161.

Shibayama, T., Aoki, T. and Sato, S., (1989), *Mud mass transport due to waves: a visco-elastic model*, International Association For Hydraulic Research, XXIII Congress, Theme: Hydraulics and the environment, Proceedings of Technical Session B: Fluvial Hydraulics, pp. B 567-574.

Spierenburg, S.E.J., (1987), *Seabed response to water waves*, dissertation, Delft University of Technology, The Netherlands.

Suhayda, J.N., (1984), *Interactions between surface waves and muddy bottom sediments*, Lecture notes on Coastal and Estuarine Studies, Vol. 14, Estuarine Cohesive Sediment Dynamics edited by A.J. Mehta, pp. 401-428.

Timoshenko, S., (1951), *Theory of elasticity*, second edition, McGraw-Hill Book Company, Inc.

Tolman, H.L., (1990), *Wind waves propagation in tidal seas*, Communications on hydraulic and geotechnical engineering, report nr. 90-1, Faculty of Civil Engineering of the Delft University of Technology, The Netherlands.

Toorman, E.A. and Berlamont, J.E., (1993), *Mathematical modelling of cohesive sediment consolidation*, Nearshore and Estuarine Cohesive Sediment transport, Coastal and Estuarine Studies, Vol. 42, edited by A.J. Mehta, pp. 167-184.

Van Leussen, W., (1988), *Aggregation of particles, settling velocity of mud flocs. A review*, Physical Processes in Estuaries, edited by J. Dronkers and W. van Leussen, Springer-Verlag, pp. 347-403.

Van Olphen, H., (1977), *An introduction to clay colloid chemistry*, Second Edition, John Wiley & Sons Inc., ISBN 0-471-01463-X.

Verruijt, A., (1992), *Offshore soil mechanics*, X2-CT2.1, Department of Civil Engineering, Delft University of Technology, The Netherlands.

Weast, R.C., (1973), *Handbook of chemistry and physics*, 54th edition, CRC PRESS.

Yamamoto, T., (1978), *On the response of a poro-elastic bed to water waves*, Journal of Fluid Mechanics, Vol. 87, part 1, pp. 193-206.

Yamamoto, T., (1981), *Wave induced pore pressures and effective stresses in inhomogeneous seabed foundations*, Ocean Engineering, Vol. 8, pp. 1-16.

Yamamoto, T., Takahashi, S., and Schuckman, B., (1983), *Physical modelling of sea-seabed interactions*, Journal of Engineering Mechanics, Vol. 109, No. 1, February 1983, pp. 54-72.

Yamamoto, T. and Takahashi, S., (1985), *Wave damping by soil motion*, Journal of Waterway, Port, Coastal and Ocean Engineering, Vol. 111, No. 1, January 1985, pp. 62-77.

930254